EVALUATING RISK OF WATERBORNE DEBRIS

A Dissertation

by

ANITA HELENE BROWN

Submitted to the Office of Graduate and Professional Studies of
Texas A&M University
in partial fulfillment of the requirements for the degree of

DOCTOR OF PHILOSOPHY

Chair of Committee,	John M. Niedzwecki
Committee Members,	Luciana R. Barroso
	Mary Beth Hueste
	H. Joseph Newton
Head of Department,	Robin Autenrieth

May 2021

Major Subject: Civil Engineering

ABSTRACT

The problem of surface and subsurface waterborne debris is of increasing concern on a global scale. Recent surges in the number and intensity of worldwide tsunami and storm events, as well as growing populations and continuous land development have exacerbated the predicament. These events have resulted in both man-made and natural debris entering outflows to coastal waterways and eventually oceans. Depending on the type and concentration of debris that is introduced into a flow field, it has the potential to increase the risk of damage to aquatic infrastructure and ecosystems. Decreased performance and failure of critical infrastructure as well as diminished health of wildlife due waterborne debris are potential consequences that have already been observed. The behavior of debris is highly dependent on the type of debris and characteristics of the waterway flow field, which makes debris transport and trajectory a complex phenomenon to model.

The need to better understand and characterize the subsets of debris behavior and interactions that lead to these negative outcomes is the focus of this research. A probabilistic model is developed to quantitatively investigate the nature of the risks associated with waterborne debris and capture the inherent uncertainties in modeling its behavior. A fault tree framework is used to establish the relationships between sub-events that lead to the disruptive behavior of waterborne debris. Specific focus is given to illustrative examples for the entanglement of whales in derelict fishing gear for the US Atlantic and Pacific coastlines and impact loading from large waterborne debris on fixed

structures in a channel. The risk of entanglement is characterized by the type of fishing gear, including its usage rates and loss rates, the region of study, and the seasonal migration of whales. The risk of impact loading is characterized by the rate of occurrence of debris-generating events, debris characteristics, channel dimensions, flow conditions, and the position and dimensions of the structure. Several methods of visualization reveal the sensitivity of the model to parameter definitions. The developed comprehensive model provides an adaptable risk-based framework for assembling available data to be interpreted into meaningful assessments for a wide range of applications.

DEDICATION

To my parents and grandfather, who have always encouraged me and pushed me to reach new heights. Without them, I would not have made it this far.

In Memory Of,

Helen Ruth Caldwell White, Irene Vashti Burns-Brown, and Pareese Rogers Brown.

ACKNOWLEDGEMENTS

I would like to thank my committee chair, Dr. Niedzwecki, for his support and guidance. I would also like to thank my committee members, Dr. Barroso, Dr. Hueste, and Dr. Newton for their contributions and guidance during the preliminary stages of this research. Additionally, thank you to the faculty and staff of the Zachry Department of Civil Engineering for both the academic support and professional development I have received while in attendance.

I would like to gratefully acknowledge the partial financial support of the Zachry Department of Civil Engineering's Engineering Graduate Merit Fellowship (EGMF) as well as partial financial support of the Department of Defense Science, Mathematics, and Research for Transformation (SMART) Scholarship during this investigation.

Thank you to all my family and friends for the encouragement and support, especially to my grandfather, Walter White; father and mother, Dwayne and Banita; siblings, Nathaniel, Kristen, and Chris; and the Barnetts. They have always encouraged me to keep learning, work hard, and go far. Thank you to my friends and colleagues from my undergraduate years at Duke University who encouraged me to pursue a graduate degree, including my advisor, Dr. Gavin. Thank you to the Black Graduate Students' Association at Texas A&M University for the warmth and comfort. Lastly, thank you to Yang, George, Yong, and Shengyi for your friendship and timely visits to my office. I will always be grateful.

CONTRIBUTORS AND FUNDING SOURCES

Contributors

This work was supervised by a dissertation committee consisting of Professor John M. Niedzwecki (advisor), Professor Luciana R. Barroso, and Professor Mary Beth Hueste of the Department of Civil Engineering and Professor H. Joseph Newton of the Department of Statistics.

All work for the thesis was completed independently by the student.

Funding Sources

Graduate study was supported by the Zachry Department of Civil Engineering's Engineering Graduate Merit Fellowship (EGMF) as well as partial financial support of the Department of Defense Science, Mathematics, and Research for Transformation (SMART) Scholarship

TABLE OF CONTENTS

Page

LIST OF FIGURES

Page

LIST OF TABLES

Page

CHAPTER 1

INTRODUCTION

As waterborne debris continues to pose a growing threat to both the natural environment and infrastructure globally, developing an understanding of the associated risks and consequences of waterborne debris becomes an increasingly important matter. The number of debris-generating events will likely increase as the global climate continues to change, and further, it is reasonable to assume that higher quantities pollution from manmade debris will be produced with the rising global population. The more prevalent waterborne debris becomes, the more imperative it will become to understand the full range of consequences and address the pertinent issues surrounding this problem.

From microplastics to drifting cargo containers, the range of risks associated with large quantities of debris is vast, and the varying properties of marine debris pose diverse sets of hazards to bodies of water and their inhabitants. Types, sizes, origins, and deterioration rates of debris are a few of the many characteristics that aid in defining these hazards. Waterborne debris can be transported at the fluid surface or within the water column, settle on coasts, riverbeds, or ocean floors, or become trapped in the ever-growing ocean gyres. According to the National Oceanic and Atmospheric Administration (NOAA), marine debris is one of the most prevalent pollution problems with regards to marine environments (NOAA Marine Debris Division, 2015). Waterborne debris has been observed to negatively affect aquatic wildlife, interfere with the inflow into power generation structures, and impact navigation, shipping, and tourism industries (Critchell

et al, 2015; Wan et al, 2017). These effects can lead to innumerable possibilities of long-term or short-term consequences on the natural environment, lives, and economics.

There is growing evidence of entanglement of marine life and ingestion of plastic debris by marine life down to the smallest marine organisms (Eriksen et al., 2014). Impairment of vital biological functions and decline of the general wellbeing of marine life are plausible consequences of these events. The entanglement of cetaceans in fishing gear is one of the most prominent threats to cetacean safety, especially for baleen whales (Dolman et al., 2018). In a review conducted by Stelfox et al. (2016) of published and grey literature from 1997 onwards pertaining to the impact of ghost fishing on marine mammals, reptiles, and elasmobranchs, it was found that marine mammals accounted for 70% of all reported entanglements included in the literature review, with humpback and North Atlantic right whales as the two highest recorded species. Although determining the full extent of these crises is difficult as most instances go unobserved, and therefore undocumented, the predicament is still evident. Preventing entanglements is best addressed by the general avoidance of areas where populations are present and through the enforcement of constructed policies (Dolman et al., 2018), however fishery operations and migration routes can overlap as whales follow sources of food.

[https://nmssanctuaries.blob.core.windows.net/sanctuaries-prod/media/archive/news/nov15/whale-entangled-lyman-hws-1200x600.jpg]

Figure 1.1 Whale entangled by fishing gear at its tail flukes. (Lyman, 2014)

Large debris such as fallen trees or shipping containers have the potential to damage riverine infrastructure once waterborne. Lateral forces generated from impacts, drag, or hydrostatic forces each contribute to the occurrences of damaged structures. In addition to lateral loading, when debris accumulates and debris jams form, the affects to the flow field can lead to the removal of sediment or flooding conditions (Diehl, 1997; Wallerstein et al., 1997). In the Madeira River, located north of Brazil in the Amazon rainforest, the accumulation of woody debris is a significant problem that regularly impacts efficient energy generation at the Santo Antonio hydroelectric power plant (Castro et al., 2018; Katsuno et al., 2018). The significant accumulation of drifting log debris resulting from the erosion of emergent and riparian trees is of constant concern. Authorities have attempted to mitigate this continued problem by establishing debris containment grids.

In 2005, Hurricane Katrina hit the southern United States and severely damaged approximately forty-five bridges in the states of Alabama, Louisiana, and Mississippi resulting in a total cost of repair and replacement estimated to be in excess of one billion dollars (Padgett et al., 2008). Although much of the damage was due to storm surge-induced loading, several were damaged due to impact loading from unconstrained barges, oil rigs, and boats. For example, the eastbound I-10 Pascagoula River Bridge was damaged after being impacted and experienced over 1 m of transverse displacement of a six-span unit (Padgett et al., 2008). More recently, twenty-two construction barges broke free of their moorings during Hurricane Sally. This hurricane event resulted in severe structural damage to the Pensacola Bay Bridge project after four barges, some of which carried mounted cranes, impacted the bridge deck structures (Robinson, 2020; Skanska, 2020; Slowey 2020).

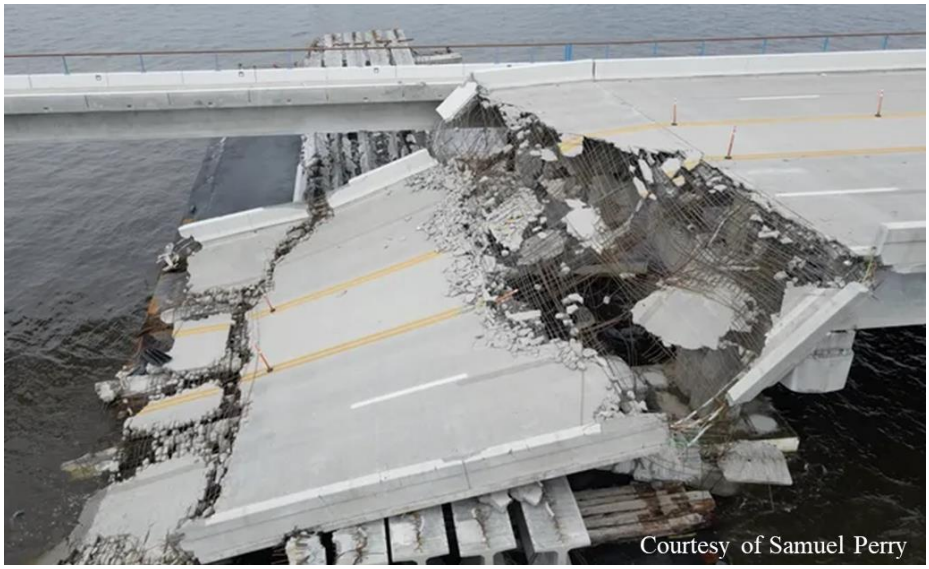

Figure 1.2 Damage to the Pensacola Bay (3 Mile) Bridge from Hurricane Sally (Robinson, 2020)

Manaadiar (2018) noted that an average of over 1500 shipping containers, of typical sizes of 2.43m (8ft) wide, 2.59m (8.5ft) high, and 6.09m (20ft) or 12.19m (40ft) long, are lost at sea per year as a result of both catastrophic and non-catastrophic losses based on surveys conducted by the World Shipping Council (WSC) from 2008 to 2016. These shipping container losses can be a consequence of adverse weather conditions, negligence, or failure to comply with limits set by the Container Securing Manual. Very recently, the ONE Apus ship suffered a catastrophic loss of 1,816 shipping containers, some of which carried "dangerous goods", in the North Pacific Ocean due to adverse weather (Maria, 2020). Daniel et al. (2002) reported that although the containers will most often sink, there is a possibility for a portion of containers to float partially submerged or release potentially harmful contents into the ocean environment. In Taiwan in 2001, Typhoon Nari caused over 1000 shipping containers to be swept into the Keelung River Basin from seven container storage yards located on a floodplain. This storm event led to blockages at 14 bridges, two of which were destroyed due to impact loading that occurred at the bridge decks. Overbank flow from blocked bridges resulted in the flooding of over 300 hectares (741.3 acres) of land in Keelung City, the loss of 11 lives, 31 injured people, and 250 inundated houses (Lee et al., 2006).

Wan et al. (2017) reported that it is generally estimated that 80% of marine debris comes from land-based sources. For manmade debris, this occurs through mechanisms such as river and atmospheric transport, littering, shipping, and fishing (Lebreton et al, 2016). Lebreton et al. (2016) correlated the production of pollution to population densities,

urban development, and seasonal changes. Once the debris becomes waterborne, its final destination and influences en route are highly dependent on the origin and type of debris. Damage to ecosystems is prominently reported on by the media in the form of entanglements, ingestion, and habitat loss. Damaged infrastructure has the potential to negatively impact regional operations and economics. Increasing incidences of debris accumulation along coasts and against structures and incidences of impact loading on structures by debris has led to increasing concerns regarding structural performance. The presence of large woody debris is particularly complex because, though it has the potential to damage infrastructure and induce flooding, it can be essential for stream ecosystems and biodiversity (Ruiz-Villanueva et al., 2016). The ability to quantify the risk associated with these events is ideal for developing preventative strategies and mechanisms.

Damage caused by waterborne debris can be cast as a probabilistic risk problem through the careful consideration of the causes and sources of debris generation, the hazards associated with debris transport, and the consequences of its presence in a body of water. These considerations make the formulation of a method to quantify the risks associated with waterborne debris highly dependent on the mechanisms that drive waterborne debris generation and the region of study. This research intends to develop and implement a risk-based model and evaluate its capabilities in making predictions. To achieve this goal, probability theory is utilized along with a fault-tree framework to construct the general risk-based model template, and relevant data from specific applications is collected from open literature to tailor the model and generate predictions. The applications of entanglement of whales in fishing gear and impact loading on

structures are chosen to demonstrate the flexibility of the developed general model. The capacity of the model to address and remedy knowledge gaps is investigated. Various visualization schema to illustrate and interpret the resulting predictions are implemented.

CHAPTER 2

BACKGROUND

In this section, a brief summary of background information related to injury to marine life due to waterborne debris and debris-structure interactions is presented. The injury to marine life background discusses the entanglement of marine mammals, specifically whales, and its connection to the phenomenon known as ghost fishing that plagues the fishing industry. This discussion will be used to identify key events in characterizing the risk of entanglement. The discussion surrounding debris-structure interactions focuses on pinpointing the key events that lead to the occurrence of negative interactions between debris and riverine structures, mainly highway bridges. Additionally, this section reviews the development of established risks models in contexts related to this research. Risk models addressing the risk of deadly collisions between boats and wildlife, the potential for the formation of debris accumulations against bridge piers, and the risk of collisions between bridge piers and aberrant vessels are discussed. Each of the presented models are relevant to how a general risk model framework can be formulated.

2.1. Injury to Marine Life

NOAA lists four main concerns for how marine animals are shown to be impacted by marine debris: ingestion, entanglement, habitat damage, and introduction of non-native species (NOAA Office of Response and Restoration, 2017). Ingestion occurs when marine debris is mistaken for food or unintentionally consumed. This occurrence can result in

starvation, poisoning, or digestive issues in marine life. Entanglement restricts the movement of animals, potentially causing injuries, drowning, starvation, or suffocation. Marine debris damages and impacts habitats by smothering plant life and polluting aquatic environments. Invasive species may travel with the introduced marine debris and modify the surrounding ecosystem.

There are innumerable amounts of literature and studies available that survey and characterize the abundance of anthropogenic marine debris for specific regions, however, there is not an adequate amount of coordination between the procedures used by researchers for collecting and reporting observed data across regions. These debris collection surveys generally focus on identifying the sources, categories, and/or sizes of the encountered debris. It is estimated that by volume at most 10% of the marine debris accumulated in oceans is attributed to fishing gear (Macfadyen et al., 2009; World Animal Protection, 2018). Factors such as environmental conditions, gear conflict, gear condition, and inappropriate disposal each contribute to the presence of derelict fishing gear (Brown and Macfadyen, 2007; NOAA Marine Debris Program, 2015). Once this fishing gear becomes derelict, most often referred to in relevant literature as abandoned, lost or otherwise discarded fishing gear (ALDFG), and is subject to the transport and flow of the body of water, it is free to negatively impact marine organisms and habitats as a source of disturbance, litter, or entanglements (Brown and Macfadyen, 2007).

Although active fishing can be found to be just as culpable as ALFDG, addressing the entanglement of whales requires understanding the phenomenon known as ghost fishing, where gear will continue to catch both target and non-target species of marine life,

even when no longer being controlled by the fishermen (Smolowitz, 1978; Brown and Macfadyen, 2007; NOAA Marine Debris Program, 2015; Gilman et al., 2016). The common categories of fishing gear are identified and explained in Table 2.1. Brown and Macfadyen (2007) pinpointed the factors that contribute to the occurrence of ghost fishing as the rate at which gear is lost, the catching efficiency of a specific type of gear, and the types of marine species that are occupying in the area, including their abundance and vulnerability. NOAA Marine Debris Program (2015) poses the following questions that are to some extent analogous to these factors:

(1) At what rate is gear lost annually?
(2) How long can gear continue to ghost fish?
(3) How effective is the gear at ghost fishing?
(4) How is value placed on the loss of both commercial AND non-commercial species?
(5) What are the costs of ALDFG on the environment?

Rates of loss, discard, and abandonment of fishing gear are commonly estimated using fisher surveys (Brown and Macfadyen, 2007; Gilman et al., 2016). The overall catching efficiency of fishing gear is related to the mortality rates of captured species and the duration of the gear's catching efficiency until it is no longer able to catch any species. Both aspects can potentially be estimated using monitored study sites and fitted regression decay models (Gilman et al., 2016).

Because many of the identified factors have a dependence on the specific study area, completing assessments across regions can be valuable. Currently there is a lack of quantitative assessment methods that allow for numerical comparisons from region to region (Dolman et al., 2018). Mattila and Lyman (2014) asserts that the remoteness of some regions and the perceived priority of the threat of entanglements influence the comprehensiveness of records and depth of investigations. Difficulties in conducting comparative research studies related to ALDFG stems from logistical and cost-prohibitive difficulties, inconsistent units of measure across regional studies, and varying international, national, and regional regulations and compliance (NOAA Marine Debris Program, 2015). Uncertainty in the repercussions and extent of ghost fishing also contribute to the complexity in quantifying the effects of ghost fishing. Therefore, quantifying the risk of entanglement regardless of region would require a flexible method that can ultimately bring together data from a variety of sources for valid interpretations.

Table 2.1 Descriptions of Fishing Gear Types (Morgan and Chuenpagdee, 2003)

Type	Description
Dredges	Large frames of various sizes towed behind vessels and used to capture benthic species.
Gillnets	Large panel of netting suspended vertically to capture benthic and pelagic species.
Hook	Individual baited hooks and lures of various sizes and weights to catch pelagic and benthic species
Longline	Long stationary line with shorter baited hooks attached to catch pelagic and benthic species.
Pots and	Frames made of wood or metal connected to a line and used to capture crustaceans and gastropods
Purse	Nets used to capture schooling pelagic species that encircles the fish and is pulled closed
Trawls	Cone-shaped net with wide mouth and narrow end, towed behind vessels

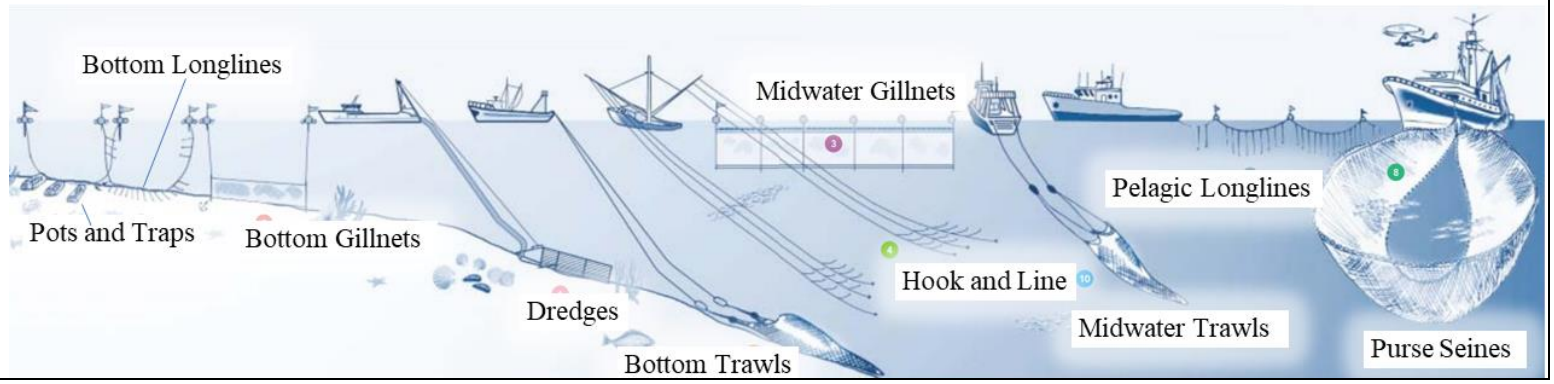

2.2. Debris-Structure Interactions

The two most common debris of concern for marine structural systems, such as bridges, are vegetation and ice debris (Briaud et al, 2006). The three types of debris hazards, with a focus on vegetative debris, to highway bridges as defined within a 1979 Federal Highway Administration (FHWA) report by Chang and Shen (1979) are:

(1) destruction from debris accumulation,

(2) destruction caused by direct impact and drag force, and

(3) other miscellaneous hazards.

The first type of debris hazard refers to the phenomenon when a piece of debris becomes lodged and, consequently, causes more debris to accumulate until flow conditions change and the waterway opening is either partially or fully blocked. This event is illustrated in Fig. 2.1. The second type comes from forceful impacts from waterborne debris. The additional pressure from accumulations can wash away embankment fill and highway approaches, cause the bridge deck to be dislodged for low lying decks, or lead to collapsed piers. The mechanisms of general accumulation are relevant to characterizing general debris-structure interactions and provide insight into the mechanisms that incite lateral loading on bridges, including impact loading.

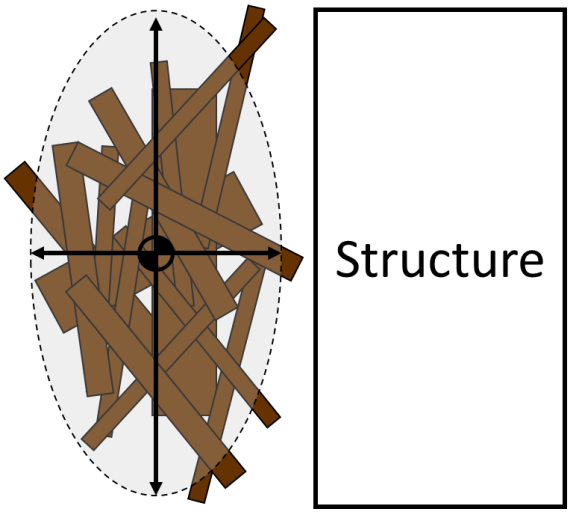

Figure 2.1 Illustration of accumulate debris

Waterborne debris will continue to be transported by currents until it reaches areas of no current, gets caught on or lodged against an obstruction in the water, or the water depth becomes too shallow (Parola et al., 2000). Overall, the accumulation of debris can be envisioned as a process that begins with a debris element that becomes lodged against an obstruction or a stabilizing element that provides a basis for a jam framework to gradually build itself around (Manners and Doyle, 2008). Debris interactions with a single pier is the most common and simplest modeling scenario for debris accumulations against a structure. Through laboratory testing, the shape of debris jams has been observed to often resemble a half-cone (Diehl, 1997, Lagasse et al., 2010; Panici and de Almeida, 2018). The major factors that lead to an accumulation have been established in literature as the channel geometry in comparison to debris dimensions and quantities, the flow field, and the existence and characteristics of obstructions (Melville and Dongol, 1992; Diehl, 1997; Lyn et al., 2006; Lagasse et al., 2010; Panici and de Almeida, 2018). As pictured in Fig.

2.2, the accumulation of debris can reach excessive heights if allowed to build up over long periods of time. Natural debris in rivers has added complexity in that it also can serve to stabilize channels, provide cover for wildlife, and add geomorphic complexity (Manners and Doyle, 2008). If designed appropriately, the existence of debris should not interfere with the performance of the structure.

Figure 2.2 Woody debris accumulated against FM 60 (Raymond Stotzer Parkway) Overpass crossing the Brazos River (Photo Credit: Anita H. Brown)

Aside from general accumulations, impact loading is typically studied and verified through laboratory testing in the context of extreme events, such as tsunamis, hurricanes, and major floods. Descriptions of published literature on conducted experimental testing

to determine the force generated by impact loading from collisions with waterborne debris are provided in Table 2.2. These tests characterize impact loads and assess the relationships between relevant factors. Analogous to the accumulation of debris, the channel geometry, flow field, debris dimensions and properties, and structural properties are all factors relevant to characterizing the impact load.

Debris control systems and debris diversion devices have been developed to attempt to mitigate these debris-structure interactions. This is done by halting the waterborne debris upstream and preventing the waterborne debris from reaching the structure, or by redirecting the waterborne debris to pass by the structure with limited to no interactions. Wallerstein et al. (1997) reviewed debris management technologies employed at riverine structures in Europe and the United States by collecting and compiling information from engineers and plant managers between September 1995 to October 1996. Bradley et al. (2005) focused on the debris control countermeasures for bridge structures and culverts. Use of these devices is catered to a specific structure location and its debris loading demands and emphasizes the need for location-based analyses.

Included within the report by Chang and Shen (1979) was a survey conducted by forty-four participating states that supports the notion that debris is a regional concern and addressing debris concerns and maintenance issues is based on local risks. Of the responses, 42 reported that debris was causing maintenance problems with 4 of the forty-two reporting a major problem, 25 moderate, and the remaining minor. According to the more recent 2019 National Bridge Inventory reports, 35.3% of highway bridges (218,028

of 617,084) reported a rating between four and six in the category of Channel and Channel Protection. The National Bridge Inspection Standards specify that a designation of six indicates that debris is slightly restricting the channel and a designation of four indicates large deposits of debris are present in the channel (U.S. DOT FHWA, 2020). Therefore, quantifying the risk of impact loading requires a flexible method that can account for each of the major factors that provoke debris-structure interactions as they pertain to a specific structure.

Table 2.2 Experimental testing for assessing impact loading from waterborne debris in extreme conditions

Test Description	Assessment	Reference
Reduced-scale and full-scale testing of wood logs	Determined the maximum impact force and the influence of collision geometry (debris orientation and eccentricity at impact)	Haehnel and Daly (2002); Haehnel and Daly (2004)
Small-scale hydraulic testing of driftwood	Estimated the maximum superposed force due to simultaneous or near-simultaneous collisions and probability of occurrence	Matsutomi (2009)
Three-dimensional numerical collision model	Developed a drift collision coupled model to analyze the collision process of drifting container due to tsunami runup	Yeom et al. (2009)
Small-scale high mass, low velocity in-air testing on shipping containers	Estimated impact force magnitude and duration based on acoustic wave propagation	Paczkowski et al. (2012)
Full-scale in-air testing of wooden utility pole and shipping container and small-scale (1:5) in-water testing	Quantified the effect of fluid on impact forces	Riggs et al. (2013); Riggs et al. (2014)
Full-scale high mass, low velocity in-air testing on a wood utility pole, steel tube, and shipping container	Estimated peak impact forces, contact stiffness, and impact durations	Aghl et al. (2014)
Small-scale (1:5) in-water testing of shipping containers	Characterized hydrodynamic effects on impact loading and duration	Ko et al. (2014)
Large-scale bore flow and in-air testing of wood logs	Quantified the relationship between collision direction angle and collision force	Ikeno et al. (2016)

2.3. Risk-Based Model Applications

There is precedent for quantifying the risk associated with hazards specific to marine life and riverine structures. Each of the following presented models uses an approach that consists of identifying the key components that bring about a specified hazard and developing methods of quantifying those components in an effort to obtain a numerical value that expresses the overall risk of the hazard. The risk models covered include the risk of deadly collisions between marine life and boats, the risk of debris accumulation at bridges, and the risk of bridge collapse due to collisions from aberrant vessels.

2.3.1. Risk of Deadly Collisions between Marine Life and Boats

Martin et al. (2015) developed a quantitative framework to investigate the risk of deadly collisions between marine wildlife, particularly marine mammals, and boats. Developing the framework required identifying the key components in the collision process and their relationships. The relationships between the key components identified by Martin et al. (2015) are organized using a conceptual diagram illustrated in Figure 2.3. The habitat characteristics describe attributes such as waterway configuration and bathymetry. The wildlife characteristics contains the size, speed, and number of wildlife, the depth at which they travel, and the number of deaths and recovered carcasses. The boat characteristics contain the size, number, and speed of boats and their compliance with relevant regulations. Each of these sets of characteristics aid in determining the likelihood of collisions and the likelihood of a collision ending in the death of the marine life.

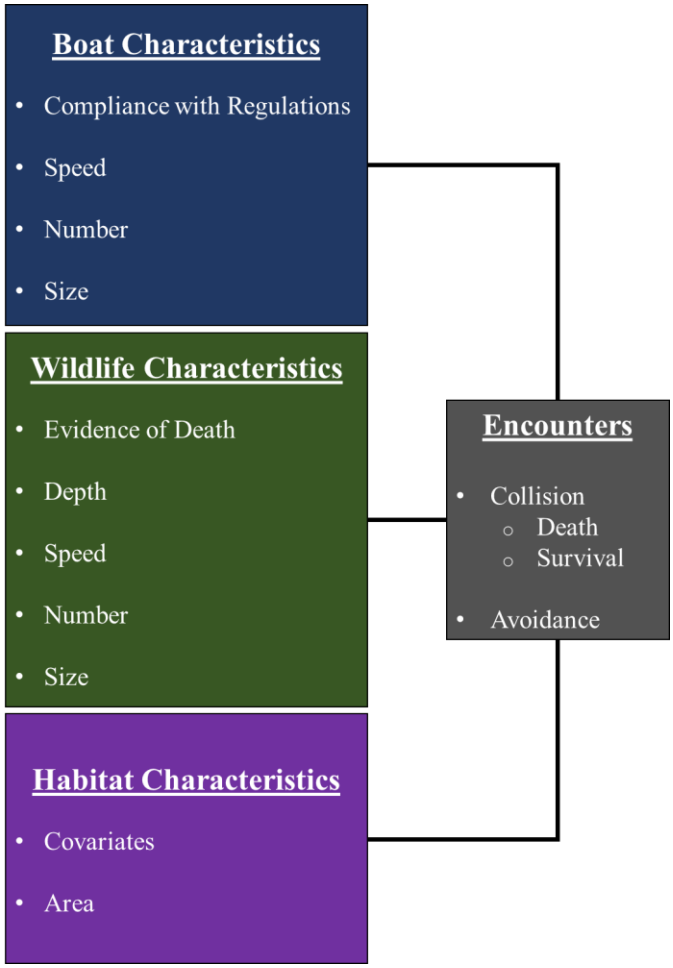

Figure 2.3 Conceptual diagram of the collision process between boats and marine life, based on illustration by Martin et al. (2015) to describe the relationships between key components.

The calculation of the rate of collision is built based upon the encounter rate between boats and marine life, that is the rate at which the trajectories of the boats and marine wildlife intersect in both time and space. The rate of collision, λ_c, is expressed as

$$\lambda_c = \lambda_e \, \mathrm{P}(\mathit{Strike\ depth}) \left(1 - \mathrm{P}(\mathit{Avoidance}_m)\right) \left(1 - \mathrm{P}(\mathit{Avoidance}_b)\right) \qquad (2.1)$$

where λ_e is the mean encounter rate between the marine mammal and a vessel, P(*Strike depth*) is the probability that the whale is within striking depth when an encounter occurs, P($Avoidance_m$) is the probability of the mammal *m* avoiding the boat, and P($Avoidance_b$) is the probability of the boat driver *b* avoiding the mammal. The death rate, λ_ε, is expressed as

$$\lambda_\varepsilon = \lambda_c \, \mathrm{P}(Death|Strike\ speed) \tag{2.2}$$

where P(*Death*|*Strike speed*) is the probability of death of the mammal given the striking speed at which the collision takes place. Evaluations using random walks and correlated random walks were conducted to run simulations and determine the general relationship between the number of encounters and vessel speed. Measures and procedures that attempt to reduce the number of ship-strikes such as slowing vessels and decreasing shipping activity in certain areas have been employed beginning with the 1999 Mandatory Ship Reporting System (Dolman et al., 2018). A similar comparative analysis was conducted by Crum et al. (2019) to quantify the differences in the relative risk of lethal vessel collisions to right whales before and after NOAA implemented a speed restriction rule with added consideration for vessel traffic data and spatially explicit estimates of right whale abundance.

2.3.2. Risk of Bridges Prone to Debris Accumulations

For bridge piers, woody debris accumulation at bridge piers can lead to exasperated scour due to acceleration and contraction of flow and increased flood risk in neighboring areas due to blocked waterway openings. Schmocker and Hager (2011) analyzed drift blocking probability for bridge decks using a scaled experimental study that emphasized the influence of drift dimension, freeboard, flow characteristics, and bridge characteristics on the resulting probability. Diehl (1997) explored guidelines to assess the potential for drift accumulation using data from published literature on 2,577 reported drift accumulations and field investigations of 144 drift accumulations. This qualitative analysis relied on flowcharts that are organized based on basin, channel, and bridge characteristics and using direct and indirect evidence. It was found that reducing the potential for drift accumulation can be done by designing bridge decks with adequate freeboard, long spans, solid and rounded piers, and strategic pier placement. Panici et al. (2020) proposed a simplified methodology that uses both direct and indirect observational data to assess the risks to bridges prone to debris accumulations using the flowchart illustrated in Figure 2.4. The direct evidence consisted of documented instances of debris accumulation at the bridge under assessment such as bridge inspection reports, photographic evidence, and repair work logs. Indirect evidence consisted of factors that were suggestive of the likelihood of debris accumulations forming based on nearby areas, such as data on upstream bridges, data on downstream bridges, and heavily forested floodplains.

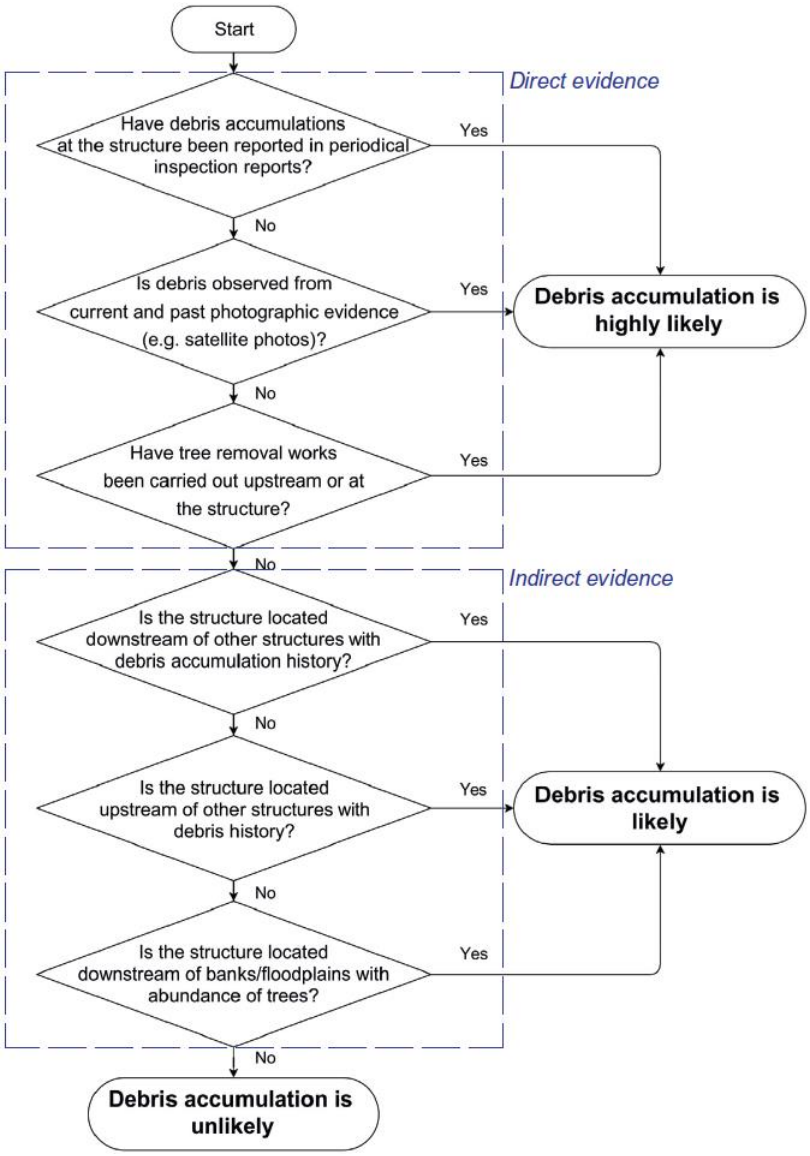

Figure 2.4 Proposed flowchart by Panici et al. (2020) for assessing debris accumulation potential at bridge piers

Based on the UK's Design Manual for Roads and Bridges BD 97/12 (2012), Panici et al. (2020) proposed that the vulnerability of a bridge can be assessed through the determination of a priority factor, P_f, with an additional factor that accounts for the likelihood of accumulations occurring. The amended equation for P_f is expressed as

$$P_f = H \cdot F \cdot M \cdot Tr \cdot V \cdot D \quad (2.3)$$

where H is dependent on the bridge scour history, M is based on the foundation material of the bridge, F is dependent on the type of foundation, Tr is dependent on the type of river, V is dependent on the type of road the bridge supports, and D is the appended factor that depends on the likelihood of debris accumulations as outlined in Figure 2.4. The assignment of values for each of these variables is based on evidence for the particular bridge being studied. The Design Manual for Roads and Bridges BD 97/12 (2012) incorporates the consequences of scour through the Relative Scour Depth, which is a ratio of the total scour depth to the depth to the underside of the foundation (Panici, 2020). The priority factor calculated from Eqn. 2.3 and the Relative Scour Depth are used to assign a Scour Risk Rating from a family of curves whose purpose is to identify bridges with a high risk of failure (DMRB, 2012). The development of this approach allows for the identification of bridges liable to debris accumulations based on direct and indirect evidence.

2.3.3. Annual Frequency of Bridge Collapse Due to Vessel Collision

The American Association of State Highway and Transportation Officials (AASHTO) used a probabilistic analysis to develop an equation that calculates the annual frequency of bridge collapse due to vessel collision (AASHTO, 2012). The annual frequency of bridge collapse due to vessel collision, AF, is expressed as

$$AF = (N)(PA)(PG)(PC)(PF) \quad (2.4)$$

where N is the annual number of vessels classified by type, size, and loading condition which can strike the bridge; PA is the probability of vessel aberrancy; PG is the geometric probability of a collision between an aberrant vessel and bridge element; and PF is an adjustment factor that accounts for protection from vessel collision. The determination of the probability of aberrancy, PA, is dependent on pilot error, adverse weather conditions, and/or mechanical failure. It is a product of a base rate of aberrancy and correction factors set based on an evaluation of accident statistics that account for bridge location, currents, crosscurrents, and vessel traffic density. The geometric probability, PG, is the conditional probability that the vessel will hit the bridge given that it is aberrant. It is dependent on factors such as geometry of the waterway, water depth, pier location and bridge clearance, vessel path and velocity, vessel size and draft, and environmental conditions. A normal distribution is typically used to describe the vessel path as illustrated in Figure 2.5. Comparable to this illustration, experimental studies have been conducted to describe debris lateral spread and mean trajectories in the context of extreme hydrodynamic events and statistically fit to normal distributions have been (Matsutomi, 2009; Stolle et al., 2018). The probability of collapse, PC, is dependent on the lateral capacity of the bridge elements to resist vessel impact force. The protection factor, PF, provides a means of adjusting the frequency of collapse when protective measures are put in place (AASHTO,

2012). Then, for a particular location with various types of vessels and multiple vulnerable bridge elements, the overall frequency of collapse of a bridge, AF_{Total}, can be expressed as

$$AF_{Total} = \sum_{i=1}^{NV} \sum_{j=1}^{NP} AF_{ij} \tag{2.5}$$

where *NV* is the number of vessel types that pass the bridge and *NP* is the number of bridge elements vulnerable to collisions (Manuel, et al. 2006).

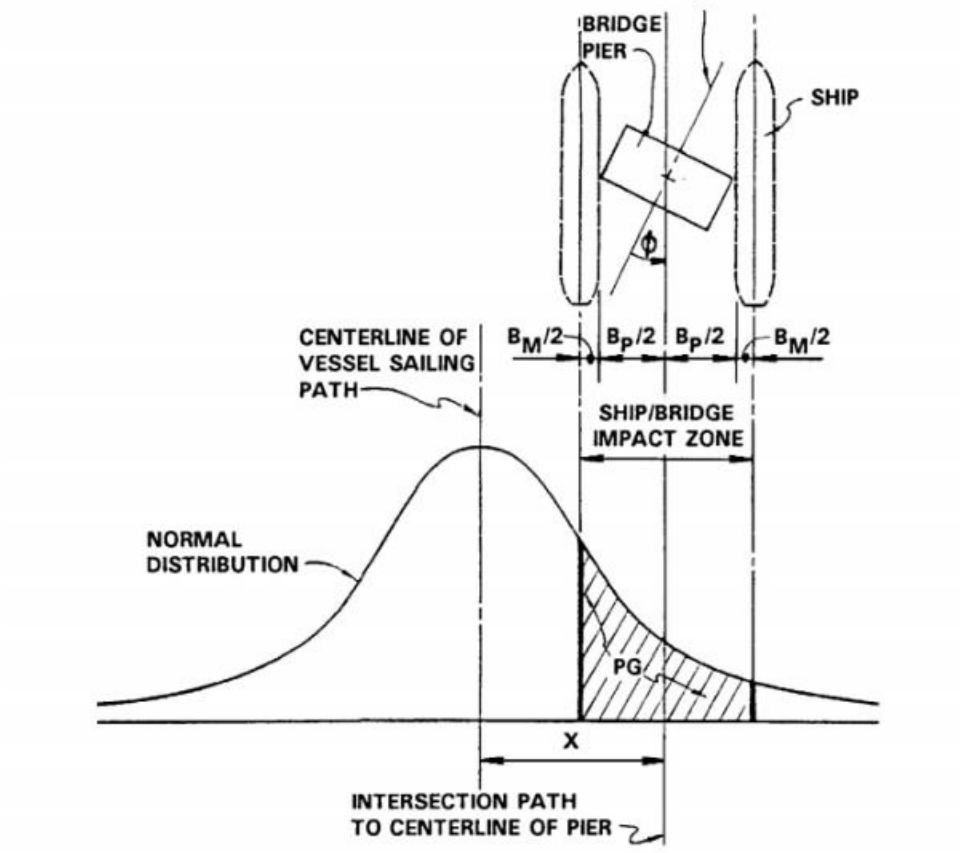

Figure 2.5 Geometric Probability of Pier Collision, where B_M = width of each vessel classification category and B_P = width of pier (AASHTO, 2012)

CHAPTER 3

MOTIVATION AND SIGNIFICANCE

Waterborne debris continues to be a growing threat to both the environment and marine infrastructure. Understanding the associated risks of waterborne debris based on causal relationships between key components enables better awareness and response. Risk analysis is a valuable tool for approaching problems involving decision making. Isolating events based on a subject's vulnerability to damages or losses due to waterborne debris requires tracing these events back to their causes. The flexibility of a risk-based model that is built on causal relationships lies in its capacity to efficiently adapt to fluctuations in the amount of available information and one's confidence in the accuracy of that information. The formulation of risk-based analyses allows for the identification of methods to prevent the occurrence of negative consequences. Aspects of the problem of interest can be specifically targeted when constructing procedures for reducing the overall risk associated with a particular event. Each of the applications and risk models explored as part of the background built their quantitative risk equations in a similar fashion. Contributing events were identified to define sub-events that caused a particular failure and evidence was gathered to properly define each event. The relationships between these sub-events were then mathematically expressed to develop a governing equation. The focus of the research presented herein is the development of probabilistic quantitative techniques to apply to the assessment of injury to marine life through the entanglement of

whales in fishing gear and debris-structure interactions through impact loading and accumulation of debris against structural elements.

ALDFG threatens the wellbeing of many marine species globally. Protecting the livelihood of these diverse species is imperative for maintaining balanced ecosystems. Lacerations and distress caused from adverse interactions with fishing gear directly influence the morbidity and mortality of marine species. Fatalities are especially damaging to marine mammal and sea turtle populations, many of which maintain endangered and protected statuses (NOAA Marine Debris Program, 2015). Use of materials such as nylon, polyethylene, and polypropylene have allowed for improved gear designs in an effort to keep up with the global demands for fish (Macfadyen et al., 2009; Stelfox et al., 2016). Unfortunately, these non-biodegradable synthetic materials that are often used in the manufacturing of fishing gear make interactions between marine species and fishing gear a prolongated issue. Any increases in the scale of global fishing operations may further exasperate this issue by generating more opportunities for potential gear loss. There is value in developing a probabilistic method that has the ability to calculate the risk associated with lost fishing gear that characterizes both the direct and indirect consequences of gear loss. The inconsistencies across regions in approaching the problem of ALDFG and the continual updates in policies over time make it necessary to develop a method of analysis that is compatible across regional sets of data and varying periods of time.

When large debris enters a marine environment, there is risk of generating waterways blockages and interfering with the uninhibited operation of infrastructure.

When impact forces from waterborne debris damage structures to the point of inoperability, economic losses due to the cost of repairs and social consequences due to broken transportation connections between areas arise. Assessing the entry of large debris into a body of water requires reviewing the frequency of instances of human error and natural causes. The design and geometry of aquatic structures and their placement within a waterway is unique to every structures as is the types of waterborne debris that may be encountered in a particular region. Once the risk of waterborne debris interacting with a structure can be assessed, further steps can be taken to ensure that the response of the structure is contained for that specific interaction. In the case of structural design, certain features can be strategically targeted to limit debris-structure interactions. For this reason, it is valuable to develop a structure-specific risk-based model that can evaluate the risk of collision for a structure and guide the process of making design decisions.

Probabilistic techniques that define the risk associated with specific events provides an adaptive means of quantifying the risk associated with any well-defined event. This research implemented a probabilistic technique for quantifying risk in the context of the entanglement of whales in fishing gear and the impact of waterborne debris against bridge piers. The loss rates of fishing gear, location, timespan, catching efficiency based on gear type, and presence of whales in the area are all used to define the risk of encountering fishing gear that can lead to the entanglement of whales. The developed model allows for comparable analyses across regions of study. The channel dimensions, debris characteristics, flow conditions, and structure position are used to define the risk of

collision between waterborne debris and a structure. The developed model can be adapted for specific structural scenarios.

3.1. Objectives

The goal of this research is to develop a methodology and framework for quantifying the risks associated with waterborne debris using a risk-based method of analysis and implement and assess the methodology in the context of the entanglement of whales by fishing gear and collisions between structures and waterborne debris.

The objectives of this research are to:

(1) Conduct literature searches to collect and examine relevant data and information available in open literature.

(2) Explore other types of models, research findings, and current practices/procedures developed to address the physical processes related to waterborne debris generation and behavior.

(3) Develop a probabilistic predictive model using reported data and available information that has the ability to evaluate the risks associated with whale entanglement due to waterborne debris and the risks associated with impact loading on bridge piers due to collisions from waterborne.

(4) Implement and evaluate the capabilities of the probabilistic predictive model to make predictions and its sensitivity to parameter definitions and identify areas for model improvement.

3.2. Research Overview

In sections 1, 2, and 3 the introduction, background and literature review, motivation, significance, and objectives of the research are presented. In section 4, the generalized template used to create event specific risk-based models and conduct risk analyses is developed as the determination of the likelihood of obtaining a certain system outcome. This section provides the theoretical basis for developing risk-based models in any context. Methods for introducing observed data into the probabilistic risk model, evaluating its sensitivity to available information, and generating model predictions are discussed.

Section 5 presents an application of the generalized risk model template to assessing the likelihood of whale entanglement using the key components of the event occurrence. The sensitivity of the model to one's confidence in the accuracy of the data and the parametrization of the model is discussed. The derivations and analyses completed in this section follow those conducted by Brown and Niedzwecki (2020). Section 6 presents an application of the generalized risk model to assessing the risk of impact loading between waterborne shipping containers and bridge piers using the key components of the event occurrence. The sensitivity of the model to one's confidence in the accuracy of the data and the parametrization of the model is discussed.

In section 7, key conclusions from each application are discussed. Suggestions are made for model improvement and future directions for this research to close revealed knowledge gaps.

CHAPTER 4

DEVELOPMENT OF EVENT SPECIFIC RISK-BASED MODELS

The development of an event specific risk-based simulation model, designed to allow for the blending of observable data and reasoned probability distributions to fill in knowledge gaps and predict the likelihood of a system outcome, is presented. The general model formulation is constructed around a fault tree framework that requires articulating the system as a synthesis of sub-events to reflect information relevant to the event being investigated. Clear descriptions of fundamental events that compose the sub-events and their interconnections that bring about the top event are of the upmost importance in making predictions using the risk-based model.

4.1. Introduction

The investigation of the behavior of systems and processes for the development of a quantitative model begins with characterization. According to Haldar and Mahadevan (2000), a system can be described as deterministic or stochastic. A deterministic system implies the availability of a mathematical expression that allows for an explicit solution based on specified parameter values; a final value can be directly evaluated. A stochastic system is one that cannot explicitly model the quantitative relationships between components of a system; multiple outcomes can be observed and are presumed to describe a random variable. For a stochastic system, probability theory is used as a tool to obtain a

final solution that states the likelihood of a certain system outcome occurring due to specified inputs.

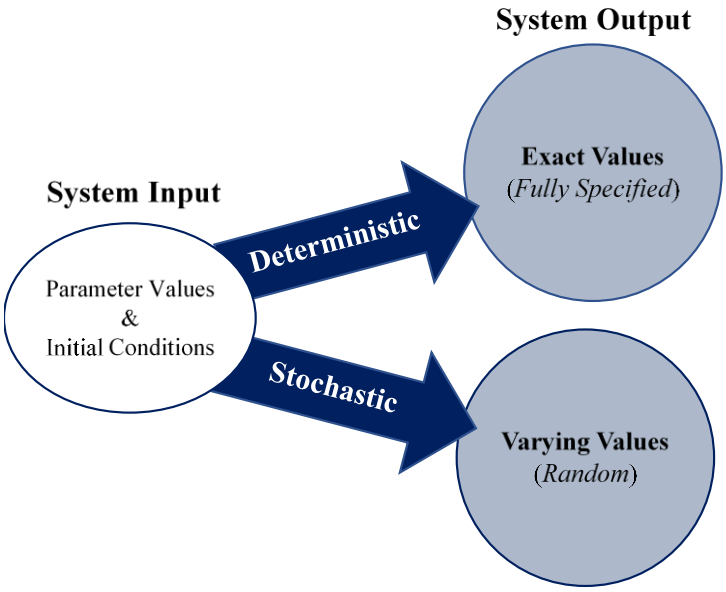

Figure 4.1 Characterizing deterministic vs. stochastic systems

Risk and reliability-based approaches rooted in probability theory become necessary when dealing with stochastic systems that rely on decision-making processes where uncertainty exists surrounding system performance and safety. In set theory, a sample space is composed of all possible outcomes. In terms of system performance, a conceived model can yield either favorable or unfavorable outcomes, where an unfavorable outcome occurs when some established limit state is violated. Reliability is typically considered the probability of maintaining a favorable outcome, while risk is the probability of experiencing an unfavorable outcome (Haldar and Mahadevan, 2000; Melchers and Beck, 2018). Therefore, when all possible outcomes in a sample space are considered and favorable versus unfavorable outcomes are mutually exclusive and

collectively exhaustive, risk and reliability act as complementary pairs that cover the entire sample space. If E_1 is used to denote favorable outcomes and E_2 denotes unfavorable outcomes, and the events are mutually exclusive and collectively exhaustive, then their relationship can be mathematically expressed as

$$P(E_1) + P(E_2) = Reliability + Risk = 1.0 \quad (4.1)$$

When one is determined, the other can be subsequently deduced. This is based on the second axiom of probability, which states that the sum of the probabilities of all possible outcomes (the probability of the sample space) is 1.0 (Haldar and Mahadevan, 2000; Ang and Tang, 2007). It becomes necessary to conceive clear descriptions for the classification of outcomes as favorable (positive) or unfavorable (negative) so that risk and reliability can each be properly addressed.

In addition to the classification of outcomes, risk involves studying negative consequences, the events that instigate a specified outcome, and the uncertainty surrounding the consequences. The important components of risk associated with the occurrence of a specific hazard event are loss and vulnerability. Specific hazard events can be specified in terms of intensity, duration, location, and probability of occurrence (Aven, 2008; Roberts et al., 2009). Loss is associated with the elements at risk, which can resemble monetary impact of damage, fatalities, and time. Vulnerability addresses factors that affect the ability of a community to prepare for, respond to, and recover from the

occurrence of a hazard. Overall, the risk associated with a particular outcome can be thought of as the probability of a negative consequence brought about by specific contributions from these identified contributing events. Each risk components plays an important role in how limit states and risk are defined when determining the risk associated with a specified event. Thus, the development of a risk-based model for a particular outcome requires the identification, articulation, and incorporation of pertinent sub-events in the model.

The uncertainties associated with these fundamental contributing events can make the modeling process quite challenging. Epistemic uncertainty, which reflects imperfect knowledge or inaccuracies in the understanding of the process being modeled (Ang and Tang, 2007), can be reduced as additional information including field data is incorporated into the model through the descriptions of the sub-events. The quantification of uncertainty associated with a risk model and the model parameters can be completed using statistical analysis.

This section focuses on the development of a general template for risk-based modeling that is constructed around a fault tree framework to organize sub-events that can be tailored to address a wide variety of specific engineering design events. Probability concepts essential to the development of a risk-based model equation are covered. Generalized sub-events that account for the identification of hazards, the elements at risk, and the vulnerability of the elements are explored to organize the fundamental contributing events in a manner that uses of available information and data. Epistemic uncertainty is

addressed through the careful interpretation of available data that is blended with carefully selected probability density functions that are used to fill in key knowledge gaps.

4.2. General Model Template for Quantifying Risk

The process of developing a general iterative template that transforms observed data for use in a risk-based predictive model, illustrated in Figure 4.2, begins with the selection of an event topic and completing an initial review of the published literature related to the chosen application. Reviewing published findings pertaining to the subject of interest allows for a better understanding of the applicability of a risk model in the field of study. For example, in a structural context, risk can be taken as the probability of failure of a system to satisfy performance criterion, including the consequences of a possible failure. Location and scenario-based data related to the types and properties of components affecting the system are extracted from the published literature and assessed and organized into sub-events. Statistical analysis is used to either convert the relevant data into discrete probabilistic information using proportions and percentages or to determine central values and variations in the data whose nature becomes captured in the parameters of analytical probability density functions that describe the sub-events. The sub-events and their interrelationships that compose the initial predictive model act as the fundamental contributing events whose descriptions encapsulate the behavior of the system and identify modes of failure. The probabilistic information is input into the initial predictive model, which is used to make predictions on encountering negative consequences, aid in interpretations of data, and visualize a range of scenarios. The resulting predictions are

critically evaluated against observations and specifics for model improvement can be noted. In this iterative process, as new information is acquired, speculative probability distribution functions used in the modeling process can be refined and the sub-events modified.

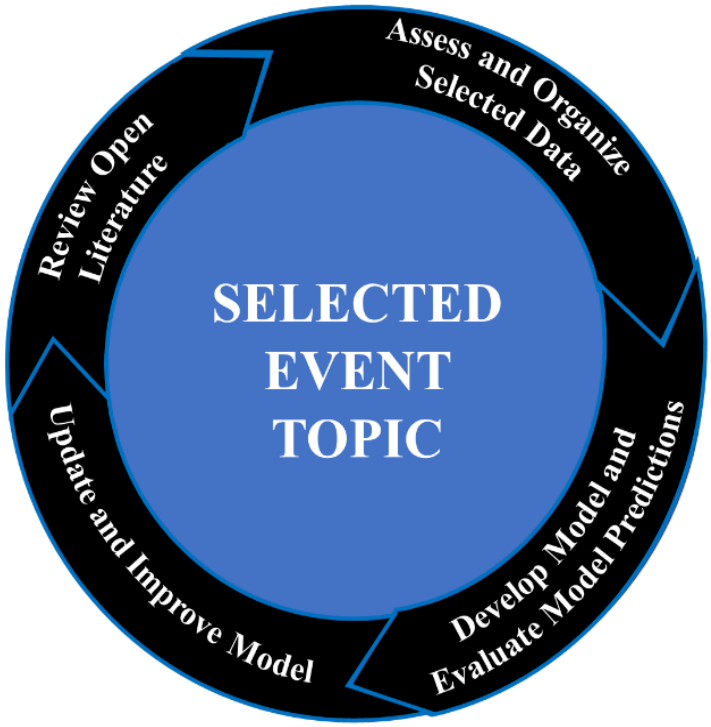

Figure 4.2 General iterative template for continued improvement of risk assessment predictions

This process is formalized using a fault tree framework as recommended by Ang and Tang (1984) to help guide the decision process for complex systems. Fault tree models aid in identifying components of a decision problem for complex systems in which outcomes representing modes of failure and consequences are identified and evaluated.

This top-down approach is effective in organizing and capturing information contributing to the top event through a series of supportive sub-events (Lee et al, 1985; Haldar and Mahadevan, 2000; Aven, 2008; Melchers and Beck, 2018). This approach is ideal for targeting specific features of a stochastic system. The risk model can be improved as new information needed to characterize additional sub-events is identified, creating an iterative process. The conceptual relationships between the sub-events and the top event dictate the mathematical development of the governing risk equation. The method for establishing a risk-based model introduced in this research merges probability theory and Boolean logic with a fault tree framework to characterize the relationships between events. The top event acts as an output, while the behavior of the sub-events act as a layered input. The use of an AND gate implies the intersection of events, where the output event occurs only if all input events occur. An OR gate implies the union of events, where the output event occurs if at least one input event occurs (Lee et al, 1985; Aven, 2008).

The probabilistic interpretation of the AND gate is the intersection of the specified sub-events, where all sub-events must occur for the top event to occur. For simplicity, sometimes it is advantageous for events to be considered independent once the sub-events are fully broken down into their individual fundamental events. This implies that the occurrence of one event does not affect the occurrence of another. For N independent events, $A_1 \ldots A_N$, the intersection of events is calculated as the multiplication of probabilities of the sub-events that lead to the top event. The mathematical representation of the intersection of N independent events is defined as

$$\mathrm{P}\left(\bigcap_{i=1}^{N} A_i\right) = \mathrm{P}(A_1 \cap \ldots \cap A_N) = \mathrm{P}(A_1) \times \ldots \times \mathrm{P}(A_N) = \prod_{i=1}^{N} \mathrm{P}(A_i) \tag{4.2}$$

where, × indicates the product between values. If the events are not considered independent, then it is necessary to acquire data connected to the conditional relationships between sub-events. Then the mathematical representation of the intersection of *N* dependent events is defined as

$$\mathrm{P}\left(\bigcap_{i=1}^{N} A_i\right) = \prod_{i=1}^{N} \mathrm{P}\left(A_i \,\middle|\, \bigcap_{j=i+1}^{N} A_j\right) \tag{4.3}$$

The probabilistic interpretation of the OR gate is the union of events, where at least one sub-event must occur for the top event to occur. For *N* mutually exclusive events, $B_1 \ldots B_N$, the union of events is calculated as the sum of probabilities of the sub-events that lead to the top event as shown in Eqn. 4.4. Mutual exclusion implies disjoint events, where only one event occurs at a time.

$$\mathrm{P}\left(\bigcup_{i=1}^{N} B_i\right) = \mathrm{P}(B_1 \cup \ldots \cup B_N) = \mathrm{P}(B_1) + \ldots + \mathrm{P}(B_N) = \sum_{i=1}^{N} \mathrm{P}(B_i) \tag{4.4}$$

If N is collectively exhaustive, spanning the set of all possible events, then Eqn. 4 will equal 1.0. Without the mutual exclusion descriptor, it is necessary to include the contributions of intersections terms. The union of N non-mutually exclusive events is written using the inclusion-exclusion principle as

$$\mathrm{P}\left(\bigcup_{i=1}^{n} B_i\right) = \sum_{c=1}^{N}\left[(-1)^{c-1} \sum_{\substack{C \subseteq \{1,\ldots,N\} \\ |C| = c}} \mathrm{P}\left\{\bigcap_{i \in C} B_i\right\}\right] \tag{4.5}$$

where, c controls the number of terms pulled into each combination without repetition of subset C for each iteration of c (Andreescu and Feng, 2004; Roberts and Tesman 2009). An example using the union of three events is given by Eqn. 6, where the notation $\mathrm{P}(B_iB_j\ldots)$ denotes the intersection of events to be calculated using Eqns. 2 or 3, depending on whether there is independence between events.

$$\begin{aligned}\mathrm{P}(B_1 \cup B_2 \cup B_3) = \mathrm{P}(B_1) + \mathrm{P}(B_2) + \mathrm{P}(B_3) - \mathrm{P}(B_1B_2) - \mathrm{P}(B_1B_3) \\ - \mathrm{P}(B_2B_3) + \mathrm{P}(B_1B_2B_3)\end{aligned} \tag{4.6}$$

Judgement on the necessity of including the intersection terms for non-mutually exclusive events and approximating the sub-events as mutually exclusive can be made based on the order of magnitudes for the probabilities and their products. Additionally, it

is possible to use de Morgan's rule to define the union of N events if the data presents itself in an appropriate way (Ang and Tang, 2007). This format makes use of the complementary events, $\overline{B}_i$, making the union of events

$$\mathrm{P}\left(\bigcup_{i=1}^{N} B_i\right) = 1 - \mathrm{P}\left(\bigcup_{i=1}^{N} \overline{B}_i\right) \tag{4.7}$$

The creation of a final risk-based equation relies on the merging of these probability concepts. Utilization of other logic gate concepts to represent exclusion or conditional relationships between events is also possible as event descriptions become more complex. It is important to note that the probabilities used to describe the fundamental events can be defined using discrete probability values or probability density functions. Describing the fundamental events as probability distributions with specified distribution parameters allows for better incorporation of uncertainty into the risk model.

4.3. Event Specific Risk Model Formulation

The process of developing a general risk-based model framework that is capable of addressing specific events using set and probability theory is presented in this section. The identification of fundamental data-driven sub-events, and how assumptions of independence and mutual exclusivity of the events affect the mathematical representation are examined. Using the organizational structure of a fault-tree, it is advantageous to generalize the types of sub-events that will present themselves when characterizing a

stochastic system. The sub-events established for the risk-based model are interconnected with the types of observable data available and should be grounded in the components of risk: hazard, loss, and vulnerability. Using this approach, the basic sub-events are considered to be a combination of spatial and temporal conditions and physical characteristics. Spatial conditions relate to location or position and can be used to account for spatial variability. Temporal conditions are those variables related to time, either as occurring over a period of time or at a specified time within a period. The temporal conditions sub-event can be used to account for factors such as seasonal changes and migrations or allow for the inclusion of mitigating factors that occur at regular intervals. Physical characteristics can be further broken down into size, shape, mass, strength, and/or type attributes. If the sub-events are acting independently and it is necessary for all the sub-events to occur for the top event to occur, then the intersection of the sub-events can be expressed mathematically as

$$\begin{aligned} &\mathrm{P}(\textit{Top Event}) \\ &\quad = \mathrm{P}(\textit{Spatial Conditions} \cap \textit{Temporal Conditions} \cap \textit{Physical Characteristics}) \\ &\quad = \mathrm{P}(\textit{Spatial Conditions}) \times \mathrm{P}(\textit{Temporal Conditions}) \times \mathrm{P}(\textit{Physical Characteristics}) \\ &\quad = s \times t \times h \end{aligned} \tag{4.8}$$

where, in the most compact notation, *s* represents the spatial conditions, *t* represents the temporal conditions, and *h* represents the necessary physical characteristics. If the sub-events are not independent, then it becomes necessary to consider the conditional relationships between events. The intersection of the sub-events would then be expressed as

$$
\begin{aligned}
&\mathrm{P}(\textit{Top Event}) \\
&\quad = \mathrm{P}(\textit{Spatial Conditions} \cap \textit{Temporal Conditions} \cap \textit{Physical Characteristics}) \\
&\quad = \mathrm{P}(\textit{Spatial Conditions} \mid \textit{Temporal Conditions} \cap \textit{Physical Characteristics}) \\
&\qquad \times \mathrm{P}(\textit{Temporal Conditions} \mid \textit{Physical Characteristics}) \\
&\qquad \times \mathrm{P}(\textit{Physical Characteristics}) \\
&\quad = (s \mid t \cap h) \times (t \mid h) \times (h)
\end{aligned}
\tag{4.9}
$$

4.3.1. Specification of Physical Characteristics

In some cases, it may be beneficial to further breakdown a particular sub-event into several distinct sub-events. For example, consider the intersection of the required physical characteristics of the system. If each physical characteristic (e.g. size, shape, mass, strength, etc.) is decomposed into its own fundamental event with index *i*, h_i, then the intersection of the *N* required independent physical characteristics of the system, can be expressed as

$$\mathrm{P}(\textit{Physical Characteristics}) = h = \bigcap_{i=1}^{N} h_i = \prod_{i=1}^{N} h_i \tag{4.10}$$

If the N required physical characteristics of the system are instead dependent events, then the probability of having the necessary physical characteristics is instead expressed as

$$\mathrm{P}(\textit{Physical Characteristics}) = h = \bigcap_{i=1}^{N} h_i = \prod_{i=1}^{N} \left(h_i \left| \bigcap_{j=i+1}^{n} h_j \right. \right) \tag{4.11}$$

If it is more accurate to represent the physical characteristics as the union of the fundamental characteristics, where only at least one physical characteristic is required, then the equation describing the physical characteristics is derived based on assumptions of mutual exclusion. Mutually exclusive physical characteristics h_i would mathematically be expressed as

$$\mathrm{P}(\textit{Physical Characteristics}) = h = \bigcup_{i=1}^{N} h_i = \sum_{i=1}^{N} h_i \tag{4.12}$$

If N is collectively exhaustive, spanning the set of all possible events, then the summation in Eqn. 4.12 will equal 1.0. The union of non-mutually exclusive physical characteristics, h_i, is written using the inclusion-exclusion principle as

$$\mathrm{P}(\textit{Physical Characteristics}) = h = \bigcup_{i=1}^{N} h_i = \sum_{c=1}^{N} \left[(-1)^{c-1} \sum_{\substack{C \subseteq \{1,\ldots,N\} \\ |C| = c}} \left\{ \bigcap_{i \in C} h_i \right\} \right] \quad (4.13)$$

where, c controls the number of terms pulled into each combination without repetition of subset C for each iteration of c (Andreescu and Feng, 2004; Roberts and Tesman 2009). If exploring the risk of the top event due to a specific physical characteristic with index i, then h_i can be substituted into Eqns. 4.8 and 4.9. Judgement on approximating the sub-events as mutually exclusive and not including intersection terms can be made on a case-by-case basis.

4.3.2. Specification of Temporal and Spatial Conditions

The concept of the union of events is especially important when considering spatial and temporal conditions because it may be necessary to combine data sets that span different intervals of space and time. Consider the risk for a period of time that can be expressed based on data in any given units (e.g. years, months, minutes). The probability of the top event occurring at time j is given by

$$\mathrm{P}(\textit{Top Event in Time } j) = (s \cap t \cap h)_j \quad (4.14)$$

where the spatial conditions and physical characteristics can also be specified for time *j*. The independence or dependence of the sub-events dictates whether Eqn. 4.14 reduces to the form of Eqn. 4.8 or 4.9. Mutual exclusivity of events over a period of time is dependent on whether the sets if sub-events are disjoint over time, i.e., whether or not the events leading to time *j* affect the occurrence of the top event at time *j*. If the sub-events are assumed mutually exclusive, then

$$\mathrm{P}(\mathit{Top\ Event}) = \sum_{j=1}^{M} (s \cap t \cap h)_j \tag{4.15}$$

where, *M* is the amount of time spanning the dataset, *h* is the physical characteristics defined using Eqns. 4.10, 4.11, 4.12, or 4.13 for time *j* to *M*, and the independence or dependence of the sub-events dictates whether Eqn. 4.15 further proceeds in the form of Eqn. 4.8 or 4.9. If considerations are given to how each physical characteristic, h_i, changes over time while maintaining any of the definitions given by Eqns. 4.10 through 4.13, then an additional subscript is given to account for these changes, h_{ij}. The total number of physical characteristics becomes N_j as opposed to *N* to represent the possibility of the number of reported physical characteristics changing with time, depending on the information available in the datasets.

When the quantity of observable data available for analysis is limited, it is reasonable to consider the combination of data from different geographic regions. The union of spatial events from mutually exclusive regions of interest can be expressed as

$$\mathrm{P}(Top\ Event) = \sum_{k=1}^{Q} \frac{1}{M_k} \cdot \left[\sum_{j=1}^{M_k} (s \cap t \cap h)_{jk} \right] \tag{4.16}$$

where, Q is the number of regions being considered, M_k is the amount of time spanning the datasets for region k, h is the physical characteristics defined using Eqns. 4.10 through 4.13, and the independence or dependence of the sub-events dictates whether Eqn. 4.16 proceeds in the form of Eqn. 4.8 or 4.9. Each physical characteristic is described as h_{ijk} if they experience concurrent changes in time and space. Thus, Eqn. 4.16 represents the central equation needed to develop an event specific risk-based model.

The relationships that one establishes between the sub-events are a subjective interpretation of the data and published findings. Assumptions regarding independence and mutual exclusivity of the events directly affects the mathematical representation of the risk equation. Knowledge of how each sub-event directly influences the top event aids in implementing preventative methods to control the occurrence of the top event. As each sub-event is better understood, the preemptive methods can be explicitly expressed. The developed template for creating a risk-based model allows for a flexible approach where the best fitting risk model can be constructed.

4.4. Risk Model Implementation and Assessment

Because of the undeniable existence of uncertainty in a stochastic system, even for a well-defined system, it is important to reflect on the sensitivity and variability of the risk model estimates to the definitions of the sub-events. Well-defined sub-events give direct

interpretations of the risk model estimates and make it possible to determine the individual contributions of each event to the overall risk. The descriptions of the sub-events should reflect how certain the researcher is about the accuracy of the data, which drives the decision of designing the model to make conservative versus precise estimates. Because the necessary data is not always available, at times the researcher will be required to use their best judgement and adopt a Bayesian-like approach where a prior distribution is conceived, and data is later incorporated, either supporting the choice or replacing it with actual data, as it becomes available.

4.4.1. Methods of Generating Model Predictions

Four practical procedures for generating model predictions and monitoring the behavior of the risk-based model are assigning specific discrete probability values to represent sub-events, considering ranges of discrete probability values, producing calculations by independent sampling from distribution functions used to represent each sub-event, and directly estimating the analytical forms of the distribution functions that characterize each sub-event based on the representation of the data. Using discrete probability values to represent each sub-event entails taking the observed data and using statistical measures of central tendency, e.g., mean, median, or mode, to approximate values for s_{jk}, t_{jk}, and h_{ijk} to substitute directly into the risk equation to calculate "average" estimates. Considering ranges of discrete probability values aids in determining how individual sub-events specifically affect the estimates of the system behavior. Conditions

and characteristics with the most influence on the risk of the top event occurring can be readily identified and interpreted if the sub-events are detailed in their descriptions.

When continuous distribution functions are introduced to represent the sub-events as random variables, then not only are the central tendencies of the observed data captured, but also the variations and uncertainty in the data and one's confidence in the assumed density function and its parameters. The appropriate density functions can be selected through the recognition of the underlying probability distribution function based on individual and multidimensional histogram representations of the data. The density functions representing the introduced general sub-events of spatial conditions, temporal conditions, and physical characteristics as random variables can be denoted as $f_S(s)$, $f_T(t)$, and $f_H(h)$. Any restrictions or decisions made on the type of probability density function chosen to represent the sub-events are dependent on the collected data. At times it will be reasonable to consider transformations and modifications of the chosen distribution. If the random variables are constrained to a specific domain, then it is recommended that a truncated distribution is used. Forming a truncated distribution is equivalent to normalizing the distribution by completing a conditional probability given that the values of the random variable fall within a given interval (Benjamin and Cornell 2014).

$$f_X(x|x \in \text{Interval}) = \frac{f_X(x)}{F_X(x \in \text{Interval})} \tag{4.17}$$

Once a density function is assumed, if estimates are made using independent sampling from sub-events, then the resulting risk estimate will also be in the form of a histogram with an underlying distribution. Alternatively, the analysis can proceed using the analytical forms of the various distribution functions describing the sub-events.

Assuming independence and mutual exclusion between sub-events becomes beneficial if it is desired to express the risk estimate in its purely analytical form. To demonstrate this, consider independent sub-events X_i which lead to a top event Y. Then, the intersection of the sub-events, $Y = X_1X_2\ldots X_N$ is the product of their individual distributions.

$$f_Y(x_1,x_2,\ldots,x_N) = f_{X_1}(x_1) \cdot f_{X_2}(x_2) \cdot \ \ldots \ \cdot f_{X_N}(x_N) \tag{4.18}$$

The summations that are introduced due to the union of mutually exclusive sub-events makes it necessary to complete convolution integrals (Benjamin and Cornell, 2014; Melchers and Beck, 2018). If the sub-events are not independent, then for the additive event $Y = X_1 + X_2$,

$$f_Y(y) = \int_{-\infty}^{\infty} f_{X_1,\, X_2}(y - x_1,\, x_1)dx_1 = \int_{-\infty}^{\infty} f_{X_1,\, X_2}(x_2,\, y - x_2)dx_2 \tag{4.19}$$

If X_1 and X_2 are independent, then the distribution describing the top event Y becomes the convolution integral

$$f_Y(y) = \left(f_{X_1} * f_{X_2}\right)(y) = \int_{-\infty}^{\infty} f_{X_1}(y - x_2) \cdot f_{X_2}(x_2) dx_2 = \int_{-\infty}^{\infty} f_{X_1}(x_1) \cdot f_{X_2}(y - x_1) dx_1 \quad (4.20)$$

For N independent events, $Y = X_1 + X_2 + \ldots + X_N$, this becomes

$$f_Y(y) = \left(f_{X_1} * f_{X_2} * \ldots * f_{X_N}\right)(y) \quad (4.21)$$

In its analytic form, the risk equation is built as a combination of the algebraic representations of probability theory introduced in Eqns. 4.18 through 4.21 based on the interrelationships of the sub-events. A change of variables is required when transforming a joint probability distribution function, $f_Y(x_1, x_2, \ldots, x_N)$, into a distribution function in terms of $f_Y(y)$ so that direct interpretations of the parameters describing the top event can be made. The change of variables is completed by solving

$$f_Y(y) = \frac{f_{X_1, X_2, \ldots, X_N}(x_1, x_2, \ldots, x_N)}{\left| \det\left(J(g^{-1}(y))\right)\right|} \quad (4.22)$$

where $Y = g(X_1, X_2, \ldots, X_N)$, $g^{-1}(y)$ is its inverse, $J(g^{-1}(y))$ is the Jacobian Matrix formed by $\{dy/dg^{-1}(y)\}$, and $|\det (J(g^{-1}(y)))|$ is absolute value of the determinant of the Jacobian (Haldar and Mahadevan 2000).

Using these methods to obtain an analytical equation can become quite complex as the risk equation becomes a more complicated description of the interrelationships between sub-events. As random variables become described by more complicated distributions and the risk-based equation becomes more complex, it is important to remember that (1) a probability density function (PDF), $f_Y(y)$, is nonnegative; $f_Y(y) \geq 0.0$; (2) a cumulative distribution function (CDF), $F_Y(y)$, is zero at $-\infty$ and one at $+\infty$; $F_Y(-\infty) = 0.0$ and $F_Y(+\infty) = 1.0$; (3) the CDF, $F_Y(y)$, is nondecreasing and $F_Y(y) \geq 0.0$; and (4) for continuous random variables, the CDF is also continuous and has a derivative, which is the PDF (Haldar and Mahadevan, 2000). As a result of the second statement, it is important to realize that over the support of the random variable, the probability density function must integrate to 1.0, that is:

$$\int_{-\infty}^{+\infty} f_Y(y)\, dy = 1.0 \tag{4.23}$$

In the case of a continuous random variable, this requirement is especially important for complex risk functions where random variables are described by different types of distributions. In some cases, when the general form of the final distribution becomes unrecognizable, the making use of proportionality and a normalizing constant is recommended for completing products and integrations.

Although the underlying probability density function does not directly give probabilities, it does provide information on the behavior of system in the form of central

tendencies and spread. In addition, the probability of either not exceeding or exceeding a specified limit, y_0, can be calculated using integration to obtain either the CDF, $F_Y(y)$, or Survival Function, $1 - F_Y(y)$.

$$\mathrm{P}(Y \leq y_0) = F_Y(y_0) = \int_{-\infty}^{y_0} f_Y(y)\, dy \tag{4.24}$$

$$\mathrm{P}(Y \geq y_0) = 1 - F_Y(y_0) = \int_{y_0}^{1} f_Y(y)\, dy \tag{4.25}$$

This assessment can provide the likelihood of the model overestimating or underestimating the risk of the top event occurring, which gives a measure of accuracy.

When a risk equation cannot be analytically determined, it is recommended that sampling and simulation methods be utilized to generate histograms to estimate the distribution function that best describes the top-event. This numerical approach to evaluation, whose results are also valid, involves repeated random sampling of values from the distributions that describe each sub-event and repeatedly calculating the risk of the top event. The sampling method and number of iterations employed are dependent on what is found to be appropriate. Aside from direct independent sampling, other sampling algorithms include Monte Carlo-based methods such as Markov Chain Monte Carlo methods (e.g. Gibbs Sampling and Metropolis-Hastings) (Ang and Tang, 1984; Hoff 2009; Melchers and Beck, 2018). From the collection of calculated values, one can use kernel density estimates and statistical methods to estimate the parameters of the underlying

probability distribution. Reflection on the specific event predictions can suggest where additional information could result in improved model predictions.

4.4.2. Methods for Evaluating Model Accuracy and Sensitivity

Exploring the sensitivity of the model to slight changes in the model structure provides insight into how the output of the model changes as the availability of data fluctuates, which variables have the most influence on the final outputs, and how well the sub-events are described by their probability density functions and parameters. Parameter estimation methods such as method of moments, method of maximum likelihood, and order statistics and statistical tests such as hypothesis testing and goodness-of-fit tests are advantageous for determining the parameters that best describe the probability distribution for a given random variable representing a sub-event based on observed data (Benjamin and Cornell, 2014; Melchers and Beck, 2018). These methods described in Table 4.1 can be applied to the distribution describing the sub-events or top event, so that the parameters of the risk model can be determined and the adequacy of the risk model in depicting each sub-event can be assessed.

Table 4.1 Parameter estimation methods and statistical tests (Benjamin and Cornell, 2014; Melchers and Beck, 2018)

Method/Test	Application
Model Parameter Estimation Methods	
Method of Moments	For estimating population parameters, used to describe central values, dispersion, symmetry, or peakedness • nth moment: $E(X^n) = \int_{-\infty}^{\infty} x^n f_X(x)\, dx$ (continuous distribution) • nth moment: $E(X^n) = \sum_{\text{all } i} [x^n p_X(x_i)]$ (discrete distribution)
Method of Maximum Likelihood	Involves maximizing a likelihood function $L(\theta\|x)$ to find under which parameter descriptions for $\theta_1, \theta_2,\ldots,\theta_m$ the observed data $y_1, y_2,\ldots,y_n$ is most probable • $L(\boldsymbol{\theta}\|\boldsymbol{x}) = \prod_{i=1}^{n} f(x_i\|\theta)$ • $\log[L(\boldsymbol{\theta}\|\boldsymbol{x})] = \sum_{i=1}^{n} \log[f(x_i\|\boldsymbol{\theta})]$ • $\sum_{i=1}^{n} \frac{\partial}{\partial \theta_j} \log[f(x_i\|\boldsymbol{\theta})] = 0$
Order Statistics	The kth order statistic is the kth value of ordered data; it is related to rank statistics, medians, extreme values, quantiles, and ranges
Statistical Testing of Parameters	
Hypothesis Testing	Procedure for drawing conclusions about parameter values based on observed data. Involves a null hypothesis, a decision rule for when to reject or fail to reject the null hypothesis, and an alternate hypothesis.
Goodness-of-fit Tests (e.g. χ^2 and Kolmogorov-Smirnov (K-S) Tests)	A model hypothesis test based on deviations between predicted values from the model and observed data. Involves a null hypothesis that is the proposed model, a decision rule reliant on a sample statistic that captures deviations between observations and model predictions, and an alternate hypothesis

4.5. Application of Template

In the sections to follow, the template developed in this section will be applied to examples related to the entanglement of whales by fishing gear and the force of collision of waterborne debris against a structure. For each unique application, the sub-events that bring about the hazard are identified and characterized using data collected through thorough literature reviews. The general iterative template illustrated in Fig. 4.2 is used as guidance for each assessment. Unraveling these examples will demonstrate the wide range of possible applications.

4.6. Discussion and Conclusions

This section presents a general methodology for developing an event specific risk-based model that predicts the likelihood of a system outcome for a variety of stochastic applications. The model integrates a fault tree framework that requires thoughtful articulation of the event of interest and its interrelated supportive sub-events. This requires a basic understanding of the physical characteristics of a system and the spatial and temporal conditions as presented in the formulation. The template introduces probabilistic and statistical methods that can be applied to mathematically characterize general sub-events that encompass the spatial conditions, temporal conditions, and physical characteristics of the system. The resulting model gives mathematical interpretations to probabilistic representations of these fundamental events. Focused descriptions of sub-events within the fault-tree makes the template applicable to many research topics for a variety of fields.

Use of the model to obtain accurate estimates is dependent on the amount of observed data available that is relevant to the fundamental events established. The event specific risk-based model as presented can be utilized to address epistemic uncertainty by the careful interpretation of available data and the careful blending of documented data with relevant probability density functions that are selected to fill in any knowledge gaps reflecting incomplete information. Refinement of the model occurs with increased data and leads to confidence in the risk-based model predictions. With the availability of parameters to help define the behavior of each sub-event, alternate scenarios can easily be explored. Characterizing the sensitivity of the risk model parameterization is possible through various visualization schema and statistical analyses. This study provides a straightforward approach for the development of risk-based models. It is expected that with the investigation of specific events, a deeper understanding of the refinement of sub-events, the need for more field data, and modeling on a larger scale will be part of the evolution process of event specific risk-based modeling.

CHAPTER 5

ASSESSING THE RISK OF WHALE ENTANGLEMENT WITH FISHING GEAR DEBRIS[*]

This section follows the work done by Brown and Niedzwecki (2020). The loss and abandonment of fishing gear has resulted in one of the most visible signs of growing pollution in the marine environment. The entanglement of whales in fishing gear has been the subject of increasing documentation. The interpretation of the documented incidents to address the risk of whale entanglement is presented. An initial risk-based model is derived that reflects published information on multi-year fishing gear accumulation rates and entanglement data. A fault tree framework is adopted to organize the data, allowing for the continual improvement of the risk-based model predictions through the incorporation of new data and inclusion of additional sub-events. Analytic distribution functions are introduced to augment incomplete data and explore hypothetical scenarios. Data reported for the US Atlantic and Pacific coastlines are used in illustrative examples, that address both regional and multi-regional applications, and the sensitivity of the risk-based predictions to the reported field data.

---

[*] Reprinted with permission from "Assessing the risk of whale entanglement with fishing gear debris." by Anita H. Brown and John M. Niedzwecki, 2020. *Marine Pollution Bulletin,* 161(2020): 111720, Copyright [2020] by Elsevier Ltd.

5.1. Introduction

The fishing industry is an international enterprise with contributions from both large corporations and local commerce. Global oversight organizations and committees have been established, but the size of the industry makes it practically impossible to track the activities of every vessel. Consequently, the actual quantities of lost fishing gear and its accumulation lurking beneath the ocean surface are not precisely known. It has been estimated that on a global scale as much as 10% of marine debris is attributed to fishing gear (Macfadyen et al., 2009; World Animal Protection, 2018) and this percentage will likely vary by region and locality. Macfadyen et al (2009) list some of the factors that affect the amount of lost fishing gear as adverse weather; cost of retrieval; gear conflicts; illegal, unregulated and unreported (IUU) fishing; vandalism/theft; and accessibility of collection facilities. Plastics used in fishing gear can take hundreds of years to break down in marine environments, only to perhaps culminate into the associated problem of microplastics (Barnes et al., 2009; Macfadyen et al., 2009). Due to currents and the connectivity of oceans and rivers, the site where the fishing gear appears is not necessarily indicative of where the fishing gear originated (Saez et al., 2020). This is observed in the appearance of naturally occurring convergence zones where debris accumulates (Macfadyen et al., 2009).

In addition to economic and social impacts, abandoned, lost or otherwise discarded fishing gear poses a particular problem for large species of marine life, such as whales. Entanglement can result in the restriction of their movement and has been documented to cause mild to severe injuries to whales, and additionally, if not removed, could lead to

drowning or suffocation. Injuries to these marine animals can affect their ability to reproduce and feed (Saez et al., 2020). Outside of the incidents of bycatch during active fishing, there is a specific risk to a variety of large marine inhabitants that also includes dolphins, seals, sea turtles, and sharks. Large marine animals, several of which maintain endangered or threatened status (Macfadyen et al., 2009; Gilman et al, 2016), tend to swim long distances during seasonal migrations, making them susceptible to crossing paths with debris in commercial fishing zones and shipping lanes while pursuing food sources.

The National Oceanic and Atmospheric Administration (NOAA) has documented large whale entanglements off the U.S. West Coast (California, Oregon, and Washington) dating back to 1982 (NOAA Fisheries, 2019; Saez et al., 2020). NOAA has recorded a generally increasing trend in the number of whale entanglement cases reported on the West Coast with the average number of confirmed cases rising from 9 confirmed cases to 41 confirmed cases between the spans of 1982 to 2013 and 2014 to 2017, respectively (NOAA Fisheries, 2019; Saez et al, 2020). Saez et al. (2020) specifically notes factors that have led to an increased public awareness and sensitivity to this problem. These contributing factors include increased monitoring of changes in the spatial distribution and abundance of whales, changes in fishing methods, and changes in ocean conditions. In the North Atlantic, it is estimated that 82% of right whales have experienced entanglement during their life (Waters, 2016), compared to the 409 population estimate of North Atlantic right whales by the North Atlantic Right Whale Consortium for the end of 2018 (Pettis et al, 2020).

Although there are entanglement cases documented, these reports are only comprised of confirmed cases. It remains unknown exactly how many marine mammals in total are affected by these incidents, and unfortunately, as more debris accumulates in the oceans, entanglement incidents can be expected to increase in frequency. Data that identifies the specific type of fishing gear that is at fault is somewhat difficult to ascertain and, though identifiable in some cases, it represents only a subsection of the total confirmed cases. A majority of the large whale entanglement cases from NOAA for the West Coast were caused by an unidentifiable source (Saez et al., 2020), and since standardization in reporting is difficult, a flexible approach is necessary in developing a predictive model. The uncertainties associated with the reported data collected suggests that probabilistic risk-based methods could prove useful in gaining more insight into this complex problem, since they are well suited for dealing with stochastic systems in which the precise relationships between components of a system cannot be quantitatively modeled (Haldar and Mahadevan, 2000). Many circumstances exist where data is available but creating meaningful interpretations of the data can be quite difficult. Thus, creating a model that can be used to estimate the probability of a specified event occurring, described by favorable or unfavorable outcomes, is valuable. This is because the probability concepts used to develop the model remain valid regardless of the quality and extensiveness of the available data (Ang and Tang, 2007). A method to quantify the threat of marine debris to large species of marine mammals that allows for the estimation and incorporation of regional risk quantities is presented.

The general iterative approach used in this study that incorporates reported data and the continual refinement of the risk-based predictive model is conceptualized in Figure 5.1. Focusing on a topic of interest leads to the review of published literature and allows for the identification of key parameters. After extracting and organizing the relevant data, it is then converted into estimates of probabilistic information needed as input for the risk model. As additional data is discovered the predictive model can be improved and updated along with new ideas that might improve the visual interpretation and predictive capabilities of the model. Illustrative examples are developed using data available for the US North Atlantic coastline, which includes Maine, New Hampshire, Massachusetts, Rhode Island, and Connecticut, and the Pacific coastline that includes Washington, Oregon, and California revealing the increasing complexity and capability of the risk-based model approach. The ability to explore patterns and scenarios using graphical visualization is used to illustrate the potential of this modelling approach.

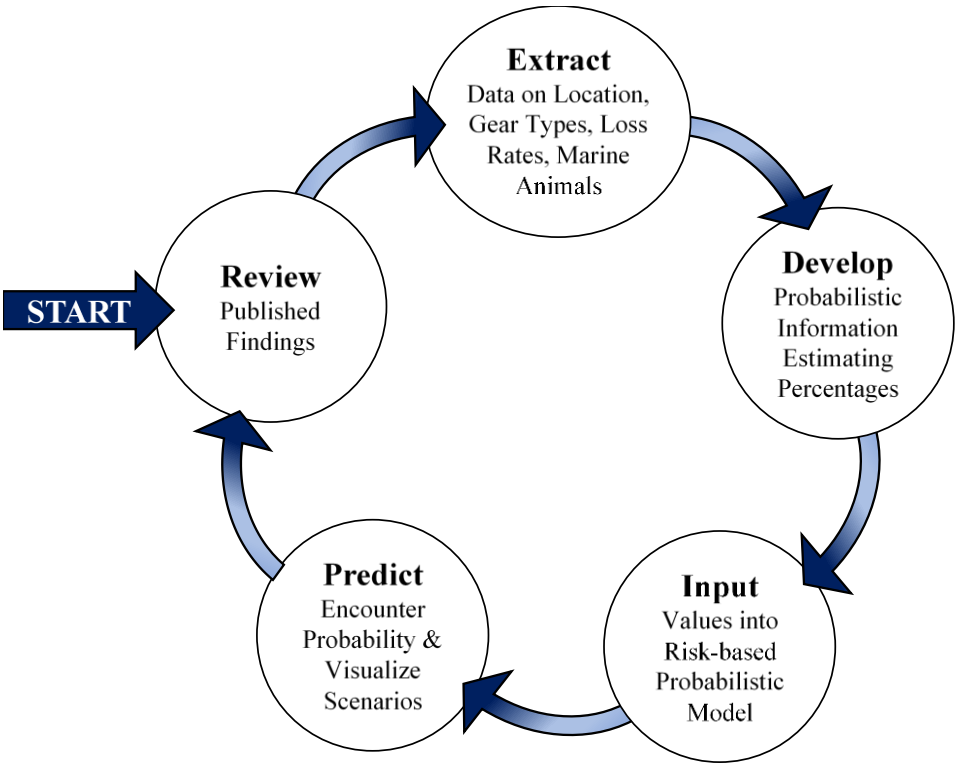

Figure 5.1 General iterative template for the continued improvement of risk assessment predictions. Reprinted with permission from Brown and Niedzwecki (2020).

5.2. Development of the Risk Model

An effective way to organize a risk model is to utilize fault trees. This organizational structure provides a logical interpretive structure for supporting a top event using sub-events, that is, basic elements that cause the top event to occur (Lee et al, 1985; Haldar and Mahadevan, 2000; Aven, 2008). This approach is ideal for targeting specific features of a subject that can be improved as new information becomes available and can also lead to the introduction of additional sub-events to improve the model predictions. In this study the top event is the entanglement of whales by fishing gear and assessing the likelihood of it occurring. The intersection of the sub-events, calculated as the product of

probabilities assuming independence between sub-events, leads to the occurrence of the top event. The regional sub-events addressed here reflect the type of fishing gear introduced into the environment, and its potential to entangle marine life in the vicinity.

The various sub-events identified are assigned numerical values tied to the data available. A fishing gear type that can result in entanglement is viewed as a combination of the proportions of gear types that are used in the region and the types of gear that have been observed to cause entanglements. The presence of whales in the region is subject to information on their migration patterns and its overlap with seasonal commercial fishing locations. Another important factor is the proportion of regional fishing gear that is lost annually or over some specified time scale. Data pertaining to these particular sub-events was collected and grouped based on the specific regional data as reported in the open literature.

The probability of the top event occurring is calculated as the intersection of the independent sub-events, and therefore, the product of the individual probabilities. These sub-events are the location overlap, fishing gear loss rates, and fishing gear type. It is assumed that the contribution of each gear type used in the region to the entanglement of marine animals is a disjoint event, therefore each gear type can therefore be considered separately. In this formulation it is assumed that there is no overlap between gear types, so the union of events is their summation without the intersection terms. Thus, the probability of encountering a specific fishing gear type i that will cause entanglement can be expressed as

$$\begin{aligned} \mathrm{P}(\textit{Encounter for Gear type } i) &= \mathrm{P}(\textit{Location}) \times \mathrm{P}(\textit{Gear Loss for type } i) \\ &\quad \times \mathrm{P}(\textit{Gear Type } i) \end{aligned} \tag{5.1}$$

$$= \lambda \times (\gamma_i \, \beta_i \, w_i) \tag{5.2}$$

where, the symbol × is used to indicate multiplication between scalar values, λ is the probability of marine life in the location, γ_i is the probability of gear loss for gear type *i*, and the product of β_i and w_i are the weighted probability of gear type *i*. For a particular location and set of data, it is necessary to consider the types of gear that have historically been the cause of entanglements in whales and how heavily that particular type of gear is used by the fishing industry in that region. The value of β_i is the percent usage of gear type *i* by the region's fishing industry and w_i is a weighting assigned based on the historical entanglement cases. Specific details identifying the domains of these variables are provided in Table 5.1.

Table 5.1 Descriptions of variables associated with the sub-events for the whale entanglement risk-based model. Reprinted with permission from Brown and Niedzwecki (2020).

Basic Event	Sym.	Description	Restrictions
P(*Location*)	λ	The probability that the fishing gear and marine animals are inhabiting the same space	[0,1]
	n	Number of gear types being considered	≥ 1
P(*Gear Loss*)	γ_i	The probability that gear type *i* is lost/mishandled	[0,1]
P(*Type*) = $\beta_i w_i$	β_i	The percent usage of gear type *i* in the region by the fishing industry. Assigned based on proportions of the all the types of gear used in the region, so must sum to 100%.	[0,1]
			$\sum_i^n \beta_i = 1$
	w_i	Weighting assigned based on culprits of previous entanglement cases in the region. Assigned based on proportion entanglements attributed to gear type *i* out of total number of cases.	[0,1]
			$\sum_i^n w_i = 1$

Then, for N fishing gear types, the probability of encountering and causing entanglement from fishing gear in the region is:

$$\mathrm{P}(\textit{Encounter}) = \lambda \times \left[\sum_{i=1}^{N} \gamma_i \beta_i w_i \right] \tag{5.3}$$

The product between the resulting probability with the total amount of gear deployed provides a means to estimate the amount of gear that will potentially have negative encounters with marine mammals. The complement of this probability provides the

amount of fishing gear that will not have negative encounters because it is properly removed, retrieved, out of range, or not an entangling type of gear.

5.3. Annual Multi-Year Fishing Gear Entanglements

Not all the fishing gear that is accidentally or intentionally lost at sea is available for entanglement of large whales. Thus, the predictive model should account for the percentage of gear that is removed by nature or other means. Of particular interest is the ability of the model to consider annual or multi-year scenarios which can account for accumulation of fishing gear. Eqn. 5.3 can be modified by introducing a debris removal rate of r_j for each year reflecting, for example, removal of fishing gear through clean-up efforts or fishing gear that has settled to where it no longer poses a risk of entanglement for the whales. Then, the contribution for Year j can be expressed as

$$P_j(Encounter) = \left(1 - r_j\right) \times \lambda_j \left[\sum_{i=1}^{N} \gamma_{ij}\, \beta_{ij}\, w_{ij}\right]_j \tag{5.4}$$

where, the term $(1 - r_j)$ represents the fishing gear that remains after removal. When determining the accumulation over a series of years, it is important to remember that the contributions of each year act as disjoint events and are additive, that is, the amount of fishing gear lost in the current or previous years does not change the amount lost in subsequent years. It is also true that what is lost in a previous year has the possibility of being removed during a subsequent year, so the fishing gear removal rate can vary and

affect multiple year events. Then, the probability of encounter for a sequence of *M* years can be expressed as

$$P_M(Encounter) = \sum_{j}^{M} \left\{ \left[\prod_{m=M}^{j} (1 - r_m) \right] \times \lambda_j \left[\sum_{i=1}^{N_j} \gamma_{ij} \beta_{ij} w_{ij} \right] \right\} \tag{5.5}$$

where r_m is the removal rate representing the percentage of gear removed in Year *m* and the product operates in reverse, counting down from *M* to *j*. The resulting equation is a stacked relationship between the current year being examined and the previous years.

To illustrate the single and multiple year estimates consider the following examples. For a single year, $M = 1$, a numerical estimate can be obtained using Eqn. 5.4. For a two-year sequence, $M = 2$, a numerical estimate can be made by expanding Eqn. 5.5, resulting in the following equation

$$\begin{aligned} P_2(Encounter) = & \left\{ (1 - r_2)(1 - r_1) \lambda_1 \left[\sum_{i=1}^{N_1} \gamma_{i1} \beta_{i1} w_{i1} \right] \right\}_{j=1} \\ & + \left\{ (1 - r_2) \lambda_2 \left[\sum_{i=1}^{N_2} \gamma_{i2} \beta_{i2} w_{i2} \right] \right\}_{j=2} \end{aligned} \tag{5.6}$$

If one is combining datasets from multiple regions, then the multi-year and multi-regional risk-based model for entanglement of whales for a variety of types of fishing gear becomes

P(*Encounter for Q Regions*)

$$= \sum_{k=1}^{Q} \left(\frac{1}{M_k} \cdot \sum_{j=1}^{M_k} \left\{ \left[\prod_{m=M_k}^{j} (1 - r_{mk}) \right] \times \lambda_{jk} \left[\sum_{i=1}^{N_j} \gamma_{ijk} \beta_{ijk} w_{ijk} \right] \right\} \right) \qquad (5.7)$$

where, Q is the number of regions being considered, M_k is the amount of time spanning the dataset for region k, and r_{mk} is the removal rate specified in time and space. The variables λ_{jk}, γ_{ijk}, β_{ijk}, and w_{ijk} have an added index to allow for specifications based in time and space.

If the data allows, the model can be further advanced by adding a spatial condition based on the region of interest and possibly time that examines the spatial overlaps between whale migration routes and regional fishery locations. Then,

P(*Encounter for Q Regions*)

$$= \sum_{k=1}^{Q} \left(\frac{1}{M_k} \cdot \sum_{j=1}^{M_k} \left\{ \left[\prod_{m=M_k}^{j} (1 - r_{mk}) \right] \times \psi_{jk} \lambda_{jk} \left[\sum_{i=1}^{N_{jk}} \gamma_{ijk} \beta_{ijk} w_{ijk} \right] \right\} \right) \qquad (5.8)$$

where ψ_{jk} is the spatial overlap that can be specified in time and space.

Macfadyen et al. (2009) specifically recommends addressing abandoned, lost or otherwise discarded fishing gear using preventative, mitigative, or curative measures. The derived equation provides the flexibility to account for efforts made in each of these categories by allowing parameters to incorporate the rate of gear loss, the ramifications of using certain types of gear without innovation or modifications, and gear removal efforts.

5.4. US North Atlantic and Pacific Coastline Data Sets

5.4.1. Assessing λ Values for the P(Location)

Based on the availability of data, P(Location) is treated as a temporal condition based on the migrations of whales. Whales participate in seasonal migrations each year due for breeding and feeding. Whale tracking is commonly used not only for tourism purposes, but also to alert the shipping industry because collisions with large ships are an additional threat to marine mammal populations (Waters, 2016). Based on data from whale watching sites it is estimated that whales spend about half the year consistently in the New England and Pacific regions (Discover New England, n.d.; Visit California, 2019). A majority of reports reference the entanglement of gray, right, and humpback whales (Johnson et al, 2005; Saez et al., 2020). Right whales are found along the North Eastern Seaboard of the United States in the spring and summer months where they migrate to feed. In the fall and winter months they travel southward for feeding; this is also typically when the calving occurs (Waters, 2016). If whales spend half of the year in a region, then a value of $\lambda = 0.5$ can be assumed.

5.4.2. Assessing γ Values for the P(Gear Loss)

Richardson et al (2019) used meta-analysis to compile information from published data on abandoned, lost or otherwise discarded fishing gear reported in different time scales as percentages, proportions, lengths, or weights from 1950 to May 2018, and then estimated the global gear loss rates by gear type. These values are listed in Table 5.2 and are used to develop an average value for γ for the model predictions, as the actual loss rates are unknown.

Table 5.2 Global estimates of fishing gear loss rates by gear type (Richardson et al., 2019). Reprinted with permission from Brown and Niedzwecki (2020).

Gear Type	Percentage (γ_i)
All Traps	8.6%
Pots/Traps	19%
Fyke Nets	4.1%
Pound Nets	2.6%
All Nets	5.7%
Gillnets and Entangling Nets	5.8%
Miscellaneous Nets	1.2%
Purse Seine Net fragments	6.6%
Seine Net fragments	2.3%
Trawl Net fragments	12%
All Lines	29%
Handlines	23%
Pole-lines	65%
Longlines	20%
Trolling lines	22%

5.4.3. Assessing β and w Values for the P(Type)

The quantity β is used to represent the percent usage of a particular fishing gear type in a specific region. This value would be best described using regional data on yearly gear deployments, but since exact data is unavailable, the value of β is estimated from the fish landing proportions in each region. Chuenpagdee et al. (2003) and Morgan and Chuenpagdee (2003) only provide information on the top 4 fishing gear types by weight, which are listed in Table 5.3 for each Fishery Management Council region. The states which comprise each Council are provided in Table 5.4. In the New England Region pots/traps make up 15% of the industry, dredges are 7%, bottom and midwater trawl nets combine for 59%, and the remaining 19% is comprised of other types of gear. In the Pacific Region pots/traps make up 4% of the industry, purse seine nets are 48%, bottom and midwater trawl nets combine for 31%, and the remaining 17% is comprised of other types of gear.

Table 5.3 Fish landing proportions by gear type (by weight) for Fishery Management Council Regions (Chuenpagdee et al., 2003; Morgan and Chuenpagdee, 2003). Modified with permission from Brown and Niedzwecki (2020).

Type (*bottom and midwater combined, ** bottom and pelagic combined)	**Percentage (β_i)**
New England	
Pots and Traps	15%
Dredges	7%
*Trawl nets	59%
Other (*Gillnets, Hooks and lines, **Longlines, Purse seine)	19%
Pacific	
Pots and Traps	4%
Purse Seine	48%
*Trawl nets	31%
Other (*Gillnets, Hooks and lines, **Longlines, Dredges)	17%
Mid-Atlantic	
Dredges	14%
Pots and traps	8%
Purse seine	60%
Trawl - bottom	6%
Other (*Gillnets, Hooks and lines, **Longlines, Trawl-midwater)	12%
South Atlantic	
Hooks and lines	5%
Pots and traps	23%
Purse seine	29%
Trawl-bottom	20%
Other (Dredges, *Gillnets, **Longlines, Trawl-midwater)	23%
Gulf of Mexico	
Pots and traps	4%
Purse seine	73%
*Trawl nets	16%
Other (Dredges, *Gillnets, Hooks and lines, **Longlines)	7%
North Pacific	
Gillnet-midwater	7%
Purse seine	16%
*Trawl nets	68%
Other (Dredges, Gillnet-bottom, Hooks and lines, **Longlines, Pots and traps)	9%
West Pacific	
Gillnet-bottom	1%
Hooks and lines	32%
Longline-pelagic	63%
Purse seine	3%
Other (Dredges, Gillnet-midwater, Longline-bottom, Pots and traps, *Trawl nets)	1%

Table 5.4 U. S. Regional Fishery Management Councils by Region (U.S. Regional Fishery Management Councils, n.d.)

Region	Description
North Pacific	Alaska, (Gulf of Alaska, Bering Sea, and Aleutian Islands)
Western Pacific	Hawai'i, Guam, American Samoa, Commonwealth of the Northern Mariana Islands, and eight remote islands
Pacific	Washington, Oregon, California
New England	Maine, New Hampshire, Massachusetts, Rhode Island, and Connecticut
Mid-Atlantic	New York, New Jersey, Pennsylvania, Delaware, Maryland, Virginia and North Carolina
South Atlantic	North Carolina, South Carolina, Georgia and east Florida to Key West
Gulf of Mexico	Louisiana, Mississippi, Alabama, Texas, and the west coast of Florida.
Caribbean	Puerto Rico, United States Virgin Islands

The quantity *w* is a weighting value that accounts for how likely a particular type of gear is to cause an entanglement. This value considers available data on reported entanglement cases in the region and the proportion of cases attributed to the gear type. For the New England Region, Johnson et al. (2005) conducted a study on the entanglement of right and humpback whales in the western North Atlantic Ocean between the years 1994 and 2002. Fishing gear involved in the entanglements were documented by the gear type, but the specific year associated with each case was not provided. A total of 61 cases were examined, but unfortunately the gear type could only be identified or recovered in 45 of those cases. The four categories of fishing gear considered were pots and traps, gillnets, other, and unknown. Considering only the 36 cases where the gear type was identifiable, 89% (32 of 36) of the gear identified in the entanglement cases were attributed

to pots and traps and gillnets. Of the 36 identifiable cases, 52.8% (19 of 36) were identified as entanglement with pots and traps, 36.1% (13 of 36) were attributed to gillnets, and 11.1% (4 of 36) were categorized as other.

For the Pacific Region, the West Coast Whale Entanglement Summaries from the US Dept of Commerce, the National Oceanic & Atmospheric Administration (NOAA), and the National Marine Fisheries Service (NMFS) were utilized to identify whale entanglement cases. In 2015 there were a total of 18 entanglement cases reported, with 13 (72.2%) attributed to pot and trap fisheries and the remaining to gillnet fisheries (NOAA Fisheries, 2019). In the subsequent years the total number of cases were twenty-nine, fourteen, and twenty-four respectively with 27 of 29 (93.1%), 10 of 14 (71.4%), and 17 of 24 (70.8%) associated with pot and trap fisheries and the remaining to gillnet fisheries. These percentages were based only on the identifiable cases, which represent only a portion of the total confirmed entanglement cases.

5.5. Example: New England Region Multi-Year Average Estimate

For the New England Region, the data used to determine the weighting, w, for whale entanglements spans from 1994 to 2002, but as previously noted is not broken down specifically by year. As a result, it is used as a single data set to perform calculations. The gear types can be isolated into the categories of pots and traps, gillnets, and other, and results a value of $N = 3$. Since only one set of data is available, Eqn. 5.3 is used for this example. The assignment of values for γ_i, β_i, and w_i are from Table 5.5 and the value of λ was selected as 0.5. The gear loss rate for the category other is assumed to be 14.43% and

is calculated as the average of the loss rates of all traps (8.6%), all nets (5.7%), and all lines (29%). The exact usage rate of gillnets is unknown and must be assumed. A value of 6% was selected because it must be < 7% based on the information provided by Chuenpagdee et al. (2003) and Morgan and Chuenpagdee (2003). Substituting these values into Eqn. 5.3, an estimate of the probability of encounter, i.e., whale entanglement can be made. Specifically,

$$\mathrm{P}(\textit{Encounter}) = \lambda \times \left[\sum_{i=1}^{N=3} \gamma_i \beta_i w_i \right] \tag{5.9}$$

$$= 0.5\left[\gamma_1 \beta_1 w_1 + \gamma_2 \beta_2 w_2 + \gamma_3 \beta_3 w_3\right]$$

$$= 0.5\ [(0.19)(0.15)(0.528) + (0.058)(0.06)(0.361) + (0.1443)(0.79)(0.11)]$$

$$\approx 0.014 \rightarrow \boldsymbol{1.4\%}$$

The interpretation of this result is that for the New England Region, approximately **1.4%** of gear deployed in a year will be available for negative encounters (entanglement) with whales. Hypothetically, say, if 100,000 units of gear are deployed off the New England Coast, then approximately 1,400 units of gear would be available for the entanglement of whales. From the 1.4% pots and traps contribute approximately 0.75%, gillnets contribute approximately 0.06%, and other types contribute approximately 0.63%. When fishing gear is abandoned, lost or otherwise discarded it is subject to transport by

storms, offshore currents, or other factors that will reduce this estimate by establishing a removal rate, as introduced in Eqn. 5.4.

Table 5.5 Assignment of values for the New England Region, used in Example 1. Reprinted with permission from Brown and Niedzwecki (2020).

i	Gear Loss (γ_i) (Table 5.2)	Gear Usage (β_i) (Table 5.3)	Weighting (w_i)
1 = Pots and Traps	γ_1 = 19%	β_1 = 15%	w_1 = 52.8%
2 = Gillnets	γ_2 = 5.8%	β_2 = 6% *assumption, < 7%	w_2 = 36.1%
3 = Other	γ_3 = 14.43% *assumption, avg	β_3 = 79%	w_3 = 11.1%

5.6. Example: Pacific Region Multi-Year Estimate

For the Pacific Region it is possible to illustrate multi-year predictions for the entanglement of whales because the data provided for determining the weighting, w, is provided yearly from 2015 to 2018. This data spans a sequence of 4 years, thus $M = 4$ in Eqn. 5.5. The gear types for each year can be isolated into the categories of pots and traps, gillnets, and other, making $N_j = 3$. Because the value of N_j is the same for all 4 years N_j becomes $N = 3$ for each year.

Assuming that γ_{ij}, β_{ij}, and λ_j are held constant annually, and that no fishing gear is removed from the region from year to year so that $r_j = 0$, only the weighting, w_{ij}, differs annually. A summary for the assignment of values is available in Table 5.6. As a result of these assignments, the product is equal to 1 and the j summation can be moved inside to obtain:

$$P_{M=4}(Encounter) = \sum_{j=1}^{M=4} \left\{ (1) \times \lambda_j \left[\sum_{i=1}^{N_j} \gamma_{ij} \beta_{ij} w_{ij} \right] \right\} \qquad (5.10)$$

$$= \lambda \times \left[\sum_{i=1}^{N=3} \left(\gamma_i \beta_i \sum_{j=1}^{M=4} w_{ij} \right) \right]$$

Table 5.7 provides guidance for completing the summation used for this example. The probability of encounter, i.e., whale entanglement, is estimated to be $P \approx 0.012 =$ ***1.2%***. The interpretation of this value is that for the Pacific Region approximately **1.2%** of gear deployed from 2015 to 2018 will be available for negative encounters (entanglement) with whales. Again, hypothetically if 100,000 units of gear are deployed per year on the West Coast, then approximately 4,800 units of gear will be available for the entanglement of whales over the 4-year period.

Table 5.6 Assignment of values for the Pacific Region, used in Example 2. Reprinted with permission from Brown and Niedzwecki (2020).

j	r_j	n_j	i	Gear Loss (γ_{ij}) (Table 2)	Gear Usage (β_{ij}) (Table 3)	Weighting (w_{ij})
1 = 2015	r_1 = 0%	n_1 = 3	1 = Pots and Traps	γ_{11} = 19%	β_{11} = 4%	w_{11} = 72.2%
			2 = Gillnets	γ_{21} = 5.8%	β_{21} = 3%	w_{21} = 27.8%
			3 = Other	γ_{31} = 14.43%	β_{31} = 93%	w_{31} = 0.0%
2 = 2016	r_2 = 0%	n_2 = 3	1 = Pots and Traps	γ_{12} = 19%	β_{12} = 4%	w_{12} = 93.1%
			2 = Gillnets	γ_{22} = 5.8%	β_{22} = 3%	w_{22} = 6.9%
			3 = Other	γ_{32} = 14.43%	β_{32} = 93%	w_{32} = 0.0%
3 = 2017	r_3 = 0%	n_3 = 3	1 = Pots and Traps	γ_{13} = 19%	β_{13} = 4%	w_{13} = 71.4%
			2 = Gillnets	γ_{23} = 5.8%	β_{23} = 3%	w_{23} = 28.6%
			3 = Other	γ_{33} = 14.43%	β_{33} = 93%	w_{33} = 0.0%
4 = 2018	r_4 = 0%	n_4 = 3	1 = Pots and Traps	γ_{14} = 19%	β_{14} = 4%	w_{14} = 70.8%
			2 = Gillnets	γ_{24} = 5.8%	β_{24} = 3%	w_{24} = 29.2%
			3 = Other	γ_{34} = 14.43%	β_{34} = 93%	w_{34} = 0.0%

Table 5.7 Solving Eqn. 5.5 using values assigned to the Pacific Region in Example 2. Reprinted with permission from Brown and Niedzwecki (2020).

i	$\lambda \gamma_i \beta_i$	j	w_{ij}	$\lambda \gamma_i \beta_i \cdot \sum_j^4 w_{ij}$
1	(0.5)(0.19)(0.04)	1	0.722	
		2	0.931	
		3	0.714	
		4	0.708	
	$\lambda \gamma_1 \beta_1$= 0.0038	$\sum w_{1j}$ = 3.075		0.012
2	(0.5)(0.058)(0.03)	1	0.278	
		2	0.069	
		3	0.286	
		4	0.292	
	$\lambda \gamma_2 \beta_2$= 0.00087	$\sum w_{2j}$ = 0.925		0.0008
3	(0.5)(0.1443)(0.93)	1	0	
		2	0	
		3	0	
		4	0	
	$\lambda \gamma_3 \beta_3$= 0.067	$\sum w_{3j}$ = 0		0
			Total Sum	1.2%

5.7. Example: Combining New England & Pacific Regions Data

Given the limited quantities of data available for analysis, it is reasonable to consider the combination of data from different geographic regions. For illustrative purposes, combining the data from the New England and Pacific Regions using Eqn. 5.7 results in a probability of encounter of **1.7%**. The interpretation is that for the combined New England and Pacific Regions approximately **1.7%** of gear deployed in a year will be available for negative encounters (entanglement) with whales. Then, for a hypothetical deployment rate of 100,000 units of gear per year, this means that approximately 1,700 units of gear available for entanglement. As noted previously, natural events can redistribute the debris and the rate of redistribution can be different for each region.

5.8. Visualization of Variability and Sensitivity

Recognizing the difficulties in consistently assessing the source and type of entanglement of large marine mammals as reflected in the data, the risk-model can be used to explore and gain insight into the resulting variability and sensitivity of the model predictions. Graphical visualization is an essential feature in understanding the numerical results and reflecting on what additional information might improve model predictions.

5.8.1. Variability

The variability of the basic risk model predictions to changes in data can initially be examined using Eqn. 5.3 and the resulting Figures 5.2 and 5.3. In order to facilitate the

interpretation, the number of variables and their range of variation is minimized. In particular, the number of fishing gear types is specified as $N = 3$ so that the values of the percent usage, β_i, and historical cases weighting, w_i, are restricted to planes. Variations in the gear type usage, β_i, weighting, w_i, location parameter, λ_i, or the gear loss rate, γ_i, result in linear changes in the final probability predictions. For these simulations the values $\lambda = 0.5$; $\beta_i = \{0.15, 0.05, 0.80\}$; $w_i = \{0.70, 0.25, 0.05\}$; and $\gamma_i = \{0.20, 0.06, 0.15\}$ were selected for consistency.

The figures are developed by selecting one variable to vary, while holding the others constant. This allows one to identify the influence of each variable on the risk model predictions. In Figure 5.2a, the gear usage, β_i, gives the percent usage for a given gear type. By varying this value along each axis, the effect of using different proportions of each gear type on the risk model predictions is revealed. Gear type $i = 1$, representing pots and traps, has the highest weighting and loss rate of the three gear categories. The weighting is defined as the proportion of documented cases in the open literature associated with a specified gear type, so having the highest weighting indicates that pots and traps are most likely to be at fault for causing entanglements, while having the highest loss rate indicates that they are most likely to be lost. Thus, in Figure 5.2a the value of β_1 has the most influence as it approaches a value of 1.0, and the increased usage of this gear type will quickly increase *P(Encounter)*. In Figure 5.2b, each axis corresponds to the weighting parameter for each of the three gear types. Gear type, $i = 3$, representing the category “other”, has the highest usage. This indicates that most of the gear used by the industry does not fall into the categories of pots and traps or gillnets. Thus, in Figure 5.2b,

w_3 has the most influence as it approaches a value of unity, and results in an increased risk of entanglement. The linear relationship between variables illustrated by these figures is intended to allow one to determine the gear types that are most at fault for whale entanglements based on documented instances and industry usage. This visualization is based on three categories, but should a new category emerge one would need to rethink the combinations of axes. This would result in additional graphs of this nature and perhaps a recombination of axes that would be used to better understand the relationships between the gear type categories.

Another possible visualization of the gear loss rates, γ_i, is presented in Figure 5.3. Here all the possible gear loss rates are restricted to vary within a cube of unit volume shown in Figure 5.3a. From Figure 5.3b it is easier make sense of this information in visualizing the *P(Encounter)* by considering horizontal slices through the cube space that correspond to a particular range of γ_1 and γ_2 values. Here the values of γ_3 = 0, 0.5, and 1.0 were selected. It can be deduced that the loss of pots and traps (γ_1) has the most control over the resulting estimate of *P(Encounter)*. This can be explained in view of the pots and traps ($i = 1$) having the largest weighting value. This high weighting indicates that pots and traps are the most at fault for causing entanglements of whales, so losing more of this type of gear would likely result in more encounters and a higher likelihood of entanglements.

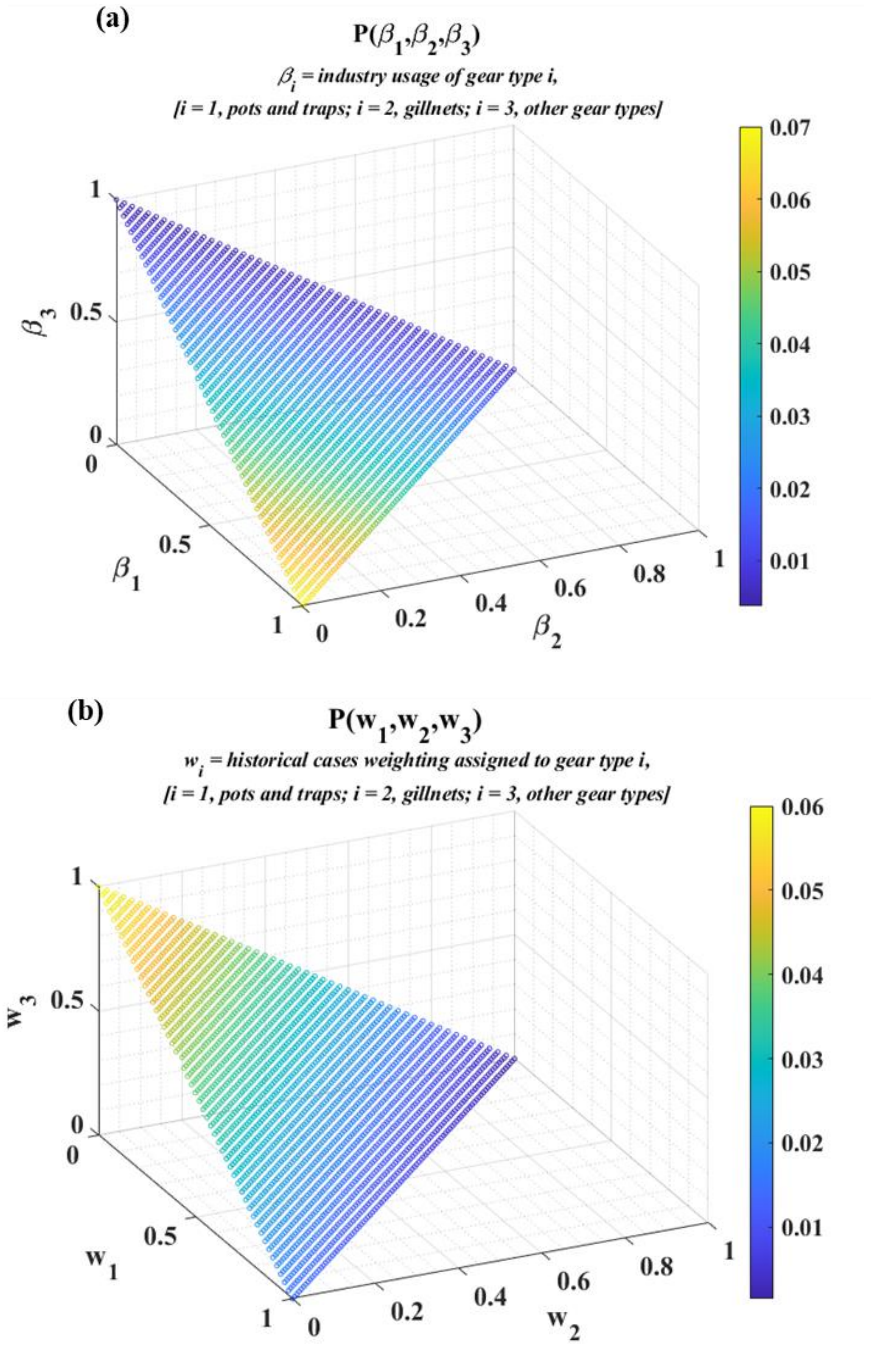

Figure 5.2 (a) The effect of industry gear usage by gear type, β_i, and (b) weighting assigned based on historical entanglement cases by gear type (w_i) on the Probability of Encounter, with gear types *1* = pots and traps, *2* = gillnets, *3* = other, and restrictions $\sum\beta_i = 1$ and $\sum w_i = 1$. Reprinted with permission from Brown and Niedzwecki (2020).

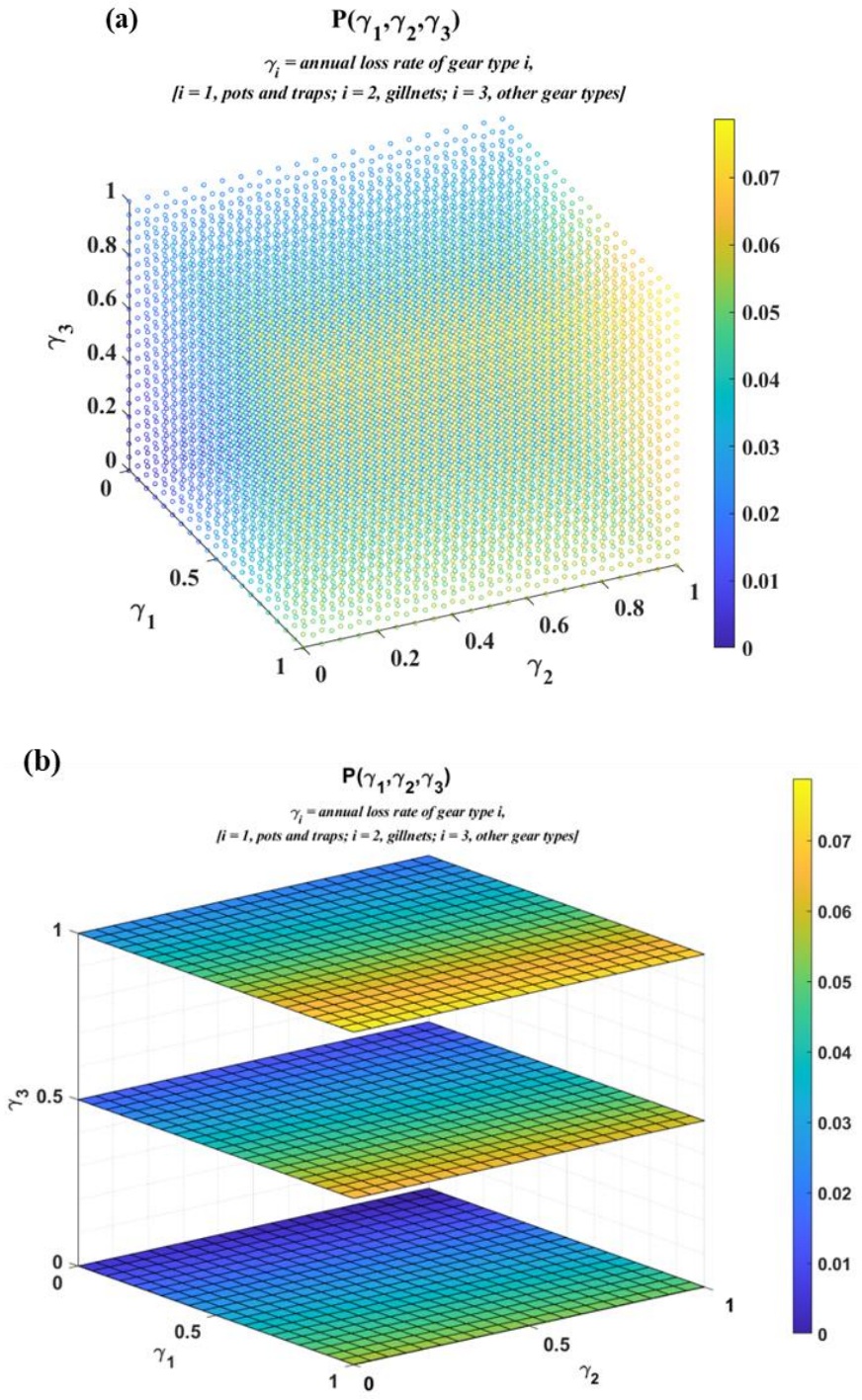

Figure 5.3 (a) The effect of gear loss rates by gear type, γ_i, on the Probability of Encounter, with γ_1 = pots and traps, γ_2 = gillnets, γ_3 = other types, and restriction $\gamma_i \in (0,1)$ and (b) sliced visualization of the Probability of Encounter with varying gear loss rates. Reprinted with permission from Brown and Niedzwecki (2020).

5.8.2. Sensitivity of Probabilistic Modeling Approach

The strength in developing a risk-based model is that, once it is established, one can explore the sensitivity of the predictions to various underlying assumptions and scenarios. Since the information is converted to probabilistic information, one can also examine the accuracy of the model predictions and can illustrate the need for improved data on specific variables. In addition, one can explore which parameters most influence on the model predictions, and then seek to improve information regarding those parameters. A series of relevant examples is presented next to illustrate this aspect.

First, we consider how $P_M(Encounter)$ based upon Eqn. 5.5 changes over a sequence of years for different values for the yearly removal rate, r_j. The base values for each of the parameters selected are assigned as $\beta_{ij} = \{0.15, 0.05, 0.80\}_{j=1,2,3}$; $w_{ij} = \{0.70, 0.25, 0.05\}_{j=1,2,3}$; $\gamma_{ij} = \{0.20, 0.06, 0.15\}_{j=1,2,3}$; and $\lambda_{j=1,2,3} = 0.5$. The two boundaries of the domain of r_i represent the cases of no lost fishing gear being removed in Year j ($r_i = 0$) and all lost fishing gear being removed in Year j ($r_i = 1$). In Figure 5.4 constant fishing gear removal each year is presented; if the fishing gear inputs remain constant, a plateau will be reached. Removing more gear annually than is input yearly ($r_i > 1$) is the only way to obtain a decrease mathematically and conceptually over time based on Eqn. 5.5.

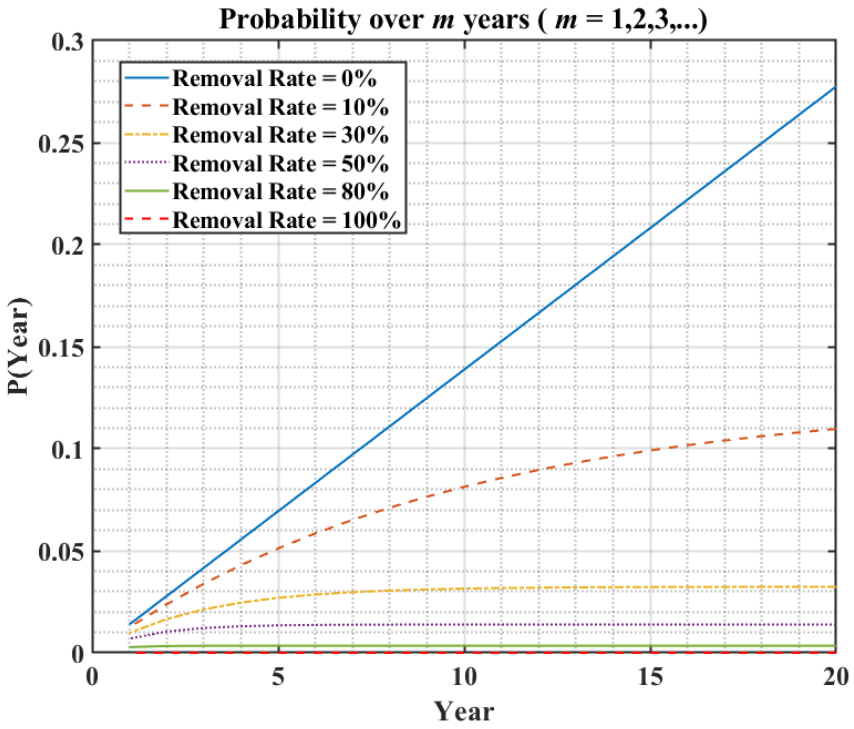

Figure 5.4 Probability of Encounter due to accumulation of gear over a period of years. Reprinted with permission from Brown and Niedzwecki (2020).

The true values of the assigned probabilities are likely unknown. In the examples presented thus far, discrete values were chosen for each sub-event based on the available data and then ranges of values were considered. As more data sets become available it becomes possible to describe each sub-event as a random variable using a probability distribution function. In instances where very limited or no data is available for a particular sub-event, one can consider a Bayesian way of thinking, where prior distributions are created and chosen based on one's beliefs. Then, selected distribution functions can act as a placeholder until evidence from collected data can later be interpreted and included in the model.

To demonstrate the incorporation of probability distributions, the removal rate is assumed to be a random variable that follows a truncated normal distribution in the interval [0,1] with mean, μ_R, and standard deviation, σ_R (Benjamin and Cornell 2014; Burkardt, 2014). The truncated normal distribution is selected because of the symmetry around the mean value. A truncated normal distribution with lower and upper truncation points of *a* and *b* respectively is described by

$$f(x;\mu,\sigma,a,b)=\begin{cases}\dfrac{\phi\left(\frac{x-\mu}{\sigma}\right)}{\Phi\left(\frac{b-\mu}{\sigma}\right)-\Phi\left(\frac{a-\mu}{\sigma}\right)} & , a\le x\le b \\ 0 & , \text{otherwise}\end{cases} \tag{5.11}$$

where μ and σ are the mean and standard deviation of the 'parent' normal distribution, and ϕ and Φ are the probability density and cumulative distribution functions of the 'parent' normal distribution (Burkardt, 2014).

The values of β_{ij}, w_{ij}, γ_{ij}, and λ_j are assumed to be discrete variables, where β_{ij} = $\{0.15, 0.05, 0.80\}_{j=1,2,3}$, w_{ij} = $\{0.70, 0.25, 0.05\}_{j=1,2,3}$, γ_{ij} = $\{0.20, 0.06, 0.15\}_{j=1,2,3}$, and $\lambda_{j=1,2,3}$ = 0.5. Samples were drawn from the truncated normal distribution describing the removal rate, *R*, with a specified mean value μ_R = 0.3 and a standard deviation σ_R = 0.1, that is, $R \sim N(0.3,0.1)$. Assuming a time span of 20 years, 100 independent samples were drawn from the distribution each year, for a total of 2000 samples. These values are presented in Figure 5.5a along with a normalized histogram in Figure 5.5b. The sampled

values from *R* were then used in Eqn. 5.5 to perform 100 simulations in order to estimate the P_M*(Encounter)* due to accumulation of fishing gear within a 20-year period.

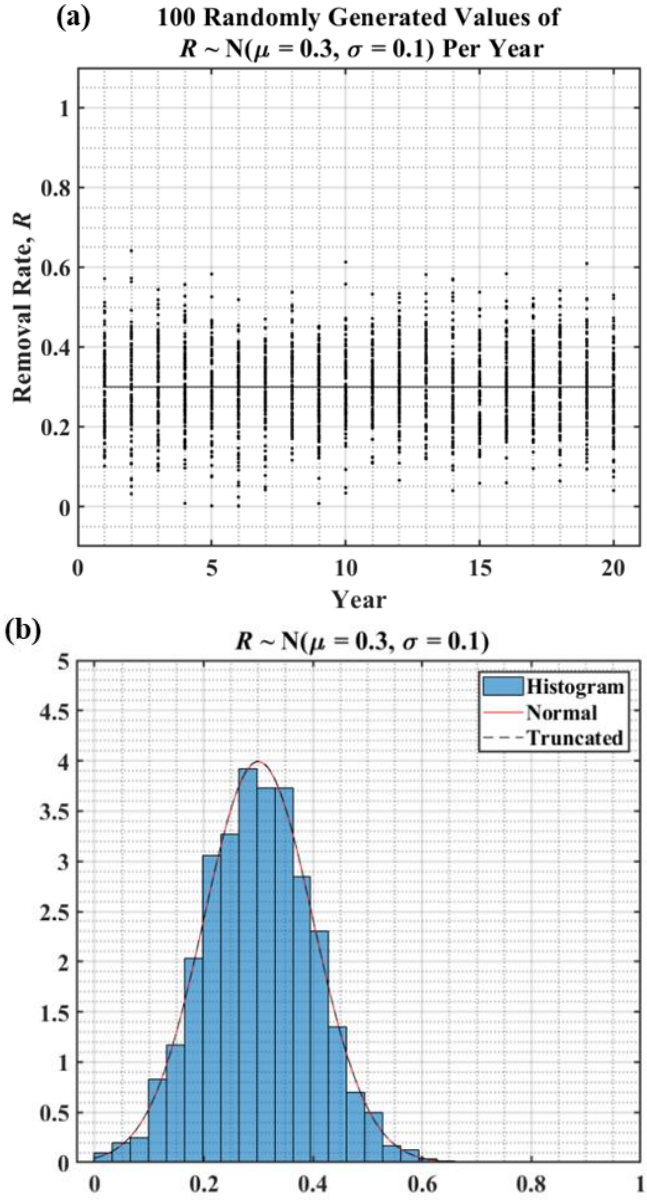

Figure 5.5 Modeling the removal rate using a truncated normal distribution (a) 100 samples drawn per year from *R ~ N(0.3,0.1)* for a span of 20 years, and (b) a normalized histogram of samples. Reprinted with permission from Brown and Niedzwecki (2020).

As time progresses the variability in the predicted results increases, as can be observed in Figure 5.6. This is due to the additive nature of Eqn. 5.5, in that the annual variability is affected by the uncertainty of previous years' predictions. It becomes possible to capture the variability of $P_M(Encounter)$ using probability distribution functions for each year, as seen with Year 10, $P_{M=10}(Encounter)$. Conducting the same analysis with different distributions to describe the removal rate, $R \sim N(\mu_R, \sigma_R)$, results in different estimates of $P(Encounter)$. Figures 5.7a, 5.7b, and 5.7c demonstrate that the final $P(Encounter)$ is highly dependent on the standard deviation assigned to the distribution of the removal rate, which is contingent on how strongly it is believed that the removal rate follows the assumed distribution function. As the standard deviation is increased, the probability distribution for the random variable R is shown in Figure 5.7c to approach that of a uniform distribution.

The mean and standard deviation of the removal rate are varied and illustrated in Figures 5.8a and 5.8b. This illustrates how parameters of a selected distribution function can be used to better reflect the information available. Smaller standard deviations can be used to reflect higher accuracy and confidence in the data. It can be observed for lower values of the standard deviation in Figure 5.8b that the $P(Encounter)$ hovers closer to the exact solutions calculated by treating the variables as discrete valued variables.

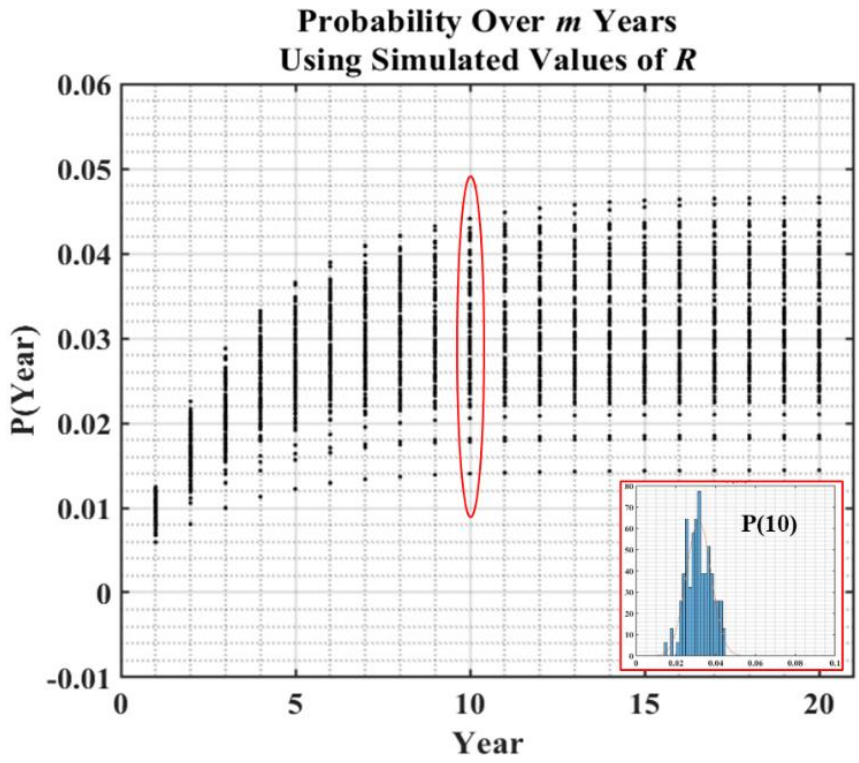

Figure 5.6 The variation of the Probability of Encounter over *m* years using removal rate values sampled from *R ~ N(0.3,0.1)* (truncated normal), with a focus on Year 10, where P(10) = $P_{(M = 10)}$(Encounter). Reprinted with permission from Brown and Niedzwecki (2020).

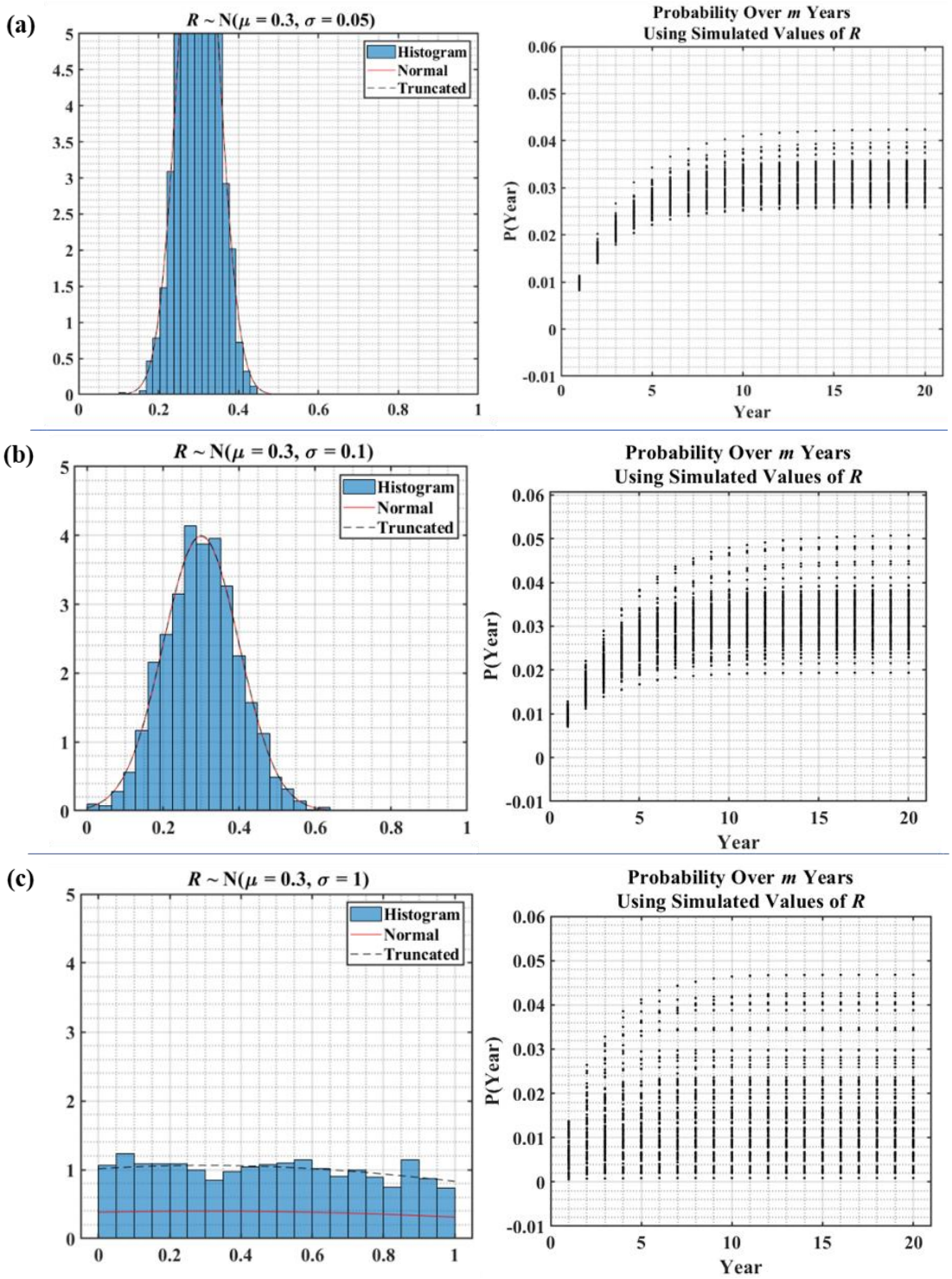

Figure 5.7 Simulations of calculating the Probability of Encounter due to accumulation of gear over *m* years; removal rate values are sampled from *R ~ N(0.3,σ)* (truncated normal) using standard deviations of (a) *σ = 0.05*, (b) *σ = 0.1*, and (c) *σ = 1.0*. Reprinted with permission from Brown and Niedzwecki (2020).

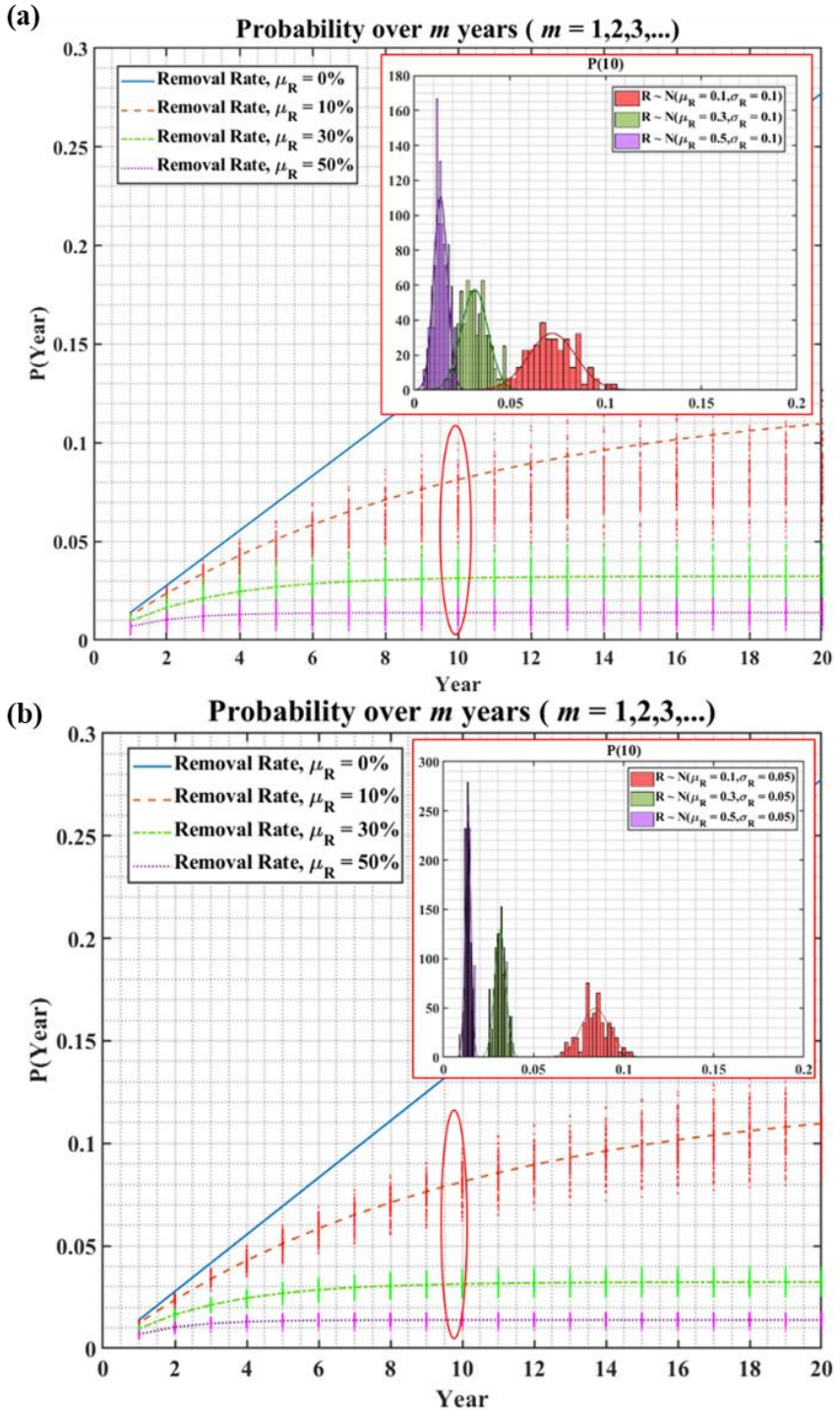

Figure 5.8 *P(Encounter)* over m years using removal rate values sampled from (a) *R ~ N(0.1,0.1)* , *R ~ N(0.3,0.1)*, and *R ~ N(0.5,0.1)* (truncated normal) and (b) from *R ~ N(0.1,0.05)* , *R ~ N(0.3,0.05)* , and *R ~ N(0.5,0.05)* (truncated normal), including distributions for Year 10, where *P(10) = $P_{(M = 10)}$(Encounter)*. Reprinted with permission from Brown and Niedzwecki (2020).

This indicates the need to check the relationship between the parameters used in the distribution function representing the removal rate and the resulting sensitivity in estimating the probability of encounter. In order to understand how the parameter selection used to describe the removal rate affects the estimates of *P(Encounter)*, the parameters of each distribution were plotted against each other for $P_{M = 10}$*(Encounter)* in Figures 5.9a and 5.9b. In Figure 5.9a, as the mean removal rate is increased, i.e. a higher portion of fishing gear is removed from the region, there is a decrease in the mean of *P(Encounter)* for each standard deviation assigned to the removal rate. In general, as the mean removal rate is increased there is seen to be less dependence on the standard deviation of the removal rate. Skewness and heavy tails for the truncated distribution led to more spread in the mean of *P(Encounter)* for lower values of the μ_R. The minimal spread occurs at a mean of $\mu_R = 0.5$, where the distribution for the removal rate becomes symmetric. In Figure 5.9b, the sensitivity of the standard deviations for *P(Encounter)* shows that as the standard deviation of the underlying distribution is increased, the values converge to an uninformative distribution. This is equivalent to knowing less information about the behavior of the random variable as would be reflected by the selection of a uniform distribution.

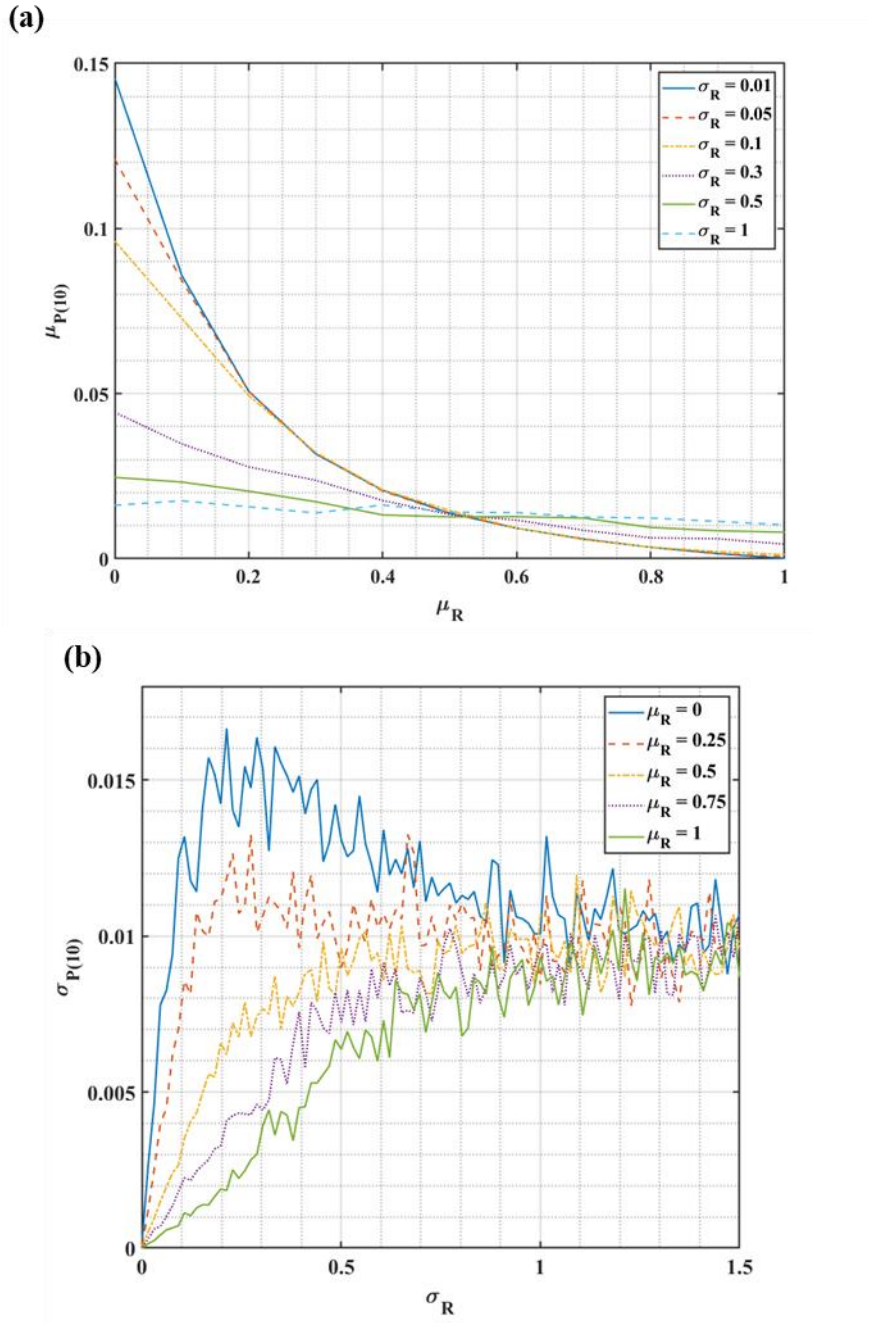

Figure 5.9 Variation of the means and standard deviations for the *P(Encounter)* in Year 10, $P(10) \sim N(\mu_{P(10)}, \sigma_{P(10)})$, using simulations of the Removal Rate, $R \sim N(\mu_R, \sigma_R)$ (truncated normal); (a) mean assessment and (b) standard deviation assessment. Reprinted with permission from Brown and Niedzwecki (2020).

Next, we consider fishing gear loss rates, γ_i, for each of the three categories of gear (pot and traps, gillnets, and other) where each are assumed to be random variables. Here it is assumed that each fishing gear type can be modeled as truncated normal distributions; $\gamma_1 \sim N(0.2,\sigma_{\gamma_1})$, $\gamma_2 \sim N(0.06,\sigma_{\gamma_2})$, and $\gamma_3 \sim N(0.15,\sigma_{\gamma_3})$. Gear loss for pots and traps was isolated by sampling from its distribution using different parameter values to directly determine its effect on *P(Encounter)* in Figures 5.10a and 5.10b. As the standard deviation is decreased from 0.5 in Figure 5.10a to 0.1 in Figure 5.10b, the three cases are shown to separate.

In order to better visualize the effects of the distribution for the gear loss rate of pots and traps, $\gamma_1 \sim N(\mu_{\gamma_1},\sigma_{\gamma_1})$, on the estimates of *P(Encounter)*, the parameters of each were plotted against each other as illustrated in Figures 5.11a and 5.11b. In Figure 5.11a, increasing the mean loss rate results in a subsequent increase in *P(Encounter)*. In Figure 5.11b the standard deviation of *P(Encounter)* increases with the standard deviation of the loss rate. As seen previously when the removal rate was treated as a random variable, the standard deviation of *P(Encounter)* begins to converge as the loss rate distribution function approaches to an uninformative uniform distribution function.

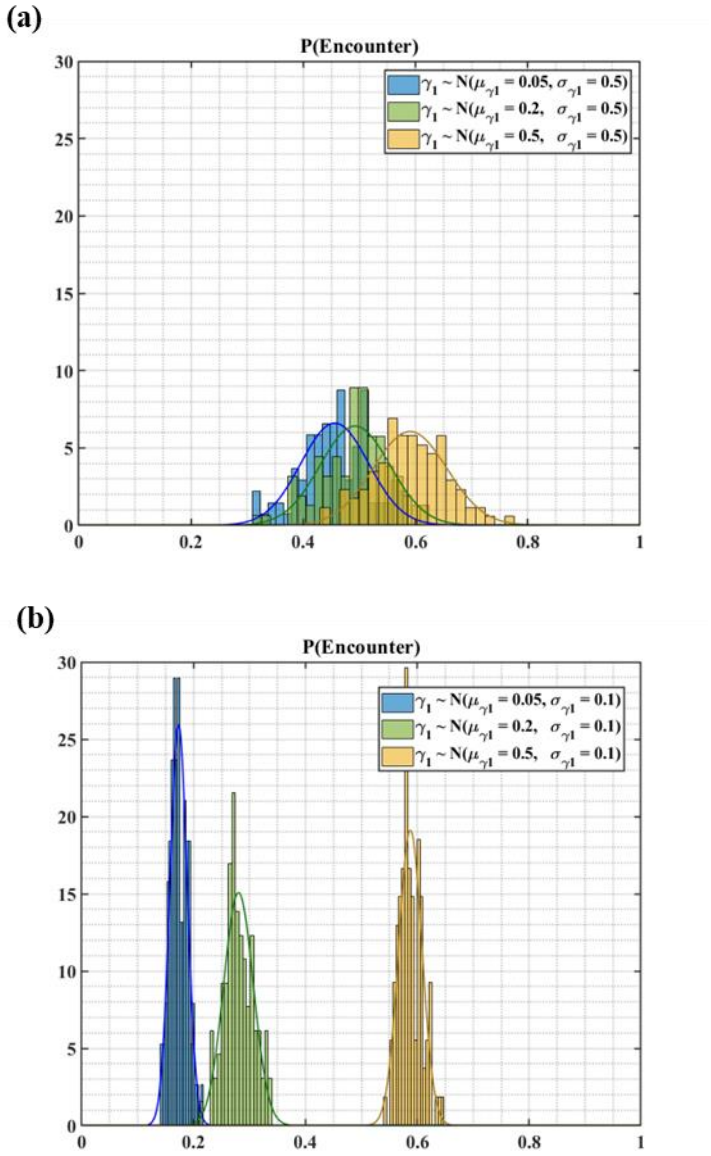

Figure 5.10 Distributions of *P(Encounter)* for differing sampling distributions for the loss rate of gear type 1 (γ_1; pots and traps); (a) $\sigma_{\gamma 1} = 0.5$ and (b) $\sigma_{\gamma 1} = 0.1$. Reprinted with permission from Brown and Niedzwecki (2020).

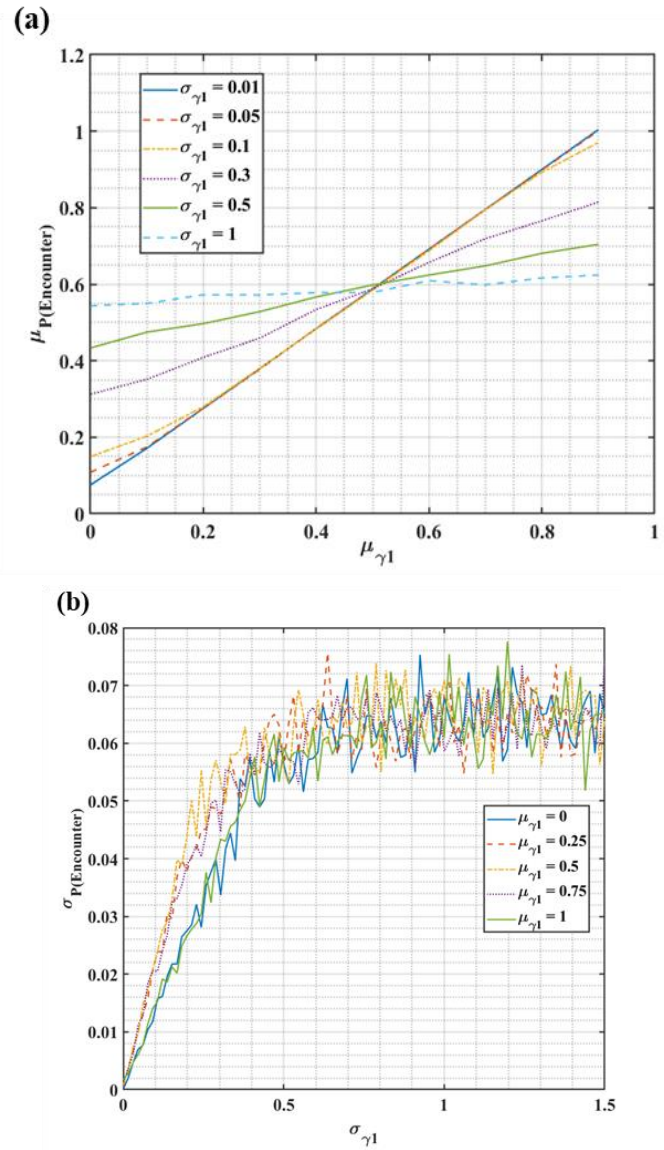

Figure 5.11 Variation of the means and standard deviations for the *P(Encounter)* ~ $N(\mu_{P(Encounter)}, \sigma_{P(Encounter)})$, using gear loss simulations of $\gamma_1 \sim N(\mu_{\gamma 1}, \sigma_{\gamma 1})$ (truncated normal) (a) mean assessment and (b) standard deviation assessment. Reprinted with permission from Brown and Niedzwecki (2020).

This insight can be utilized when revisiting the earlier Examples 1 and 2 by interpreting the values presented in Tables 5.5 and 5.6 as the mean values for the random variable γ_i and treating the other variables as deterministic values. The parameters for the

estimated distributions of *P(Encounter)* and $P_{M=4}$*(Encounter)* are given by Table 5.8 for different assigned standard deviations of γ_i. The alignment of these predictions with the results from Examples 1 and 2 illustrates that when there is more confidence in assigning distribution parameters, there is better alignment between results using random variables versus a deterministic approach.

Table 5.8 Evaluation of distribution parameters for P(Encounter) using data from the New England and Pacific Regions. Reprinted with permission from Brown and Niedzwecki (2020).

Standard Deviation for Gear Loss	Parameters of *P(Encounter)*
Example 1 – New England Region (Table 5.5)	
$\sigma_{\gamma i} = 0.01$	$\mu_P = 0.0148$
	$\sigma_P = 0.0031$
$\sigma_{\gamma i} = 0.1$	$\mu_P = 0.0169$
	$\sigma_P = 0.0055$
$\sigma_{\gamma i} = 0.5$	$\mu_P = 0.0374$
	$\sigma_P = 0.0166$
Example 2 – Pacific Region (Table 5.6)	
$\sigma_{\gamma i} = 0.01$	$\mu_{P(4)} = 0.012$
	$\sigma_{P(4)} = 0.0007$
$\sigma_{\gamma i} = 0.1$	$\mu_{P(4)} = 0.0141$
	$\sigma_{P(4)} = 0.0014$
$\sigma_{\gamma i} = 0.5$	$\mu_{P(4)} = 0.0292$
	$\sigma_{P(4)} = 0.0041$

By introducing the analytical form of the various distribution functions describing the sub-events, it is possible to both model the information gathered from various sources and to directly assess the accuracy of the risk-based model predictions. To demonstrate

this, Eqn. 5.2 is used, where *P(Encounter)* is calculated for a specific gear type. Due to the independence between each of the variables, a product of the individual distributions can be used represent a joint distribution function. Suppose the probability of gear loss for a particular gear type and the percent usage of a particular gear type are treated as random variables while the location parameter and the weighting assigned to each gear type retain their discrete distributions. The exact losses due to both the commercial and local fishing industries are difficult to estimate and the exact contributions of each to the proportions of gear usage are unknown, making the model parameters difficult to quantify. This makes fishing gear loss and gear usage suitable variables to be described using probability distribution functions. Based on this idea, one can express the distribution function describing the probability of encounter mathematically as

$$f_{P(Encounter)}(\lambda, \gamma, \beta, w) = f_{\Lambda}(\lambda) \cdot f_{\Gamma}(\gamma) \cdot f_{\mathrm{B}}(\beta) \cdot f_{W}(w) \tag{5.12}$$

where the product of the probability density functions for the location parameter, gear loss, gear usage, and weighing are shown on the right-hand side of Eqn. 5.12. Assume that the gear loss rate can be modeled as a truncated normal distribution, $\gamma \sim N(\mu_{\gamma},\sigma_{\gamma})$, and the gear usage follows a truncated Rayleigh distribution as a function of the parameter θ_{β}, where $\beta \sim Rayleigh(\theta_{\beta})$; both are confined to the interval 0 to 1. Let the location and weighting distribution functions be described as discrete distributions where they are only valid for values of λ_0 and w_0, respectively. That is,

$$f_{\Gamma}\left(\gamma\,;\,\mu_{\gamma}\,,\,\sigma_{\gamma}\,,\,0\,,\,1\right)=\begin{cases}\dfrac{\phi\left(\dfrac{\gamma-\mu_{\gamma}}{\sigma_{\gamma}}\right)}{\Phi\left(\dfrac{1-\mu_{\gamma}}{\sigma_{\gamma}}\right)-\Phi\left(\dfrac{0-\mu_{\gamma}}{\sigma_{\gamma}}\right)} & ,\ 0\le\gamma\le 1\\ 0 & ,\text{ otherwise}\end{cases} \tag{5.13}$$

$$f_{\mathrm{B}}(\beta;\,\theta_{\beta})=\begin{cases}\dfrac{\dfrac{\beta}{\theta_{\beta}^{\,2}}\exp\left(-\dfrac{1}{2}\left(\dfrac{\beta}{\theta_{\beta}}\right)^{2}\right)}{1-\exp\left(-\dfrac{1}{2}\left(\dfrac{1}{\theta_{\beta}}\right)^{2}\right)} & 0\le\beta\le 1\\ 0 & \text{elsewhere}\end{cases} \tag{5.14}$$

$$f_{\Lambda}(\lambda)=\begin{cases}1 & \lambda=\lambda_{0}\\ 0 & \text{elsewhere}\end{cases} \tag{5.15}$$

$$f_{W}(w)=\begin{cases}1 & w=w_{0}\\ 0 & \text{elsewhere}\end{cases} \tag{5.16}$$

Based on these assumptions, the resulting joint distribution function for the probability of encounter can be expressed as the joint distribution of λ, γ, β, and w as expressed in Eqn. 5.12. A change of variables is required to reconstruct this joint probability distribution function, $f_{P(Encounter)}(\lambda,\gamma,\beta,w)$, in terms of the probability of encounter, $f_{P(Encounter)}(p)$, where p is the random variable of *P(Encounter)*. The change of variables is completed by solving,

$$f_{P,\Lambda,B,W}(p,\lambda,\beta,w)\;=\frac{f_{\Gamma,\Lambda,B,W}(\gamma,\lambda,\beta,w)}{\left|\det\left\{\dfrac{\partial(p,\lambda,\beta,w)}{\partial(\gamma,\lambda,\beta,w)}\right\}\right|}$$

$$= \frac{f_\Gamma(\gamma) \cdot f_\Lambda(\lambda) \cdot f_B(\beta) \cdot f_W(w)}{\left| \det \begin{Bmatrix} \frac{\partial p}{\partial \gamma} & \frac{\partial p}{\partial \lambda} & \frac{\partial p}{\partial \beta} & \frac{\partial p}{\partial w} \\ \frac{\partial \lambda}{\partial \gamma} & \frac{\partial \lambda}{\partial \lambda} & \frac{\partial \lambda}{\partial \beta} & \frac{\partial \lambda}{\partial w} \\ \frac{\partial \beta}{\partial \gamma} & \frac{\partial \beta}{\partial \lambda} & \frac{\partial \beta}{\partial \beta} & \frac{\partial \beta}{\partial w} \\ \frac{\partial w}{\partial \gamma} & \frac{\partial w}{\partial \lambda} & \frac{\partial w}{\partial \beta} & \frac{\partial w}{\partial w} \end{Bmatrix} \right|}$$

$$= \frac{f_\Gamma(\gamma) \cdot f_\Lambda(\lambda) \cdot f_B(\beta) \cdot f_W(w)}{\left| \det \begin{Bmatrix} \lambda\beta w & \gamma\beta w & \lambda\gamma w & \lambda\gamma\beta \\ 0 & 1 & 0 & 0 \\ 0 & 0 & 1 & 0 \\ 0 & 0 & 0 & 1 \end{Bmatrix} \right|}$$

$$= \frac{f_\Gamma(\gamma) \cdot f_\Lambda(\lambda) \cdot f_B(\beta) \cdot f_W(w)}{\lambda\beta w}$$

$$= \frac{f_\Gamma\left(\frac{p}{\lambda\beta w}\right) \cdot f_\Lambda(\lambda) \cdot f_B(\beta) \cdot f_W(w)}{\lambda\beta w} \qquad (5.17)$$

Then, the marginal density function that characterizes the probability of encounter can be calculated from the joint distribution using integration.

$$f_P(p) = \int_{-\infty}^{+\infty} \int_{-\infty}^{+\infty} \int_{-\infty}^{+\infty} f_{P,\Lambda,B,W}(p,\lambda,\beta,w)\, d\lambda\, d\beta\, dw$$

$$= \int_{-\infty}^{+\infty} \int_{-\infty}^{+\infty} \int_{-\infty}^{+\infty} \frac{1}{\lambda\beta w} \cdot f_\Gamma\left(\frac{p}{\lambda\beta w}\right) \cdot f_\Lambda(\lambda) \cdot f_B(\beta) \cdot f_W(w)\, d\lambda\, d\beta\, dw \qquad (5.18)$$

The limits of integration are dependent on the support of the distribution describing the variables. In this case, because each of the random variables is describing a probability, their domains are from 0 to 1 inclusive. Because the weighting and location parameters are assigned discrete distributions and only take specified values, the equation can be further simplified to

$$f_{P(Encounter)}(p) = \int_0^1 f_B(\beta) \cdot f_\Gamma\left(\frac{p}{\lambda\,\beta\,w}\right) \cdot \frac{1}{\lambda\,\beta\,w}\, d\beta \tag{5.19}$$

In terms of the assigned probability distributions that is,

$$f_{P(Encounter)}(p)$$

$$= \int_0^1 \frac{\frac{\beta}{\theta_\beta^{\,2}} \exp\left(-\frac{1}{2}\left(\frac{\beta}{\theta_\beta}\right)^2\right)}{1 - \exp\left(-\frac{1}{2}\left(\frac{1}{\theta_\beta}\right)^2\right)} \cdot \frac{\phi\left(\frac{\frac{p}{\lambda_0\,\beta\,w_0} - \mu_\gamma}{\sigma_\gamma}\right)}{\Phi\left(\frac{1 - \mu_\gamma}{\sigma_\gamma}\right) + \Phi\left(\frac{\mu_\gamma}{\sigma_\gamma}\right) - 1} \cdot \frac{1}{\lambda_0\,\beta\,w_0}\, d\beta \tag{5.20}$$

Converting the probability density so that it is in terms of *P(Encounter)* is advantageous for making direct interpretations of the parameters describing the probability of encounter distribution function. Then, to determine the Probability of Exceedance of a specified value, p_0, the complementary cumulative distribution is written as

$$1 - F_{P(Encounter)}(p_0) \quad = \Pr\left(\mathrm{P}(Encounter) \geq p_0\right)$$

$$= \int_{p_0}^{1} f_{P(Encounter)}(p)\, dp \tag{5.21}$$

$$= \int_{p_0}^{1} \int_{0}^{1} \frac{\frac{\beta}{\theta_\beta{}^2} \exp\left(-\frac{1}{2}\left(\frac{\beta}{\theta_\beta}\right)^2\right)}{1 - \exp\left(-\frac{1}{2}\left(\frac{1}{\theta_\beta}\right)^2\right)} \cdot \frac{\phi\left(\frac{p}{\lambda_0\, \beta\, w_0} - \mu_\gamma}{\sigma_\gamma}\right)}{\Phi\left(\frac{1 - \mu_\gamma}{\sigma_\gamma}\right) + \Phi\left(\frac{\mu_\gamma}{\sigma_\gamma}\right) - 1} \cdot \frac{1}{\lambda_0\, \beta\, w_0}\, d\beta\, dp \tag{5.22}$$

As noted previously, by adopting the analytical form of the probability density functions it is possible to assess the accuracy of the risk-based model and the sensitivity of its predictions to incomplete information.

Including the debris removal rate requires an additional variable in Eqns. 5.12-5.22. It is best to specify its distribution as the complementary event, $f_{1\text{-}R}(1\text{-}r)$, representing the percentage of fishing gear that is left behind, to allow for the product to be used in the joint distribution. If the function describing the removal rate, $f_R(r)$, is known, then the complementary event can be found by shifting the function. Then,

$$f_{P(Encounter)}(\lambda, \gamma, \beta, w, r) = f_\Lambda(\lambda) \cdot f_\Gamma(\gamma) \cdot f_\mathrm{B}(\beta) \cdot f_W(w) \cdot f_R(1 - r) \tag{5.23}$$

Because of the assumption of independence between sub-events, layered convolution integrals based on the concept previously introduced in Eqn. 4.21 can be utilized to address the summations over *i*, *j*, and *k*.

$$f_{P_I}(p) = \left(f_{P_{i=1}} * f_{P_{i=2}} * \ldots * f_{P_{i=N_{jk}}}\right)(p) \tag{5.24}$$

$$f_{P_J}(p) = \left(f_{P_{I,j=1}} * f_{P_{I,j=2}} * \ldots * f_{P_{I,j=M_k}}\right)(p) \tag{5.25}$$

$$f_{P_K}(p) = \left(f_{P_{I,J,k=1}} * f_{P_{I,J,k=2}} * \ldots * f_{P_{I,J,k=Q}}\right)(p) \tag{5.26}$$

The modeling of incomplete data can be achieved by recognizing the underlying probability density functions or exploring the impact of possible distributions on the predictions. The recognition of an underlying distribution is demonstrated in Figures 5.12a and 5.12b, where simulated data is fit with continuous distributions. For the example provided, the data is simulated from known probability distribution functions, however in reality, it is unlikely that data will be available with this resolution. As the quantities of accurate data related to whale entanglement via fishing gear increases, smaller bin sizes and better characterization of the behavior of the data using continuous distribution functions will result. Figures 5.12c, 5.12d, 5.12e, and 5.12f provide comparative plots between proceeding with the analysis for determining the risk of entanglement using simulated discrete data versus an idealization of the discrete data using continuous distribution functions. If the analysis proceeds using the discrete data, the result is as

shown in Figure 5.12c and 5.12d, where multidimensional histograms and pulses of color provide a rigid representation of how the risk-model behaves. Proceeding with continuous representations of the data as in Figure 5.12e and 5.12f allows for smoother visualization of the 3-dimensional and contour graphics. Although the two methods provide different levels of visualization, the accuracy of results of each analysis is entirely dependent on how well the continuous distribution functions match the behavior of the data.

It can be seen that continuous distribution functions result in reasonable representations of discrete data, and with some adjustment, could be further refined if necessary. This is illustrated in Figures 5.13a, 5.13b, 5.13c, and 5.13d where slight changes in each of the parameter assignments for β and γ are shown to alter the contours of the joint distribution functions. This demonstrates how alternate scenarios could be implemented, as this approach is not limited to the probability density functions explored in this study. So, if more appropriate analytical functions are deemed to better fit the data, the formulation of the joint distributions can be modified and introduced into the risk-based model.

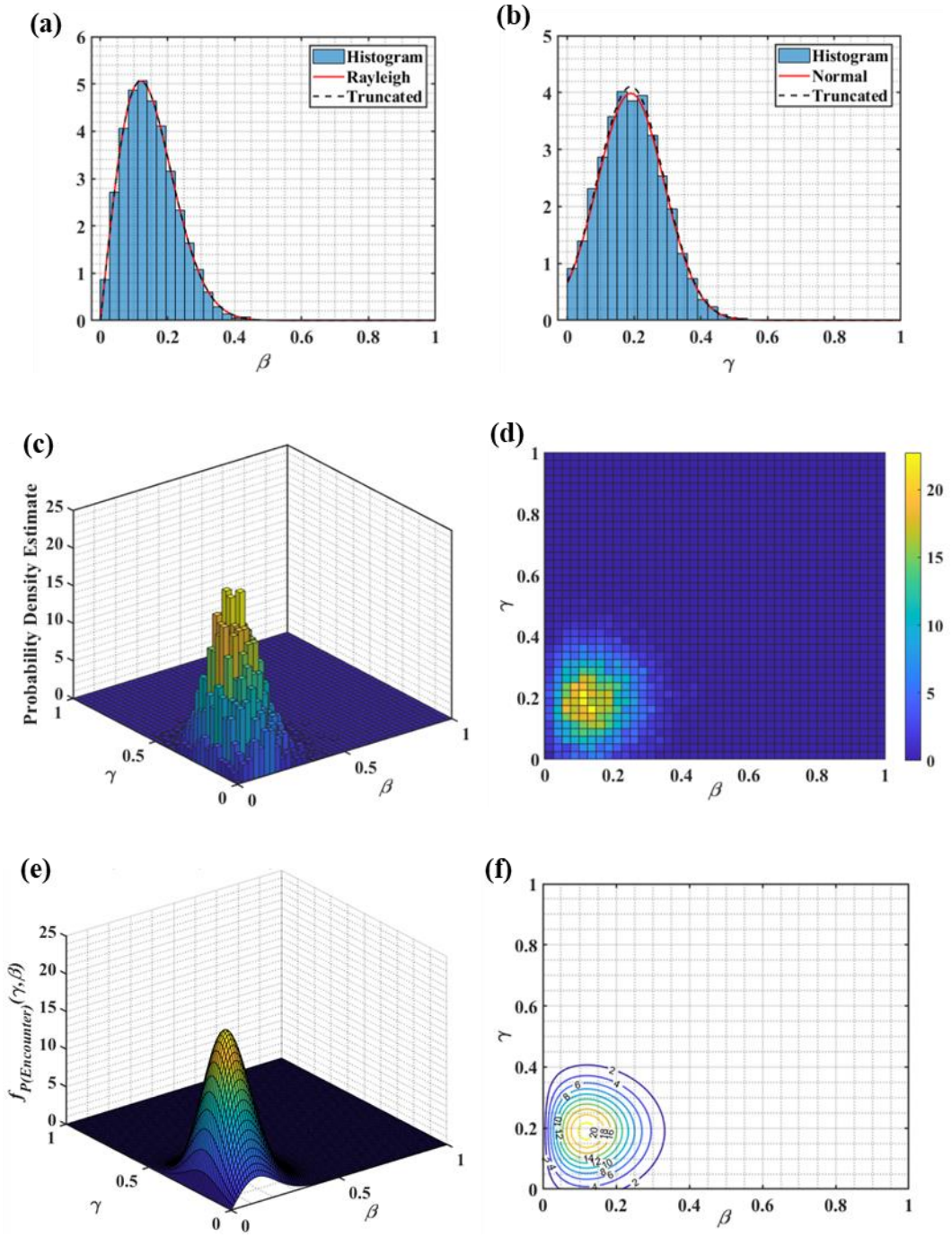

Figure 5.12 Simulated data for (a) β ~ Rayleigh($\theta_\beta = 0.15\sqrt{(2/\pi)}$) and (b) $\gamma \sim N(\mu_\gamma = 0.19, \sigma_\gamma = 0.1)$ to compare resulting (c) 3-D histogram and (d) heat map of data to (e) 3-D and (f) contour visualization of fitted continuous distribution functions. Reprinted with permission from Brown and Niedzwecki (2020).

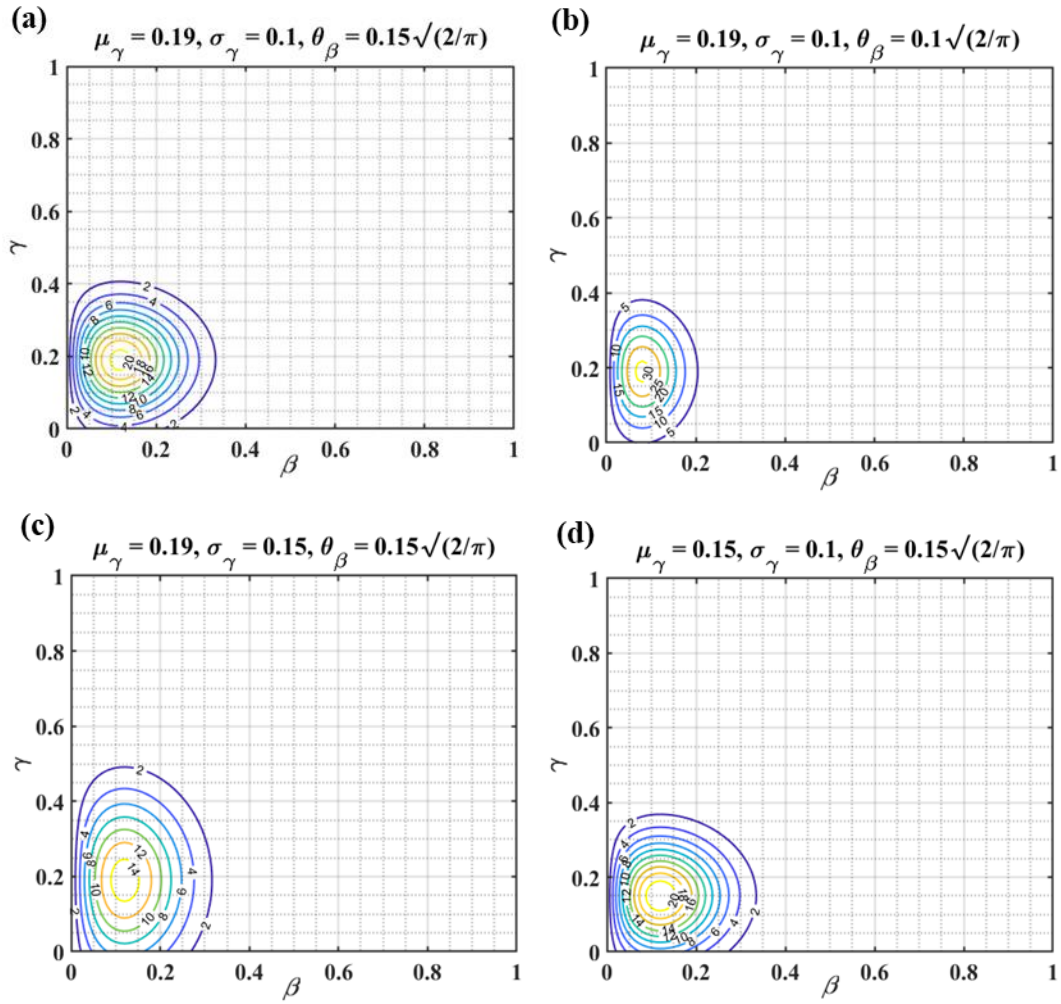

Figure 5.13 Comparison of the contours of the analytical joint distribution functions modeling the probability of encounter, $f_{P(Encounter)}(\gamma, \beta)$, with incremental changes in parameter values. Specifically, (a) $\mu_\gamma = 0.19$, $\sigma_\gamma = 0.1$, $\theta_\beta = 0.15\sqrt{(2/\pi)}$; (b) $\mu_\gamma = 0.19$, $\sigma_\gamma = 0.1$, $\theta_\beta = 0.1\sqrt{(2/\pi)}$; (c) $\mu_\gamma = 0.19$, $\sigma_\gamma = 0.15$, $\theta_\beta = 0.15\sqrt{(2/\pi)}$; and (d) $\mu_\gamma = 0.15$, $\sigma_\gamma = 0.1$, $\theta_\beta = 0.15\sqrt{(2/\pi)}$. Reprinted with permission from Brown and Niedzwecki (2020).

In order to check the effect of these parameter changes on the estimates for the probability of encounter the mean value of the probability of encounter distribution for each variation was taken as the informative measurement for comparison. It is worth noting that the mean values calculated using the joint distribution in Eqn. 5.12 matched

those of the distribution introduced in Eqn. 5.20, so calculations can be completed using either format. The base parameters were assigned so that the mean of each distribution matched the values used in calculating the contribution of pots and traps to whale entanglement in the New England Region for Example 1.

The parameter assignments of $\mu_\gamma = 0.19$, $\sigma_\gamma = 0.1$, and $\theta_\beta = 0.15\sqrt{(2/\pi)}$ with $\lambda = 0.5$ and $w = 0.528$, shown in Figure 5.13a, resulted in a mean value of 0.76% and standard deviation of 0.05% which is well within a standard deviation of the 0.75% estimate calculated using discrete values in Example 1. The interpretation of the calculated mean value is that, on average, the model will report that 0.76% of pots and traps deployed in a year in the New England Region will be available for entanglements with whales. The next variation in Figure 5.13b has the parameter assignments of $\mu_\gamma = 0.19$, $\sigma_\gamma = 0.1$, and $\theta_\beta = 0.1\sqrt{(2/\pi)}$ with $\lambda = 0.5$ and $w = 0.528$. This is equivalent to decreasing the mean of the Rayleigh distribution describing β to 0.1 and underestimating the portion of pots and traps being used by industry. The resulting distribution has a mean of 0.51% and standard deviation of 0.02%, which is noticeably less than the initial estimate and results in an underestimate. Figure 5.13c uses the parameter assignments of $\mu_\gamma = 0.19$, $\sigma_\gamma = 0.15$, and $\theta_\beta = 0.15\sqrt{(2/\pi)}$ with $\lambda = 0.5$ and $w = 0.528$. In this case, the standard deviation of the distribution describing γ is increased to reflect less certainty in the choice of distribution to represent the loss of pots and traps. This variation now provides a conservative estimate for the probability of encounter with a mean of 0.85% and standard deviation of 0.08%. Lastly, Figure 5.13d uses the parameter assignments of $\mu_\gamma = 0.15$, $\sigma_\gamma = 0.1$, and $\theta_\beta = 0.15\sqrt{(2/\pi)}$ with $\lambda = 0.5$ and $w = 0.528$ to represent estimating less pots and traps lost each

year than the true amount. This results in an underestimation of the probability of encounter with a mean of 0.64% and standard deviation of 0.04%. Any changes to the definitions of the location parameter, λ, and weighting, w, which would reflect spatial or temporal changes in the presence of whales and additional information on past entanglement cases respectively, result in linear changes in the mean value of the probability of encounter because of their current discrete distribution definitions.

The likelihood of the risk-model underestimating the probability of encounter can be calculated using the probability of exceedance introduced in Eqn. 5.22. The probability that the true value exceeds the estimated value, if the estimated value is taken as the mean value of the distribution, was approximately 41% for the parameter assignments in Figures 5.13a and 5.13b, and approximately 40% for the parameter assignments in Figures 5.13c and 5.13d. This means that the model has approximately a 40% likelihood of underestimating the true number of whale entanglements using the current definitions of the sub-events and generated data. With sufficient amounts of accurate data and well-defined sub-events, the accuracy of the risk-based model can be assessed in this manner. In addition to comparisons to the results of the discrete valued examples, other methods can be used for model comparisons as more data is compiled. Goodness-of-fit tests and confidence intervals become advantageous for selecting an underlying continuous distribution to model the data of each sub-event. Visualization will become more challenging as more sub-events are introduced to refine the risk-based model, and the use of coupled graphical representations will be needed.

5.9. Discussion and Conclusions

This research addresses the development of a methodology for quantifying the risk associated with abandoned, lost or otherwise discarded fishing gear as it pertains to the entanglement of whales. The model presented introduces parameters that provide a means to quantify the impact of mishandling of fishing gear, the types of fishing gear used by industry, and gear subject to transport by storms, offshore currents, or other factors that reduce the amount of fishing gear in a particular region. The examples presented illustrate different scenarios for how the model can be applied both for discrete representations of data and analytical functions. In the first example, data relevant to the New England region was used to calculate the risk of entanglement for whales in the region using average estimates. The next example demonstrated the ability of the model to generate multi-year entanglement estimates by combining Pacific region datasets. The third example further demonstrated the process for combining data from different geographic regions, specifically using information from the New England and Pacific regions. For situations where data is sparse or nonexistent, the use of continuous distribution functions was introduced as an alternative to accommodate these knowledge gaps. This approach allows one to investigate the sensitivity of the model to specific sub-event information. For sub-events where incomplete information exists, distributions can be selected that allow their parameter values to be defined to approach a uniform distribution when no information is available. The risk-based model predictions can be used to estimate the units of gear available for entanglement based on deployment rates or can be used to calculate the likelihood of underestimating the true risk. As the accuracy of the data used in the risk-

based model is increased, the model has the potential to be used as guidance to decrease the number of entanglement events.

The risk-based model as currently implemented is focused on independent entanglement events by gear type and does not explore multiple entanglement events by an individual whale. Other kinds of entanglements, including that from active and fixed gear, could be modeled as additional sub-events based on spatial variability between seasonal whale migration routes and regional fishery locations that attract the migrating whales. The lack of field data remains the biggest challenge to improving the breadth and accuracy of the risk model predictions. The information used in this research represents data reported in the open literature as well as idealizations of that data. In practice, one might consider introducing a reasonable distribution based on experience and use that in the modeling process until additional data is available to confirm or disprove the choice.

The strength of the methodology presented is its ability to take varied amounts of field observations and recast it for mathematical interpretation to be used in the risk-based model predictions. The general framework developed allows researchers to examine alternative hazard scenarios by incorporating additional data on both regional and global scales in a structured way and is not limited to this specific application. The fault tree approach allows one to address other research topics in a similar fashion through the focused descriptions of compiled field data, which can then be used to define an outcome based on the selection of the sub-events. The use of a variety of visualization schema is essential in characterizing possible scenarios in determining the sensitivity of the risk

model parameterization. The approach presented in this study provides a starting point for developing other risk-based models for quantifying threats to marine life.

CHAPTER 6

ASSESSING THE RISK OF DEBRIS-STRUCTURE INTERACTIONS DUE TO IMPACT LOADING

Interpretations of available information to address the risk of waterborne debris colliding with a structure are presented. A risk-based model is derived that reflects published information on large waterborne debris generation and behavioral data. The fault tree framework previously developed to organize data and allow for the continual improvement of risk-based model predictions is adapted for this new application. This objective is completed through the redevelopment of sub-events based on available data reported on shipping containers and extreme hydrodynamic events which is used in illustrative examples. The debris collision is characterized in terms of the debris characteristics, channel dimensions, flow conditions, the geometry of the target structure, and rate of occurrence of debris-generating events. The risk-based model is used to develop graphs characterizing the collision force magnitude as a function of the probability of collision for a given return period. The occurrence of either single or sequential collision events are illustrated and discussed. Analytic distribution functions are introduced to develop a joint distribution function of the top event that supports clear interpretations of result. The sensitivity of the risk-based predictions to the reported field data is investigated.

6.1. Introduction

Extreme hydrodynamic events such as tsunamic, hurricanes, and major flooding are global occurrences that can at times disturb necessary regional and international economic and social connections. Bridges and channels are necessary for the transport of goods and services, power generation structures provide essential hydroelectricity to localities, and dams hold back substantial amounts of water to protect downstream areas. Damage to any of these structures could result in catastrophic consequences for a region, especially loss of life, and inhibit emergency services. With these extreme events, fallen trees and large debris that would not be capable of being transported during typical conditions become liberated with the heighted floodwaters and higher flow velocity and free to impact aquatic structures.

The severity of threats to every structure are unique to each structure and location. Heavily forested regions will likely be prone to damage after collisions from large woody debris. Coastal regions close to ports and shipyards will be wary of aberrant vessels and loose shipping containers. Naito et al. (2014) developed a procedure to assess the site-specific potential for debris impact in the context of tsunamis using a debris classification strategy. The strategy involves determining the type of debris that will be present and understanding its capacity to impart structural damage based on the debris mass, stiffness, size, and buoyancy. Although extreme events are often required to move the debris and make it waterborne, the generation of this debris can come from a variety of circumstances. Natural occurrences such as rates of tree mortality and seasonal changes, or human activities such as mechanical failures or human error also affect the production

of significant quantities of large-size waterborne debris (Chang and Shen, 1979; Manners and Doyle, 2008; Manuel et al., 2006).

Because each structure is unique in the threats it faces, a flexible approach is necessary in developing a predictive model that can be used for numerous structural contexts. The uncertainties associated with the conditions required for a collision to occur suggest that a probabilistic risk-based method would be best for gaining insight into this application. Similar to the model development for the entanglement of whales, a method to develop meaningful interpretations of available data and quantify threats of waterborne debris that allows for the estimation and incorporations of regional specifics is valuable. Illustrative examples are developed using data available on the collisions of waterborne debris with bridge piers to further reveal the increasing complexity and capability of the risk-based model approach.

6.2. Development of the Risk Model

Riverine and coastal structures are constantly susceptible to damage from large debris that has entered a body of water due to anthropogenic behavior, natural hazards, or seasonal changes. This damage can occur due to impact loading or through the accumulation of debris against a structure. The focus here is on quantifying the risk of damage to a structure due to impact loading from waterborne debris. The actual response of the structure to the load can be treated a separate problem and is not addressed in this study. The sub-event requirements for a collision generating a certain force against a structure are that debris enters the body of water and becomes waterborne, the path of the

waterborne debris intersects with the placement of the structure causing a spatial overlap, and the waterborne debris collides at a certain force. The likelihood of debris entering a body of water uncontrolled is a physical characteristic sub-event dependent on the type of debris and its origin. For example, large woody debris requires consideration of tree mortality, bank erosion, weather conditions, and logging practices (Chang and Shen, 1979; Manners and Doyle, 2008), while aberrant vessels require focus on natural hazards, weather conditions, pilot error, or mechanical failure (Manuel et al., 2006). The path of the waterborne debris intersecting with the placement of the structure is a spatial condition sub-event that is a function of the channel morphology, debris size and orientation, and flow conditions. The force of the collision is regarded as a physical characteristic sub-events that is dependent on the mass and stiffness of the waterborne debris and the velocity at which it is transported. For this example, the sub-events are assumed to be independent and the risk of each collision is considered independent and a disjoint event. The risk calculated using this formulation is per collision event for a single element of debris. The types of debris are also assumed mutually exclusive.

6.2.1. Mathematical Representation of Sub-Events

To create the risk equation, we begin by first considering the risk of a collision of a force associated with specified types of debris such as drifting ships or barges, shipping containers, or large woody debris. The probability of a collision and the subsequent force due to a debris type i can be expressed as

$$\begin{aligned} &\text{P}(\textit{Collision with Debris Type } i) \\ &\quad = \text{P}(\textit{Becomes Waterborne} \cap \textit{Spatial Overlap} \cap \textit{Debris Force}) \\ &\quad = \eta_i \times \psi_i \times \delta_i \end{aligned} \tag{6.1}$$

where, in this discrete notation, η_i is the probability of debris type i becoming waterborne, ψ_i is the probability of the path of waterborne debris of type i overlapping with the placement of the structure, and δ_i is the probability of a specified impact loading from waterborne debris type i. In terms of the notation used in Eqns. 4.8 through 4.16, $\psi_i = s$, the spatial condition, and $\{\eta_i, \delta_i\} = \{h_1, h_2\}$, the physical characteristics. In this discrete representation of the probability of collision, each variable represents a discrete probability value and is thus bound to the interval [0,1]. The path and force are both functions of some combination of the waterborne debris orientation, velocity, mass, stiffness, and size. To determine the path and force, information regarding the waterborne debris properties must be known. Then, the probability of a collision of a certain force due to debris type i is more specifically given by

$$\begin{aligned} &\text{P}(\textit{Collision with Debris Type } i) \\ &\quad = \eta_i \times \left(\psi_i \mid \theta_i \cap v_i \cap \mu_i \cap \ell_i\right) \times \left(\delta_i \mid \theta_i \cap v_i \cap \mu_i \cap \kappa_i\right) \end{aligned} \tag{6.2}$$

where, θ_i describes the orientation distribution at which waterborne debris of type i is likely to travel, v_i describes the velocity distribution, μ_i describes the mass distribution, ℓ_i describes the size distribution, and κ_i describes the stiffness distribution. When combining the risk associated with various debris types, the designation of debris types as mutually exclusive allows for a summation of events. Then, for N types of debris, the probability of collision becomes

$$\mathrm{P}(\mathit{Collision}) = \left[\sum_{i=1}^{N} \eta_i \times \left(\psi_i \mid \theta_i \cap v_i \cap \mu_i \cap \ell_i\right) \times \left(\delta_i \mid \theta_i \cap v_i \cap \mu_i \cap \kappa_i\right)\right] \tag{6.3}$$

This resulting equation reveals itself to be comparable to that used to calculate the annual frequency of bridge collapse due to collisions from aberrant vessels (Manuel et al., 2006; AASHTO, 2012).

To account for regular changes that might occur in a dataset that spans a specific time interval, an added temporal condition can be introduced into Eqn. 6.3. This term can be interpreted as a mitigation factor that accounts for the introduction of preventative methods, such as debris-diversion techniques that are intended to decrease the risk of collisions. Specifically,

$$\mathrm{P}(\mathit{Collision}) = \left[\sum_{i=1}^{N} (1 - r_i) \times \eta_i \times \left(\psi_i \mid \theta_i \cap v_i \cap \mu_i \cap \ell_i\right) \times \left(\delta_i \mid \theta_i \cap v_i \cap \mu_i \cap \kappa_i\right)\right] \tag{6.4}$$

where the techniques used can vary in effectiveness based on the type of debris. In its current form, Eqn. 6.4 provides a means to evaluate the risk at a specific structure. Further, when considering the risk over longer periods of time using available debris collision data that can be associated with different structures, if the collision events at each structure are considered mutually exclusive, they are additive. Then a multi-structure risk equation for Q structures can be expressed as

$$\mathrm{P}(\textit{Collision}) \tag{6.5}$$

$$= \sum_{k=1}^{Q} \left\{ \frac{1}{M_k} \cdot \sum_{j=1}^{M_k} \left[\sum_{i=1}^{N_{jk}} (1 - r_{ijk}) \eta_{ijk} \times \left(\psi_{ijk} | \, \theta_{ijk} \cap \nu_{ijk} \cap \mu_{ijk} \cap \ell_{ijk} \right) \times \left(\delta_{ijk} \mid \theta_{ijk} \cap \nu_{ijk} \cap \mu_{ijk} \cap \kappa_{ijk} \right) \right] \right\}$$

where N_{jk} are the number of debris types at time j for structure k, M_k is the time span of the dataset for structure k. Each sub-event can be specified by debris type, time, and location.

6.3. Continuous Representation of the Risk Model

In order to address the risk probability as developed in Eqn. 6.5 analytically, consider the basic representation of the probability of collision using continuous density functions noted in the development of Eqn. 6.1, that is

$$f_{P(Collision)}(\eta, \psi, \delta) = f_H(\eta) \cdot f_\psi(\psi) \cdot f_\Delta(\delta) \tag{6.6}$$

With the use of a continuous representation for the probability of collision, it becomes possible to describe the variables η, ψ, and δ in greater detail without the domain restriction of [0,1] imposed by the discrete representation. The function describing the probability of becoming waterborne, $f_H(\eta)$, can be determined based on rate of occurrence of debris-generating events, where a value η_0 would describe an upper limit for the period being studied. Specifying the functions that describe the transport path of waterborne debris, $f_\Psi(\psi)$, and the force a collision generates, $f_\Delta(\delta)$, requires a clear understanding of the physics involved.

6.3.1. Modeling Waterborne Debris Colliding with a Fixed Structure

In order to determine the probability of collision between a structure and floating debris, the placement of the structure and the path of the transported debris leading to a collision requires predicting the lateral and vertical position of the debris relative to both the width and depth of the channel and the position of the structure as illustrated in Fig. 6.1a, 6.1b, and 6.1c. Debris transport most often occurs along the thalweg which is the point of highest flow velocity (Parola et al., 2000). If debris transport is assumed to follow the shape of the flow field, then the flow field can be used to estimate the path of the debris. The level of submersion relative to the vertical position of the structure is relevant for problems where the structure does not cover the entire depth or when a specific point of structural vulnerability such as a bridge deck during heavy flooding conditions is

examined. For a supporting bridge pier, let ψ_{ijk} represent the path of the debris, then the probability of the collision with the structure can be expressed as

$$\mathrm{P}\left(x_{jk} - \frac{\ell_{str,\,jk}}{2} - \frac{\ell_{ijk}}{2}\sin\theta_{ijk} \le \psi_{ijk} \le x_{jk} + \frac{\ell_{str,\,jk}}{2} + \frac{\ell_{ijk}}{2}\sin\theta_{ijk}\right) = \int_{x_{jk} - \frac{\ell_{str,\,jkr}}{2} - \frac{\ell_{ijk}}{2}\sin\theta_{ijk}}^{x_{jk} + \frac{\ell_{str,\,jkr}}{2} + \frac{\ell_{ijk}}{2}\sin\theta_{ijk}} f_{\Psi_{ijk}}\left(\psi_{ijk}\right) d\psi_{ijk} \quad (6.7)$$

where, x_{jk} is the lateral position of the structure, $\ell_{str,\,jk}$ is the length of the structure perpendicular to the direction of flow, ℓ_{ijk} is the longest length measurement of the debris, and θ_{ijk} is the orientation of the debris in the flow. Both the debris length and orientation can be treated as random variables if desired and sampled from distributions, $f_{\Theta}(\theta)$ and $f_{L}(\ell)$. If the vertical component is included, then double integration is required to account for both directions. The new limits of integration for the vertical direction are determined similarly to that of the lateral direction, but the vertical location of the critical point, z_{jk}, is used and the path, ψ_{ijk}, now has two directional components, $\psi_{(1),ijk}$ and $\psi_{(2),ijk}$ that account for lateral movement and debris buoyancy.

$$\mathrm{P}\left(\begin{array}{c} x_{jk} - \frac{\ell_{str,\,jk}}{2} - \frac{\ell_{ijk}}{2}\sin\theta_{ijk} \le \psi_{(1),\,ijk} \le x_{jk} + \frac{\ell_{str,\,jk}}{2} + \frac{\ell_{ijk}}{2}\sin\theta_{ijk} \\ \cap \\ z_{jk} - \frac{b_{ijk}}{2} \le \psi_{(2),\,ijk} \le z_{jk} + \frac{b_{ijk}}{2} \end{array}\right)$$

$$= \int_{x_{jk} - \frac{\ell_{str,\,jkr}}{2} - \frac{\ell_{ijk}}{2}\sin\theta_{ijk}}^{x_{jk} + \frac{\ell_{str,\,jkr}}{2} + \frac{\ell_{ijk}}{2}\sin\theta_{ijk}} \int_{z_{jk} - \frac{b_{ijk}}{2}}^{z_{jk} + \frac{b_{ijk}}{2}} f_{\Psi_{ijk}}\left(\psi_{ijk}\left(\psi_{(1),\,ijk}, \psi_{(2),\,ijk}\right)\right) d\psi_{(2),\,ijk}\, d\psi_{(1),\,ijk} \qquad (6.8)$$

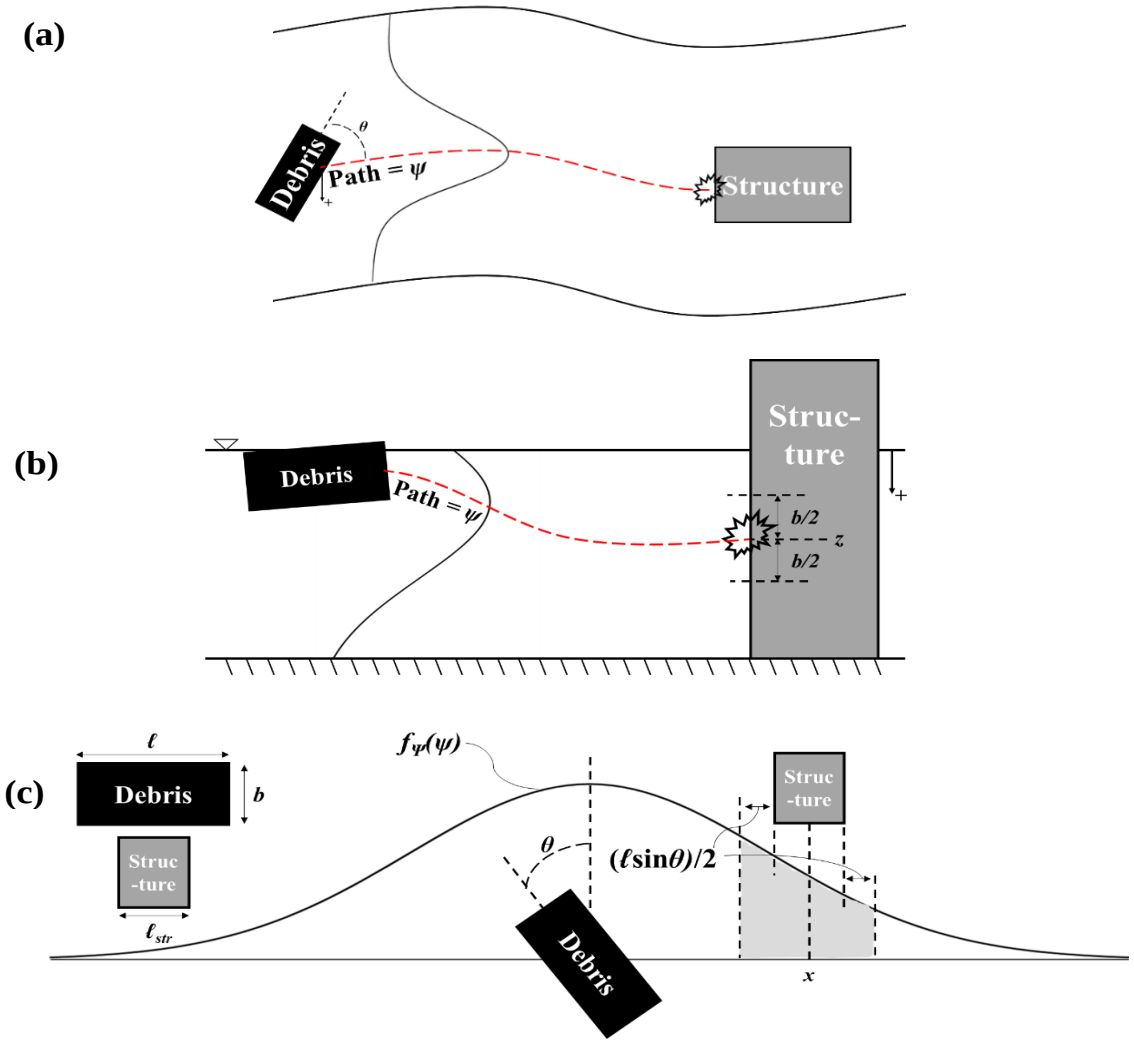

Figure 6.1 Path of waterborne debris relative to a structure: (a) lateral movement, (b) vertical movement, and (c) overlap between the path of the debris and position of the structure

6.3.2. Modeling the Collision Force

The impact force can be predicted empirically using collision tests or calculated using established equations. Although there is no true consensus on how to model impact loading from debris, the force of collision is often treated as a single degree of freedom system that assumes structural stiffness and inertia are large enough to prevent movement

at impact. The three main approaches used to estimate the force generated in impact problems are a contact stiffness approach, that uses a 1DOF spring-mass system illustrated in Fig. 6.2 with an associated stiffness from the interaction between the debris and structure; an impulse momentum approach that requires assumptions on stoppage time and the shape of the force function with time; and a work-energy approach, that requires knowledge of the stopping distance for the debris (Haehnel and Daly, 2004; Ko et al., 2014).

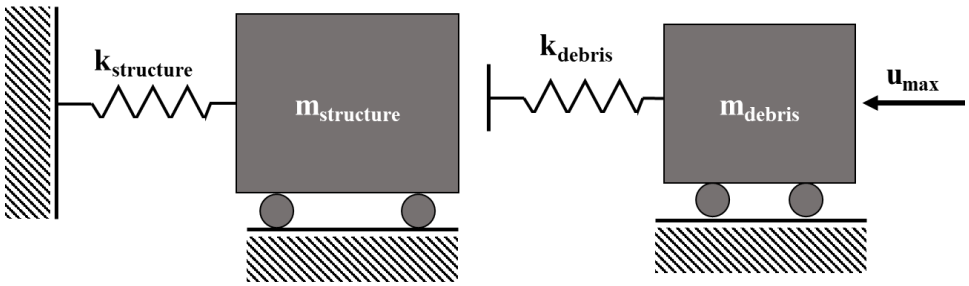

Figure 6.2 1DOF spring-mass system

The American Society of Civil Engineers (ASCE) addresses debris impact loading from tsunamis with a minimum inundation depth of 3 ft or greater and impact loading from flooding (ASCE, 2017). The load is applied at critical flexure and shear points within the inundation depth for members. Several equations for quantifying the force of impact are compiled in Table 6.1.

Table 6.1 Debris impact loading equations
(Haehnel and Daly, 2002; Ko et al., 2014; ASCE, 2016)

Approach	Equation	Variables
Impulse-Momentum	$F = \frac{\pi m_p v_I}{2\Delta t}$	F = Maximum impact force m_p = Total mass of the debris v_I = Impact velocity of the debris Δt = Time to reduce the debris velocity to zero
Work-energy	$F = \frac{mu^2}{S}$	F = Maximum impact force m = Total mass of the debris u = Impact velocity of the debris S = Stopping distance of the debris (from point of contact)
Flexible Impact	**2008 FEMA** $F_i = C_m v_I \sqrt{km}$ **2012 FEMA Modification** $F_i = 1.3\, u_{max} \sqrt{km_d\,(1+c)}$	F_i = Impact force C_m = Added mass coefficient (2.0) v_I = Flow velocity at the site k = Effective stiffness of the debris m = Mass of the debris u_{max} = Flow velocity m_d = Mass of debris c = Hydrodynamic mass coefficient
ASCE (tsunami)	$F_{ni} = u_{max}\sqrt{km_d}$ $F_i = I_{tsu} C_o F_{ni}$	F_{ni} = Nominal max instantaneous debris impact force F_i = Design instantaneous debris impact force u_{max} = Max flow velocity at site with depth sufficient to float debris k = Minimum of effective stiffness of impacting debris (EA/L) and lateral stiffness of the impacted structural elements deformed by impact m_d = Mass of the debris I_{tsu} = Importance Factor C_o = Orientation coefficient, 0.65 for logs and poles, shipping containers
ASCE (flood)	$F = \frac{\pi W V_b C_I C_O C_D C_B R_{max}}{2g\Delta t}$	F = Impact force W = Debris weight V_b = Velocity of object (assume equal to water velocity) g = Acceleration due to gravity Δt = Impact duration (time to reduce velocity to zero) C_I = Importance coefficient C_O = Orientation coefficient C_D = Depth coefficient C_B = Blockage coefficient R_{max} = Maximum ratio for impulsive load

For this example, the unmodified flexible impact equation, which allows one to account for the stiffness of the impacting debris, assuming it is less than that of the structural element, illustrated in Eqn. 6.9 is used to define the force as a probability density function. The flexible impact equation is analogous to the contact stiffness approach, which Haehnel and Daly (2002) found to align most accurately with their scaled laboratory tests.

$$F = u\sqrt{km_d} \tag{6.9}$$

where u is the max flow velocity, k is the effective stiffness, and m_d is the mass of the debris. In terms of the notation used introduced previously, that is,

$$\delta_{ijk} = v_{ijk}\sqrt{\kappa_{ijk}\mu_{ijk}} \tag{6.10}$$

In order to use Eqn. 4.22 to complete the change of variables needed to obtain $f_{\Delta}(\delta)$ from the joint distribution, $f_{\Delta}(v,\kappa,\mu)$, let the functions $f_V(v)$, $f_K(\kappa)$, and $f_M(\mu)$ represent the distributions describing the velocity, stiffness, and mass of debris, respectively. For the following derivation, the indices ijk are implied at each step but not included to facilitate the derivation:

$$f_{\Delta,K,M}(\delta,\kappa,\mu) = \frac{f_{V,K,M}(v,\kappa,\mu)}{\left|\det\left\{\frac{\partial(\delta,\kappa,\mu)}{\partial(v,\kappa,\mu)}\right\}\right|} \tag{6.11}$$

$$= \frac{f_V(v)\cdot f_K(\kappa)\cdot f_M(\mu)}{\left|\det\begin{Bmatrix}\frac{\partial\delta}{\partial v} & \frac{\partial\delta}{\partial\kappa} & \frac{\partial\delta}{\partial\mu}\\ \frac{\partial\kappa}{\partial v} & \frac{\partial\kappa}{\partial\kappa} & \frac{\partial\kappa}{\partial\mu}\\ \frac{\partial\mu}{\partial v} & \frac{\partial\mu}{\partial\kappa} & \frac{\partial\mu}{\partial\mu}\end{Bmatrix}\right|}$$

$$= \frac{f_V(v)\cdot f_K(\kappa)\cdot f_M(\mu)}{\left|\det\begin{Bmatrix}\sqrt{\kappa\mu} & \frac{\mu v}{2\sqrt{\kappa\mu}} & \frac{\kappa v}{2\sqrt{\kappa\mu}}\\ 0 & 1 & 0\\ 0 & 0 & 1\end{Bmatrix}\right|}$$

$$= \frac{f_V(v)\cdot f_K(\kappa)\cdot f_M(\mu)}{\sqrt{\kappa\mu}}$$

$$= \frac{f_V\left(\frac{\delta}{\sqrt{\kappa\mu}}\right)\cdot f_K(\kappa)\cdot f_M(\mu)}{\sqrt{\kappa\mu}} \tag{6.12}$$

Then, the marginal density function in terms of force can be calculated from the joint distribution derived in Eqn. 6.12 by integrating over the stiffness and the mass.

$$f_\Delta(\delta) = \int_{-\infty}^{+\infty}\int_{-\infty}^{+\infty} f_{\Delta,K,M}(\delta,\kappa,\mu)\,d\kappa\,d\mu$$

$$= \int_{-\infty}^{+\infty} \int_{-\infty}^{+\infty} \frac{1}{\sqrt{\kappa\mu}} f_V\left(\frac{\delta}{\sqrt{\kappa\mu}}\right) \cdot f_K(\kappa) \cdot f_M(\mu)\, d\kappa\, d\mu \qquad (6.13)$$

Then the distribution function describing the probability of the collision force exceeding some value, δ_0 is then given by

$$\mathrm{P}(\delta \geq \delta_0) = \int_{\delta_0}^{+\infty} f_\Delta(\delta)\, d\delta$$

$$= \int_{\delta_0}^{+\infty} \int_{-\infty}^{+\infty} \int_{-\infty}^{+\infty} \frac{1}{\sqrt{\kappa\mu}} f_V\left(\frac{\delta}{\sqrt{\kappa\mu}}\right) \cdot f_K(\kappa) \cdot f_M(\mu)\, d\kappa\, d\mu\, d\delta \qquad (6.14)$$

An alternate method to obtain probability distributions that describe the chance of overlap and impact force is to use sampling methods using the probability distributions built from observed laboratory data on debris transport and impact force. Repetitive experimental procedures such as the collision experiments documented in Table 2.2 are ideal for building distributions. If enough data points are gathered through laboratory experiments, histograms representations can be used to get a sense of the proper distribution that best describes the variable.

6.3.3. Modeling the Probability of Debris-Structure Collision

Introducing the functions describing $f_H(\eta)$, $f_\Psi(\psi)$, and $f_\Delta(\delta)$, allows the cumulative joint distribution based on Eqn. 6.6, $F_P(\eta,\psi,\delta)$, that describes the probability of a collision with a force of at least δ_0 occurring within time η_0, to be expressed as

$$F_{P_{ijk}}\left(\eta_{ijk}, \psi_{ijk}, \delta_{ijk}\right)$$

$$= \int_0^{\eta_0} f_{\mathrm{H}_{ijk}}\left(\eta_{ijk}\right) d\eta_{ijk} \cdot \int_{x-\frac{\ell_{str}}{2}-\frac{\ell_i}{2}\sin\theta_i}^{x+\frac{\ell_{str}}{2}+\frac{\ell_i}{2}\sin\theta_i} f_{\Psi_{ijk}}\left(\psi_{ijk}\right) d\psi_{ijk} \cdot \int_{\delta_0}^{+\infty} f_{\Delta_{ijk}}\left(\delta_{ijk}\right) d\delta_{ijk} \quad (6.15)$$

The probability of the collision estimate is controlled by the period of time being studied through η_0, the placement and geometry of the structure through the limits of integration on $f_\Psi(\psi)$, and the amount of force generated, δ_0. As derived in Eqn. 6.7, the path of the debris must overlap with the location of the structure. The force distribution derived in Eqn. 6.14 allows for the calculation of the probability of a collision that exceeds a force, δ_0, during time period η_0. The indices *i*, *j*, and *k* specify the type of debris, time within the span of the dataset, and structure of interest, respectively. Including the mitigation factor, *r*, requires an additional variable in Eqns. 6.6 and 6.15. It is best to specify its distribution as the complementary event, $f_{1\text{-}R}(1\text{-}r)$, representing the debris that is not prevented from passing debris-diversion devices. If the function describing the mitigative factor, $f_R(r)$, is known, then the complementary event is a function translation. Then,

$$f_{P(Collision)}(\eta, \psi, \delta, r) = f_H(\eta) \cdot f_\Psi(\psi) \cdot f_\Delta(\delta) \cdot f_R(1-r) \quad (6.16)$$

Because of the assumption of independence between subevents, layered multidimensional convolution integrals based on the concept introduced in Eqn. 4.21 can be utilized to address the summations over *i*, *j*, and *k* for each type of debris, time interval, and structure.

$$f_{P_I}(\eta,\psi,\delta) = \left(f_{P_{i=1}} * f_{P_{i=2}} * \ldots * f_{P_{i=N_{jk}}}\right)(\eta,\psi,\delta) \tag{6.17}$$

$$f_{P_J}(\eta,\psi,\delta) = \left(f_{P_{I,\,j=1}} * f_{P_{I,\,j=2}} * \ldots * f_{P_{I,\,j=M_k}}\right)(\eta,\psi,\delta) \tag{6.18}$$

$$f_{P_K}(\eta,\psi,\delta) = \left(f_{P_{I,\,J,\,k=1}} * f_{P_{I,\,J,\,k=2}} * \ldots * f_{P_{I,\,J,\,k=Q}}\right)(\eta,\psi,\delta) \tag{6.19}$$

6.4. Illustrative Event: Impact of Lost Shipping Containers

6.4.1. Estimating P(Collision) with a Single Shipping Container

Consider the risk of shipping containers with 6.1 m (20 ft) and 12.2 m (40 ft) length classifications colliding with a single structure. To model this scenario let $N = 2$, $M = 1$, and $Q = 1$. In this example, only the lateral position in the channel is addressed, with no assumptions made about level of submergence or buoyancy of containers. Evaluating P(*Collision*) requires specifying the parameters of the probability distributions for $f_H(\eta)$, $f_\Psi(\psi)$, $f_\Theta(\theta)$, $f_L(\ell)$, $f_V(v)$, $f_K(\kappa)$, and $f_M(\mu)$.

Allow $f_H(\eta)$, the probability that a certain type of debris becomes waterborne, to be described by an exponential distribution. An exponential distribution is given by

$$f_Y(y) = \lambda e^{-\lambda y} \tag{6.20}$$

where, λ is the rate parameter and $y \geq 0$. If the event of debris entering a waterway and becoming waterborne is thought of as a Poisson process, then the time between events can be modeled as an exponential distribution. Then, for an interval of time being studied, the probability of becoming waterborne is dependent on the time for the event to occur and

the probability of the event occurring within η_0. The rate parameter can be assigned for each debris type based on the reason the debris becomes waterborne, i.e. rate of occurrence of storms and flooding, container ship spills, etc. For this example, let $\lambda_{(i = 1,2)} = 0.0125$, which is equivalent to an 80-year return period. This emulates the event produced by Typhoon Nari in 2001, which caused over 1000 shipping containers to be swept into the Keelung River Basin in Taiwan (Lee et al, 2006).

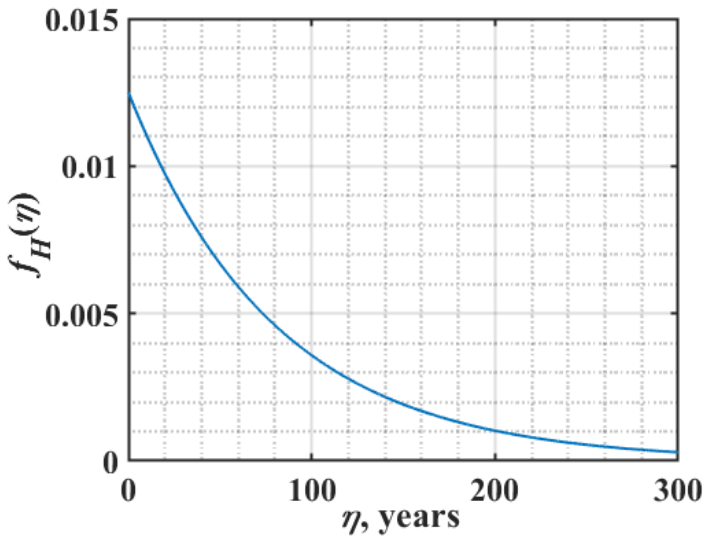

Figure 6.3 Exponential distribution function characterizing the occurrence of a debris generating event with an 80-year return period

Allow the functions characterizing the mass, $f_M(\mu)$, stiffness, $f_K(\kappa)$, and velocity, $f_V(v)$, to be described by lognormal distributions. Use of this density function assumes that the natural log of a random variable is normally distributed. The lognormal distribution is given by

$$f_Y(y) = \frac{1}{y\,\zeta_Y\sqrt{2\pi}} \exp\left[-\frac{1}{2}\left(\frac{\ln y - \lambda_Y}{\zeta_Y}\right)^2\right] \tag{6.21}$$

$$\zeta_Y^2 = \mathrm{Var}(\ln y) = \ln\left[1 + \left(\frac{\sigma_Y}{\mu_Y}\right)^2\right] \tag{6.22}$$

$$\lambda_Y = \mathrm{E}(\ln y) = \ln \mu_Y - \frac{1}{2}\zeta_Y^2 \tag{6.23}$$

where, λ_Y and $(\zeta_Y)^2$ are the expected value and variance of ln(y), respectively, and the support is 0 inclusive to ∞. The restriction of this probability density function to the positive domain is ideal for random variables such as these that will not take negative values. For defining the mass and stiffness, ASCE 7-16 Table 6.11-2 (ASCE, 2017) states the typical mass (weight) of a 6.1 m (20 ft) shipping container as approximately 2,270 kg (5 kips) empty and 13,150 kg (29 kips) loaded with a stiffness of 42,900 kN/m (245 kip/in). A 12.2 m (40 ft) shipping container is typically 3,810 kg (8.4 kips) empty and 17,240 kg (38 kips) loaded with a stiffness of 29,800 kN/m (170 kip/in). For illustrative purposes, the loaded mass of each container size was taken as the mean of each distribution describing the mass, that is $\mu_{M(i\,=\,1)}$ = 13,150 kg and $\mu_{M(i\,=\,2)}$ = 17,240 kg. The mean of each distribution describing the stiffness was taken as $\mu_{K(i\,=\,1)}$ = 42,900 kN/m and $\mu_{K(i\,=\,2)}$ = 29,800 kN/m. Standard deviations were set as $\sigma_{M(i\,=\,1,2)}$ = 2000 kg for mass and $\sigma_{K(i\,=\,1,2)}$ = 2000 kN/m for stiffness. If large amounts of surveyed data are available on container properties, then that information can alternatively be used to assign a distribution. For

other types of debris where direct estimates of stiffness are not available, the stiffness distribution parameters can be estimated using $k = EA/L$.

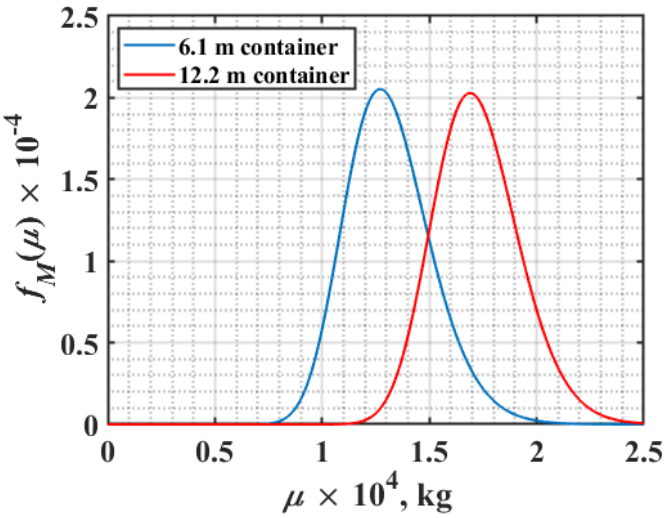

Figure 6.4 Lognormal distribution characterizing the mass of a shipping container of length 6.1 m or 12.2 m with parameters $\mu_{M(i=1)}$ = 13,150 kg, $\mu_{M(i=2)}$ = 17,240 kg, and $\sigma_{M(i=1,2)}$ = 2000 kg

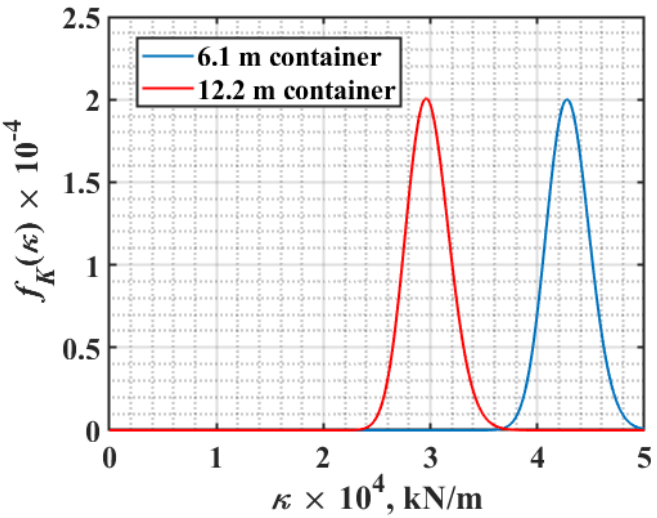

Figure 6.5 Lognormal distribution characterizing the stiffness of a shipping container of length 6.1 m or 12.2 m with parameters $\mu_{K(i=1)}$ = 42,900 kN/m, $\mu_{K(i=2)}$ = 29,800 kN/m, and $\sigma_{K(i=1,2)}$ = 2000 kN/m

When considering impact loading for large debris, it is often assumed that the debris velocity is equal to or less than the water flow velocity. The reduction allows for the possibility of capturing energy losses due to dragging against the channel bed or interactions between other debris (ASCE, 2017). The mean velocity of the distribution was selected to be $\mu_{V(i\,=\,1,2)}$ = 7 m/s because 4.5 m/s to 9 m/s is said to be a reasonable, expected flow speed for containers (Paczkowski et al., 2012). The standard deviation was set as $\sigma_{V(i\,=\,1,2)}$ = 2 m/s.

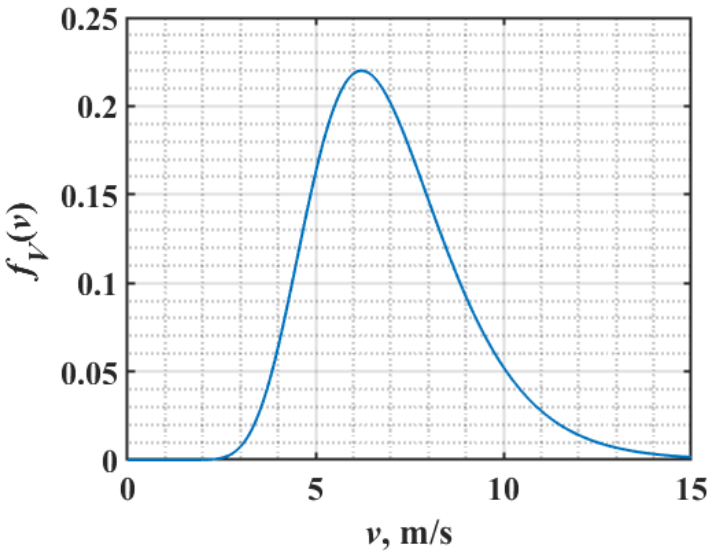

Figure 6.6 Lognormal distribution characterizing the flow velocity with parameters $\mu_{V(i\,=\,1,2)}$ = 7 m/s and $\sigma_{V(i\,=\,1,2)}$ = 2 m/s

Because the lengths of containers are standardized, the distribution describing the length, $f_L(\ell)$, is defined using discrete distributions valid for $\ell_{0,(i\,=\,1)}$ = 6.1 m (20 ft) and $\ell_{0,(i\,=\,2)}$ = 12.2 m (40 ft). The discrete distribution is given by

$$f_L(\ell) = \begin{cases} 1 & \ell = \ell_0 \\ 0 & \text{elsewhere} \end{cases} \tag{6.24}$$

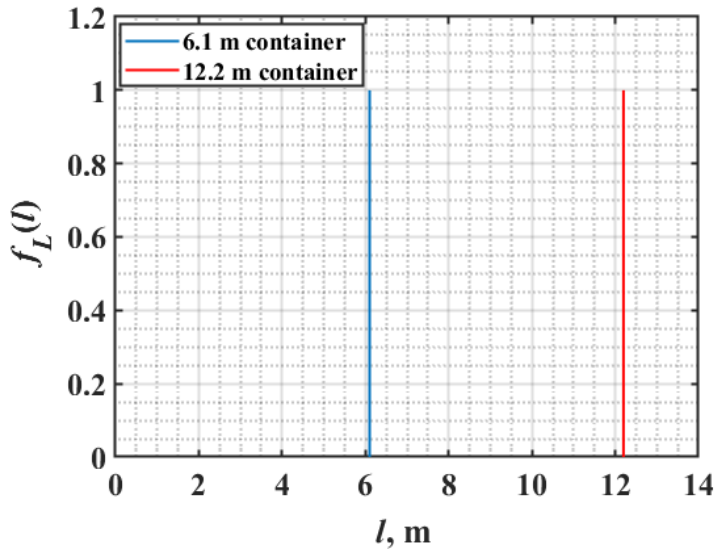

Figure 6.7 Discrete distributions characterizing the shipping container lengths of $\ell_{0,(i=1)}$ = 6.1 m and $\ell_{0,(i=2)}$ = 12.2 m

Although it is possible to assign a continuous distribution to describe how the container is likely to align itself with the flow, the orientation, $f_\Theta(\theta)$, is initially also assigned a discrete probability distribution with $\theta_{0,(i=1,2)} = 90°$. This assignment assumes that the containers will align to where the longest dimension is perpendicular to the flow to capture the largest surface area. A continuous distribution is recommended if the force equation is dependent on the debris orientation at impact (e.g., oblique impacts).

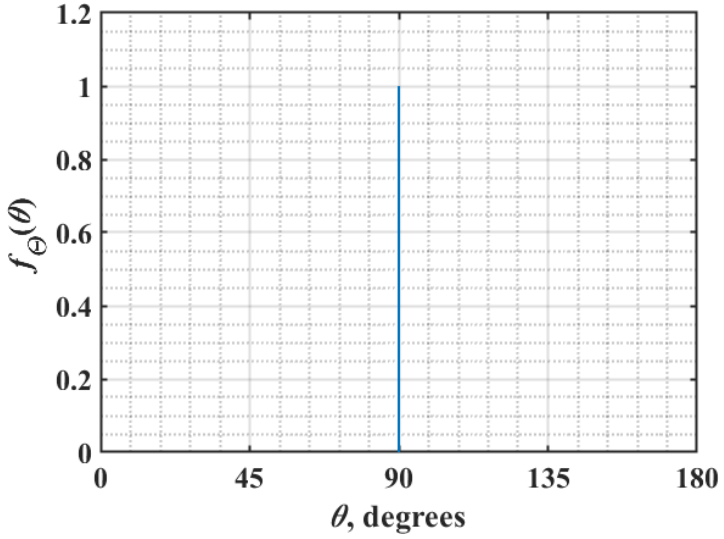

Figure 6.8 Discrete distribution characterizing the shipping container orientation as $\theta_{0,(i=1,2)}$ = 90°

Lastly, allow the path of the debris, $f_\Psi(\psi)$, to be described by a truncated normal distribution given by

$$f_Y(y) = \frac{\frac{1}{\sigma_Y\sqrt{2\pi}}\exp\left[-\frac{1}{2}\left(\frac{y-\mu_Y}{\sigma_Y}\right)^2\right]}{\Phi\left(\frac{b-\mu_Y}{\sigma_Y}\right) - \Phi\left(\frac{a-\mu_Y}{\sigma_Y}\right)} \tag{6.25}$$

The choice of the zeroed position can be made based on the path of highest flow or the center of the channel. With either designation the positive and negative domains are necessary to describe the position of the structure relative to the path, and the distribution must be truncated to fit the width of the channel, W_c, where the flow becomes zero. If it is assumed that the debris will most likely travel in the point of highest flow, then the mean

of $f_\Psi(\psi)$ can be assumed to always be zero. For this demonstration, the center of the channel and the point of highest flow are assumed to align, so the mean is defined as $\mu_{\Psi(i = 1,2)} = 0$. The more uncontrolled the flow and higher the flow velocity, the more the path distribution should flatten towards a uniform distribution, based on the standard deviation. For this example, a standard deviation of $\sigma_{\Psi(i = 1,2)} = 20$ is selected to flatten the distribution for a channel of width $W_c = 30$ m.

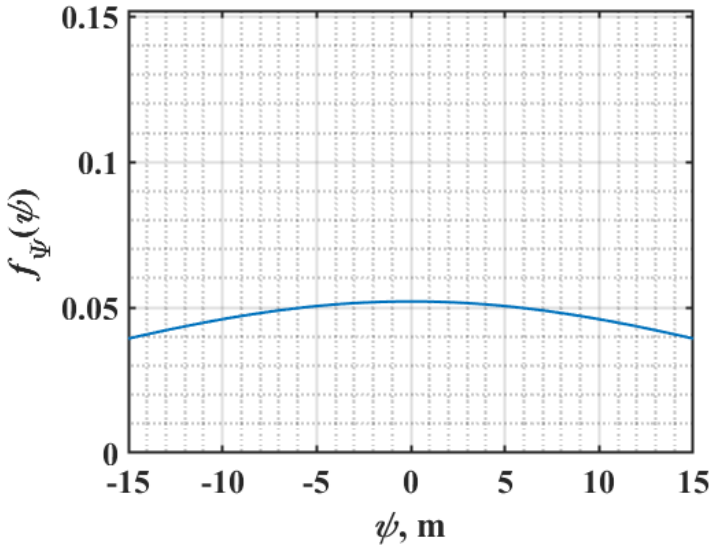

Figure 6.9 Normal distribution function characterizing the debris path with parameters $\mu_{\Psi(i = 1,2)} = 0$ and $\sigma_{\Psi(i = 1,2)} = 20$ for a channel width of 30 m

Using these parameter assignments for each variable, the distribution describing the force generated by an impact is given by

$$f_{\Delta_i}(\delta_i) = \int_0^{+\infty}\int_0^{+\infty} \frac{1}{\sqrt{\kappa_i\,\mu_i}} f_{V_i}\left(\frac{\delta_i}{\sqrt{\kappa_i\,\mu_i}}\right)\cdot f_{K_i}(\kappa_i)\cdot f_{M_i}(\mu_i)\,d\kappa_i\,d\mu_i$$

$$= \int_0^{+\infty}\int_0^{+\infty} \frac{1}{\sqrt{\kappa_i\,\mu_i}}\cdot\frac{1}{\frac{\delta_i}{\sqrt{\kappa_i\,\mu_i}}\,\zeta_{V_i}\sqrt{2\pi}}\exp\left[-\frac{1}{2}\left(\frac{\ln\frac{\delta_i}{\sqrt{\kappa_i\,\mu_i}}-\lambda_{V_i}}{\zeta_{V_i}}\right)^2\right] \tag{6.26}$$

$$\cdot\frac{1}{\kappa_i\,\zeta_{K_i}\sqrt{2\pi}}\exp\left[-\frac{1}{2}\left(\frac{\ln\kappa_i-\lambda_{K_i}}{\zeta_{K_i}}\right)^2\right]\cdot\frac{1}{\mu_i\,\zeta_{M_i}\sqrt{2\pi}}\exp\left[-\frac{1}{2}\left(\frac{\ln\mu_i-\lambda_{M_i}}{\zeta_{M_i}}\right)^2\right]d\kappa_i d\mu_i$$

$$\propto \int_0^{+\infty}\int_0^{+\infty}\left\{\frac{1}{\delta_i\,\kappa_i\,\mu_i}\exp\left[-\frac{1}{2}\left(\left(\frac{\ln\frac{\delta_i}{\sqrt{\kappa_i\,\mu_i}}-\lambda_{V_i}}{\zeta_{V_i}}\right)^2+\left(\frac{\ln\kappa_i-\lambda_{K_i}}{\zeta_{K_i}}\right)^2+\left(\frac{\ln\mu_i-\lambda_{M_i}}{\zeta_{M_i}}\right)^2\right)\right]\right\}d\kappa_i d\mu_i$$

To evaluate this integral, an independent sampling method was utilized to determine the distribution describing the force, δ. The result of this method is illustrated in Fig. 6.10a. Due to its shape, the force was fit with a lognormal distribution with parameters $(\mu_\Delta, \sigma_\Delta)_{(i\,=\,1)}$ = (5225.3, 1569.8) kN and $(\mu_\Delta, \sigma_\Delta)_{(i\,=\,2)}$ = (5099.5, 1533.4) kN using maximum likelihood estimates. The survival functions of these distributions illustrated in Fig. 6.10b give the probability of the force exceeding a value δ_0 for a specific debris type. For example, the probability of the force exceeding 5000 kN is approximately 50.3% and 46.8%, while the probability of exceeding 8000 kN is 5.3% and 3.6% for a 6.1 m loaded container and 12.2 m loaded container, respectively.

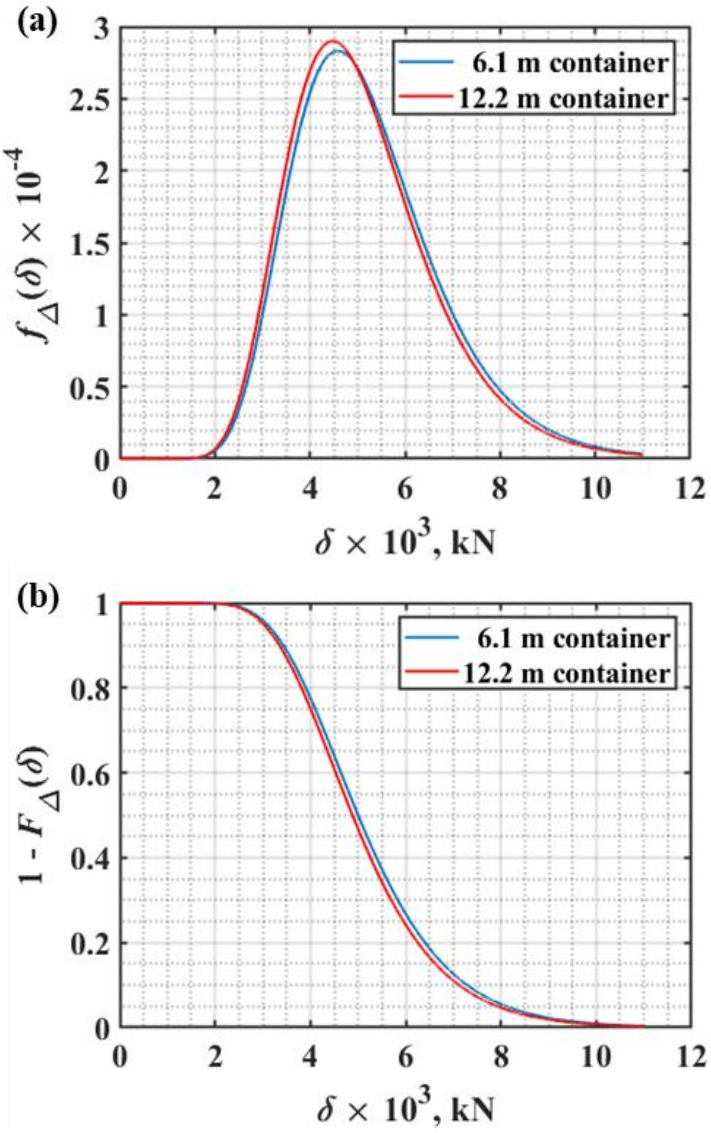

Figure 6.10 Lognormal probability of generating a collision force δ (a) probability density function and (b) survival function of δ for shipping containers with lengths 6.1 m (20 ft) and 12.2 m (40 ft)

The distribution estimating the probability of a collision at a force of at least δ_0 is given by

$$F_P(\eta,\psi,\delta) = \int_0^{\eta_0} f_{\mathrm{H}_{ijk}}\left(\eta_{ijk}\right) d\eta_{ijk} \cdot \int_{x-\frac{\ell_{str}}{2}-\frac{\ell_i}{2}\sin\theta_i}^{x+\frac{\ell_{str}}{2}+\frac{\ell_i}{2}\sin\theta_i} f_{\Psi_{ijk}}\left(\psi_{ijk}\right) d\psi_{ijk} \cdot \int_{\delta_0}^{+\infty} f_{\Delta_{ijk}}\left(\delta_{ijk}\right) d\delta_{ijk}$$

$$= \left\{\int_0^{\eta_0} \lambda_i \exp[-\lambda_i\,\eta]\, d\eta_i\right\} \cdot \left\{\int_{x-\frac{\ell_{str}}{2}-\frac{\ell_i}{2}\sin\theta_i}^{x+\frac{\ell_{str}}{2}+\frac{\ell_i}{2}\sin\theta_i} \frac{\frac{1}{\sigma_{\Psi_i}\sqrt{2\pi}}\exp\left[-\frac{1}{2}\left(\frac{\psi_i-\mu_{\Psi_i}}{\sigma_{\Psi_i}}\right)^2\right]}{\Phi\left(\frac{\frac{W_c}{2}-\mu_{\Psi_i}}{\sigma_{\Psi_i}}\right)-\Phi\left(\frac{\frac{-W_c}{2}-\mu_{\Psi_i}}{\sigma_{\Psi_i}}\right)} d\psi_i\right\}$$

$$\cdot\left\{\int_{\delta_0}^{+\infty} \frac{1}{\delta_i\,\zeta_{\Delta_i}\sqrt{2\pi}}\exp\left[-\frac{1}{2}\left(\frac{\ln\delta_i-\lambda_{\Delta_i}}{\zeta_{\Delta_i}}\right)^2\right] d\delta_i\right\}$$

$$= \left\{1-\exp\left[-\lambda_i\,\eta_0\right]\right\} \cdot \left\{\frac{\Phi\left(\frac{x+\frac{\ell_{str}}{2}+\frac{\ell_i}{2}\sin\theta_i-\mu_{\Psi_i}}{\sigma_{\Psi_i}}\right)-\Phi\left(\frac{x-\frac{\ell_{str}}{2}-\frac{\ell_i}{2}\sin\theta_i-\mu_{\Psi_i}}{\sigma_{\Psi_i}}\right)}{\Phi\left(\frac{\frac{W_c}{2}-\mu_{\Psi_i}}{\sigma_{\Psi_i}}\right)-\Phi\left(\frac{\frac{-W_c}{2}-\mu_{\Psi_i}}{\sigma_{\Psi_i}}\right)}\right\} \qquad (6.27)$$

$$\cdot\left\{1-\Phi\left(\frac{\ln\delta_{0,i}-\lambda_{\Delta_i}}{\zeta_{\Delta_i}}\right)\right\}$$

As illustrated in Fig. 6.11, for each calculation, the lateral position of the structure, *x*, is set at 0, as if the structure intersects with the path of highest flow and the width of the structure perpendicular to the flow, ℓ_{str}, is 3 m.

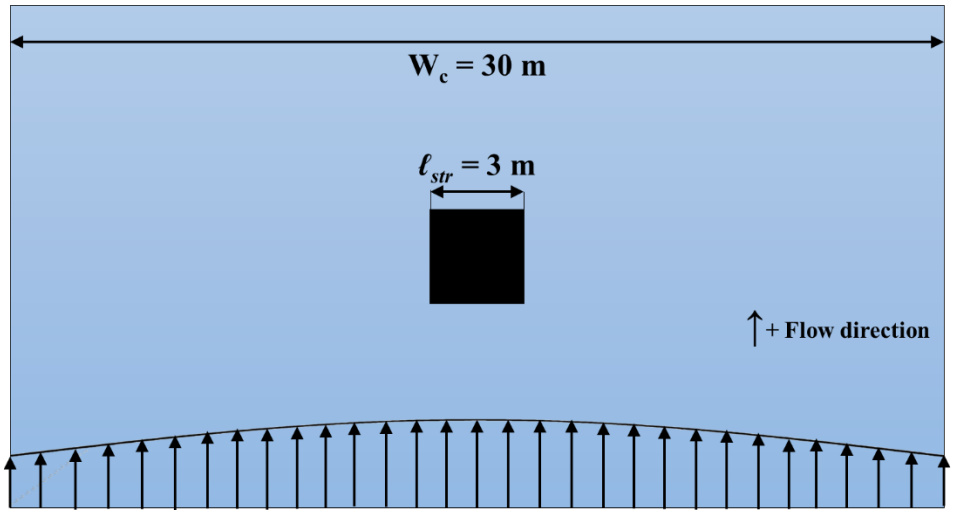

Figure 6.11 Flow conditions for example problem

Three-dimensional representation of the joint distribution, $f_{P(Collision)}(\eta,\psi,\delta)$, using the distribution assignments for $f_H(\eta)$, $f_\Psi(\psi)$, and $f_\Delta(\delta)$ and varying parameter values is illustrated by Fig. 6.12a, 6.12b, 6.12c, and 6.12d. The sensitivity of the joint distribution function to the definitions of the underlying distributions describing the sub-events becomes evident. Fig. 6.12a contains the original parameter definitions. In Fig. 6.12b, the mean of the exponential distribution describing η is increased. This is analogous to decreasing the return period of the debris-generating event. In Fig. 6.12c, the standard deviation of the normal distribution describing ψ is decreased to represent the waterborne debris following a more specified path. Lastly Fig. 6.12d illustrates an increased standard deviation in the lognormal distribution describing δ, which represents less certainty in the force generated by a collision. Visualizing how variations in the parameters used to express uncertainty in the assigned probability distributions in this manner reveals the

variability of the risk-model behavior and its sensitivity to parameter selection. Model visualization becomes more complex as additional variables and dimensions are added.

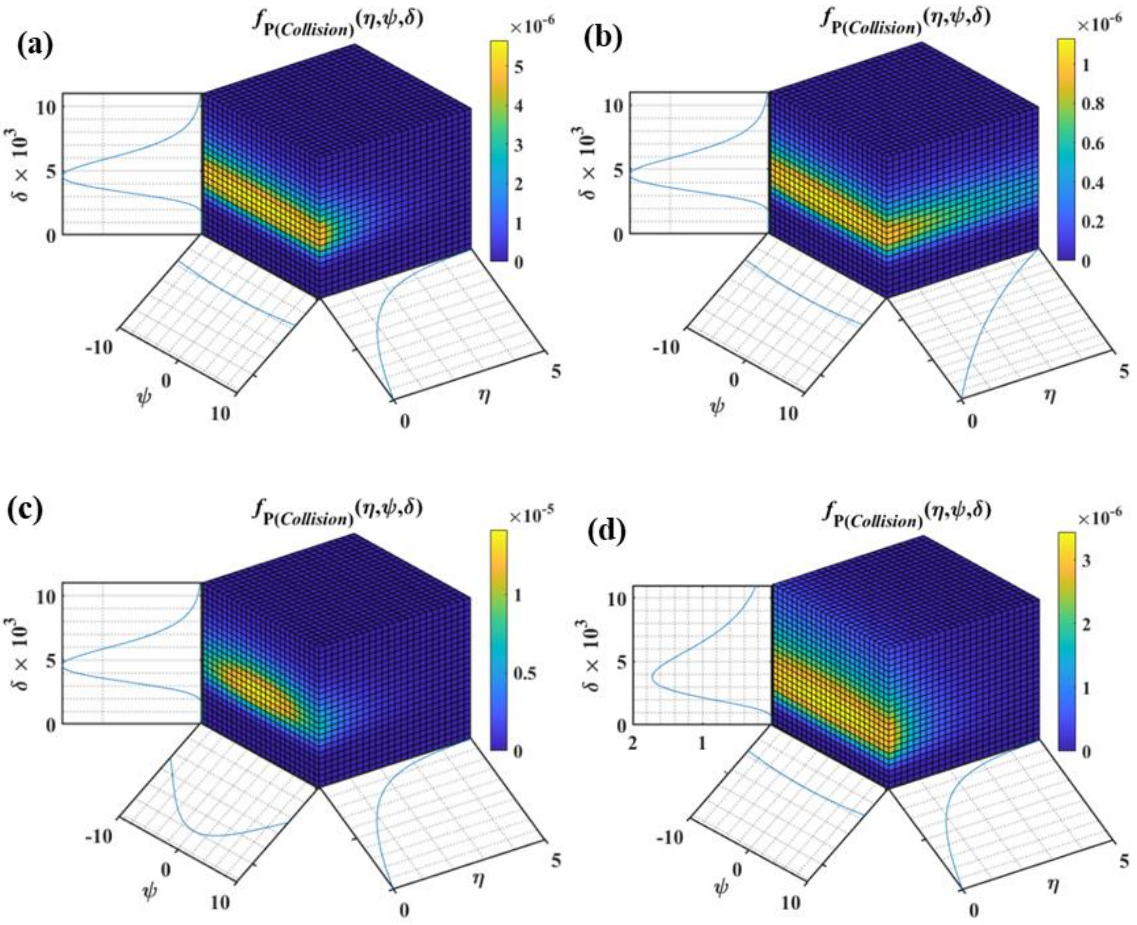

Figure 6.12 Illustration of the joint distribution functions and their sensitivity to (a) the original parameter definitions, (b) an increased mean for the exponential distribution describing η, (c) a decreased standard deviation for the normal distribution describing ψ, and (d) an increased standard deviation for the lognormal distribution describing δ.

The cumulative joint distribution function, $F_{P(Collision)}(\eta,\psi,\delta)$, describes the likelihood of a collision force of δ_0 or greater occurring within timeframe η_0 with a specified structure. For a 6.1 m container, the likelihood of a collision of force 5000 kN

or greater to occur within a year is 0.20% using an 80-year return period for the debris-generating event and positioning a 3 m wide structure at $x = 0$ within a 30 m wide channel. For a 12.2 m container, the same likelihood of collision is 0.31%. Figure 6.13 illustrates the probability of collision exceeding a force δ for each container size as a function of force for a debris-generating event occurring within a given year with a 1-year, 10-year, or 80-year return period. It is evident that lower return periods and larger debris each result in an increase in the likelihood of a collision. The likelihood of collision for a return period of 10 years increases to approximately 1.6% for a 6.1 m container and 2.5% for a 12.2 m container. The breakdown of that 2.5% risk of collision for a 12.2 m container is calculated as the product of a 54.2% chance of overlap, 46.8% chance of the force generated from a collision being at least 5000 kN, and a 10% likelihood of a debris-generating event occurring within a year.

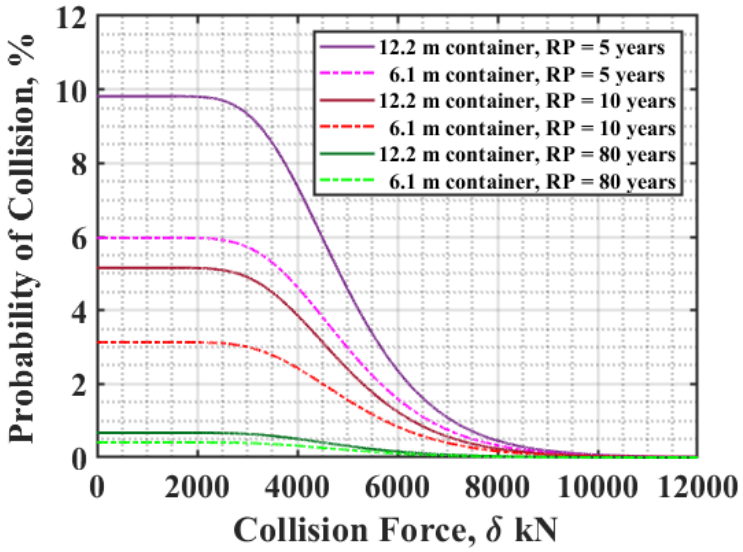

Figure 6.13 Probability of Debris Collision as a function of collision force δ and return period *RP*.

The union of collision events between the two container sizes to obtain the likelihood of collision from either container size requires a convolution integral between $f_{P(i=1)}(\eta,\psi,\delta)$ and $f_{P(i=2)}(\eta,\psi,\delta)$ as introduced in Eqns. 4.21 and 6.17. Because the rate of occurrence for the debris-generating event is defined as the same event for both debris types, the convolution is completed over only the force and overlap distributions. This resulted in a combined risk of collision of approximately 0.49% due to a 51.7% chance of overlap, 76.6% chance of the collision force exceeding 5000 kN, and a 1.25% likelihood that a debris-generating event occurs within a year. The combined probability of collision exceeding a force δ as a function of force for a debris-generating event occurring within a given year with a 5-year, 10-year, or 80-year return period is illustrated in Figure 6.14.

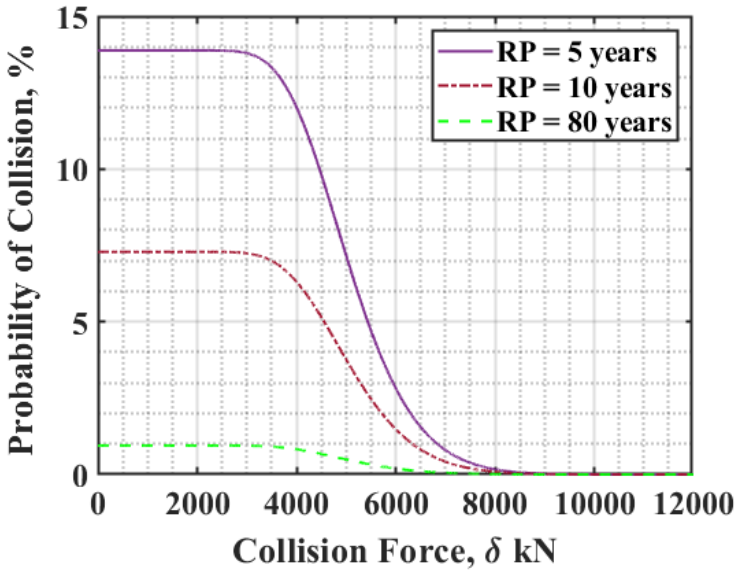

Figure 6.14 Probability of Debris Collision due to either container size as a function of collision force δ and return period *RP*.

6.4.2. Modeling Multiple Container Collisions and Accumulation of Debris

The current model evaluates the risk of a broadside impact for a single container of length 6.1 m or 12.2 m. The force equation used does not account for oblique impacts or multiple collisions within the same event, whether simultaneously as a cluster or sequentially. For a cluster of debris entering a waterway, estimates on the center of mass, the "stiffness", and the "mass" of the cluster are required to treat the situation as a single collision. The cluster would theoretically collide with the structure and potentially break apart.

The approach for sequential collisions involves additional considerations. For each specific debris type, accounting for multiple collisions for a single debris-generating event is the intersection of collision events and therefore the product over the number of containers for each specific size. The process of each individual collision is similar to the

approach used previously, however extra consideration must be given to the probability of overlap based on the channel characteristics, debris path, and structure dimensions and to the probability distribution describing the force generated by each collision. The debris-generating event is still defined based on the type of debris. The union across debris types would still require a convolution as applied previously, but the convolution integral would occur after each product over the number of items per type is taken. Using the discrete representation that is,

$$\mathrm{P}(\mathit{Collision}) = \left\{ \sum_{i=1}^{N} \eta_i \times \left[\prod_{h=1}^{D_i} \left(\psi_{hi} \mid \theta_{hi} \cap \nu_{hi} \cap \mu_{hi} \cap \ell_{hi} \right) \times \left(\delta_{hi} \mid \theta_{hi} \cap \nu_{hi} \cap \mu_{hi} \cap \kappa_{hi} \right) \times e_{hi} \right] \right\} \quad (6.28)$$

where D_i is the number of debris elements for type i that enter the waterway, and each sub-event must be adjusted based on the debris element and the variable e_{hi} describes the stability of each collision. Adjusting the distribution functions for the force generated and probability of overlap requires an assumption on whether the debris element that strikes the structure prior to element h is shed. The shedding of a debris element is dependent on the stability of the collision. If the previous elements remain, then for the collision force calculation, they act as a buffer or damper that lessens the impact force with each added container. Because of this occurrence, instead of considering the impact force it becomes more valuable to examine the generation of other lateral forces, especially the drag force. The drag force is given by

$$F_D = \frac{1}{2}\,\rho\,(v_w)^2 C_D\,A \tag{6.29}$$

where ρ is the fluid density, v_w is the fluid velocity, C_D is the drag coefficient, and A is the projected area. Then, a drag coefficient will need to be assumed based on an estimated accumulation shape. Derivation of the analytical form of the probability distribution function for the drag force proceeds in a manner analogous to the derivation of the impact force distribution in Eqns. 6.9 through 6.14.

$$f_{\Delta,V_w}(\delta,v_w) = \frac{f_{A,V_w}(a,v_w)}{\left|\det\left\{\frac{\partial(\delta,v_w)}{\partial(a,v_w)}\right\}\right|} \tag{6.30}$$

$$= \frac{f_A(a)\cdot f_{V_w}(v_w)}{\left|\det\begin{Bmatrix}\frac{\partial\delta}{\partial a} & \frac{\partial\delta}{\partial v_w}\\ \frac{\partial v_w}{\partial a} & \frac{\partial v_w}{\partial v_w}\end{Bmatrix}\right|}$$

$$= \frac{f_A(a)\cdot f_{V_w}(v_w)}{\left|\det\begin{Bmatrix}\frac{1}{2}\,\rho\,(v_w)^2 C_D & \rho v_w C_D\,A\\ 0 & 1\end{Bmatrix}\right|}$$

$$= \frac{f_A(a)\cdot f_{V_w}(v_w)}{\frac{1}{2}\,\rho\,(v_w)^2 C_D}$$

$$= \frac{f_A\left(\frac{2\delta}{\rho\,C_D\,(v_w)^2}\right)\cdot f_{V_w}(v_w)}{\frac{1}{2}\,\rho\,(v_w)^2 C_D} \tag{6.31}$$

Then, the marginal density function in terms of force can be calculated from the joint distribution derived in Eqn. 6.31 by integrating over the fluid velocity. This gives a drag force distribution function of

$$f_{\Delta}(\delta) = \int_{-\infty}^{+\infty} f_{\Delta, V_w}(\delta, v_w)\, dv_w$$

$$= \int_{-\infty}^{+\infty} \frac{2}{\rho\, C_D\, (v_w)^2}\; f_A\left(\frac{2\delta}{\rho\, C_D\, (v_w)^2}\right) \cdot f_{V_w}(v_w)\, dv_w \qquad (6.32)$$

where the distribution functions $f_{Vw}(v_w)$ and $f_A(a)$ describe the velocity of the fluid and the projected area of the accumulation, respectively. Here the fluid density and drag coefficient are treated as constants and therefore discrete values. Then probability of the force exceeding some value, δ_0 is given by

$$\mathrm{P}(\delta \geq \delta_0) = \int_{\delta_0}^{+\infty} f_{\Delta}(\delta)\, d\delta$$

$$= \int_{\delta_0}^{+\infty} \int_{-\infty}^{+\infty} \frac{2}{\rho\, C_D\, (v_w)^2}\; f_A\left(\frac{2\delta}{\rho\, C_D\, (v_w)^2}\right) \cdot f_{V_w}(v_w)\, dv_w\, d\delta \qquad (6.33)$$

The likelihood of overlap can be expected to grow with the number of accumulated elements, as the addition of accumulated elements leads to an increase in the effective width of the structure. In the analytical representation of the probability distribution

functions, this will influence the limits of integration on Eqn. 6.7 for each debris element and each iteration of the simulation.

6.4.3. Estimating P(Collision) for Accumulated Shipping Containers

Rather than developing analytical formulas as in the first example for impact loading, this application will demonstrate the use of probabilistic based simulations based on the identified sub-events. To allow for the example to be envisioned two-dimensionally, the container draft is held constant at 0.914 m for all containers, the nominal draft of a full container (Paczkowski et al., 2012). Only 6.1 m containers are included in this simulation of near-simultaneous collisions. The simulation begins with determining the number of containers to enter the waterway. This value can be treated as a random variable, however, here it is set at 50 waterborne containers (6.1 m) per simulation. The lateral position of a container in the waterway is randomly drawn from the normal distribution for the debris path ψ, $f_\Psi(\psi)$. An orientation θ is randomly drawn using a normal distribution truncated from 0° to 180° with parameters $\mu_\theta = 90°$ and $\sigma_\theta = 45°$, and the projected length of the element is then calculated. The stability of the collision is assigned based on the position of the debris element relative to the position of the structure. The closer the element is to the structure, the more likely it is to interact and become caught. The tipping point around the corner of the structure for an element is used to determine develop a piecewise function that characterizes the stability. The maximum of the piecewise function was a probability of $e_h = 0.95$ for an interval of $-\ell_{str}$ to ℓ_{str} and linearly declines to 0 in either direction to $\pm(\ell_{str} + \ell/2)$. The stability assigned is used to

draw from a Bernoulli distribution, which yields a 1 or 0 to determine if the debris becomes stuck. For each element that becomes stuck, the width of the structure is updated to account for the increased effective width. This process is repeated sequentially for every debris element.

Because the collisions are considered to be near-simultaneous, the drag force from the accumulated debris is calculated after all the debris elements have been considered. The projected area is estimated by taking the product of the final width and the nominal draft. As illustrated in Fig. 6.15a and Fig. 6.15b, the random selection from probability distributions allows the configuration of the accumulated debris to change with each simulation. Only the elements that become caught during the simulation are shown. In Fig. 6.15a, the longitudinal position of each element corresponds to the order in which the debris elements enter the accumulation. Alternatively, Fig. 6.15b assigns the same longitudinal position to each debris element as only the width of the accumulation is used to conservatively calculate the drag force. The global geometry of the accumulation is not utilized.

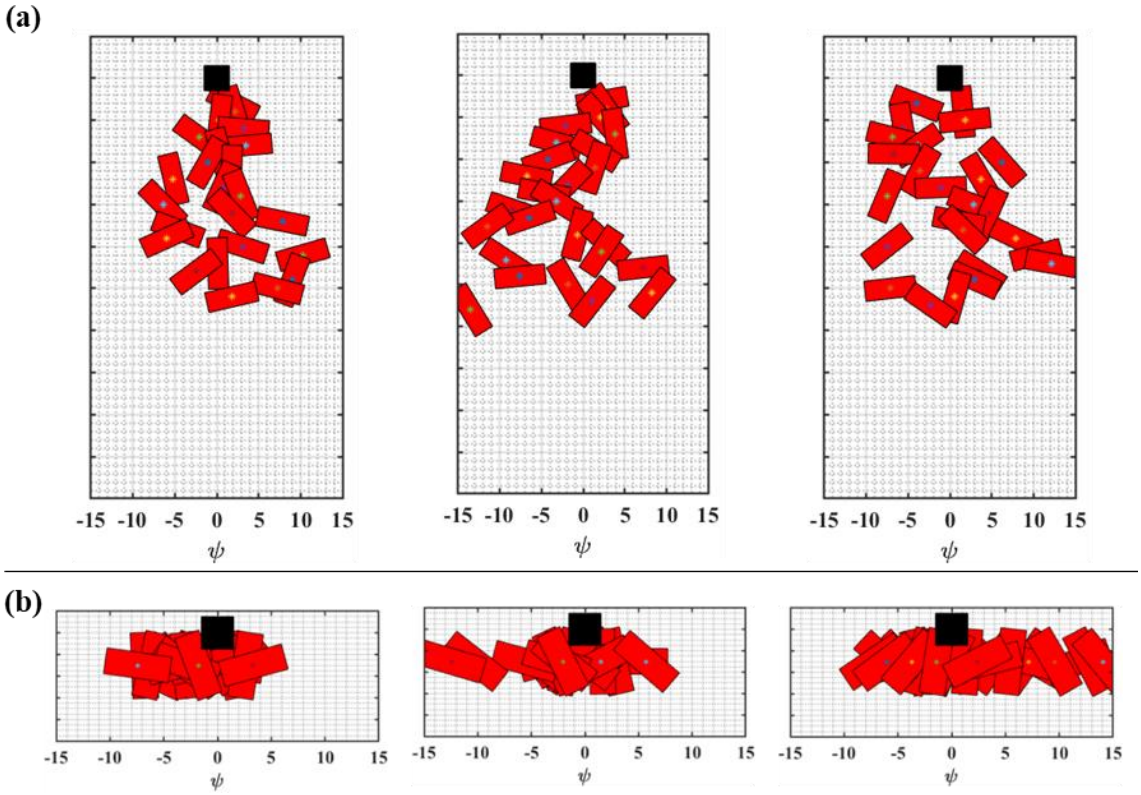

Figure 6.15 Example container spill simulations used to calculate the lateral accumulated area and drag force.

The flow velocity, v_w, is drawn from a lognormal distribution as with the previous application, but with parameters μ_{vw} = 10 m/s and σ_{vw} = 2 m/s because the flow velocity is expected to be greater than the speed at which the debris was traveling. The drag coefficient, C_D = 2.1 is approximated from the plot generated by Bearman and Trueman (1972) from experimental data on rectangular prisms. The fluid density is assigned as the density of water, ρ_w = 997 kg/m^3. This simulation is repeated 1000 times, each time calculating the drag force, to generate a histogram of the drag force that estimates a distribution $f_\Delta(\delta)$. The resulting histogram was fit with a lognormal distribution with parameters μ_δ = 1911.5 kN and σ_δ = 1121.6 kN.

With knowledge of the force distribution, the probability of collision generating a drag force greater or equal to some value δ_0 can be calculated by incorporating the probability of the debris generating event occurring, 0.0125. For a drag force of 5000kN or greater the resulting probability of collision is 0.03% with a 2.07% chance that the containers will collide in a manner that generates a force of at least 5000kN and a 1.25% likelihood of the debris generating event occurring. The probability increases to 0.17% for a drag force of at least 3000kN with a 13.5% probability that the containers will collide in a manner that generates a drag force of 3000kN or greater and 1.25% probability of the debris generating event occurring. Similar to the previous application, the probability of collision exceeding a drag force δ is illustrated in Fig. 6.16. as a function of force for a debris-generating event occurring within a given year with a 5-year, 10-year, or 80-year return period. Each of these events were based on 50 waterborne containers. This simulated probabilistic approach provides a computationally efficient process for making conservative predictions compared to particle tracking methods and computational fluid dynamics techniques.

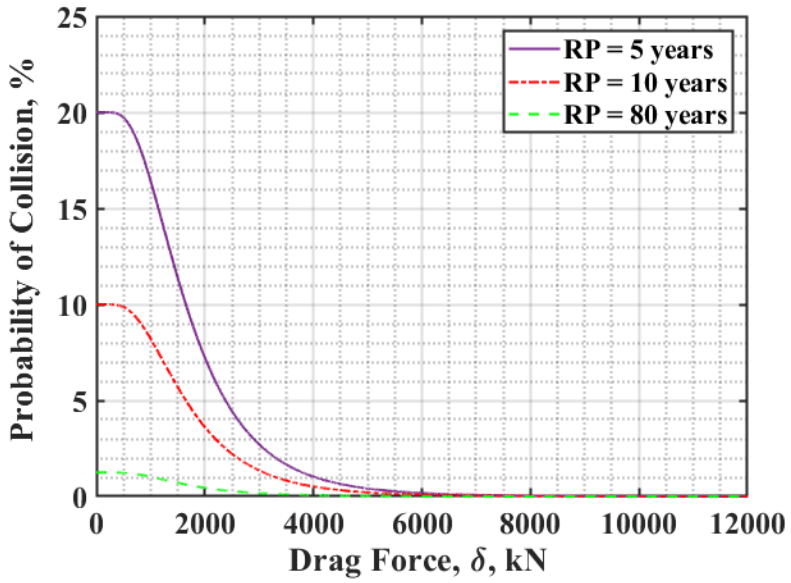

Figure 6.16 Probability of Debris Collision as a function of collision drag force δ and return period *RP*.

6.5. Discussion and Conclusions

The ability of the model to address the increasing complexity for a specific event was illustrated in the example of the floating debris impact with a structure, as the impact evolved from single to multiple impacts and debris accumulation. The incorporation of existing design formulae relevant to a specific event was illustrated prior to any numerical evaluation and the comparison of different design criteria could also be incorporated into the eventual numerical simulations. The examples also demonstrated risk-based model predictions could be used to predict the magnitude of specific events as a function of the probability of occurrence for specified return periods. As the complexity of the modeling process increased, the value of visualizing the process of debris accumulation was shown to be of importance in understanding the numerical predictions. The demonstrated

example is based on the usage of the unmodified flexible impact model and must be modified if completing calculations for other force models. The parameters of the distributions describing the mass, stiffness, and velocity are dependent on data collection. Laboratory testing and surveyed data will aid in assigning parameter values and determining the relationships between variables so that accuracy can be increased and events such as force due to oblique impacts can be explored and included. Other types of debris where lengths are not standardized, such as woody debris, can also be explored using continuous distributions rather than the discrete distributions used in this application to represent the lengths of shipping containers. Considerations for the vertical position of debris can also be explored by expanding the model. Calculations from this risk model can be used for design decisions given its ability to adjust for channel morphology and behavior, structural properties, and debris types. The rate of occurrence of a debris-generating event was based on the return period of a storm event in the presented example, however other types of debris-generating events can also be explored. Recognizing the flexibility of the formulation presented, one could modify the event focus to be the bridge deck, make adjustments to the channel morphology and flow behavior, modify the structural properties and geometry, and interchange the debris type. Then, for a given structure, the probability of a collision occurring given specific design considerations can be calculated, and designs can be adjusted in order to minimize the risk of collision.

CHAPTER 7

CONCLUSIONS

The introduction of debris into aquatic environments has long resulted in damaged ecosystems and infrastructure. The consequences of waterborne debris are closely related to its origin and characterization which can be incorporated into carefully defined sub-events that capture the uncertainty and randomness of these processes. This research provides the ability to quantify the risks associated with waterborne debris, which is important for developing preventative strategies and addressing concerns.

In this research, probability theory and statistical concepts are adopted to develop a generalized framework for quantifying risk that aids in decision making and design processes. The methodology developed can be used to create new and more complex quantitative risk models for a wide variety of applications, or it can be used to update existing risk-based models. The formulation of the models to assess the risk of whale entanglement due to fishing gear and the risk of collision of large debris with infrastructure in this research has demonstrated the flexibility of this approach. Parametric definitions for the probability distributions functions carefully selected to represent the identified sub-events reveal the model sensitivity and the ability of the model to adapt for varying amounts of data.

The main objectives of this research were to conduct literature searches to collect and examine relevant data and information available in open literature; explore the applications of other types of models, research findings, and current practices/procedures developed to address the physical processes related to waterborne debris generation and

behavior; and develop a probabilistic predictive model that utilizes reported data and available information that has the ability to evaluate the risks associated with whale entanglement due to waterborne debris and the risks associated with impact loading on bridge piers due to collisions from waterborne. Implementation and evaluation of the probabilistic predictive model's capacity to make predictions and its sensitivity to parameter definitions aided in identifying areas for model improvement.

In sections 1, 2, and 3 the introduction, background, motivation, significance, objectives, and research overview are presented. These sections establish the key information needed to initiate the understanding of the problem of waterborne debris, specifically its relation to the entanglement of whales in fishing gear and interactions between large debris and infrastructure. Other risk models are briefly explored. The problem of lost fishing gear was found comparable to the phenomenon known as ghost fishing. Laboratory and field experiments for large debris were investigated.

In section 4, the methodology for developing an event-specific risk-based model is established. Basic sub-events that can describe any event are identified as physical characteristic, temporal conditions, and spatial conditions. Specific applications require focused descriptions of each sub-event. The mathematical representation of the generalized model is developed through the introduction of probability theory and statistical concepts. Methods for generating predictions are discussed and four main methods are isolated that use either discrete representations of data to calculate statistical measures of central tendency or modifiable continuous probability density functions to additionally evaluate statistical measures of variability.

Section 5 concentrates on the application of whale entanglement along the US North Atlantic coastline and the Pacific coastline. The identified sub-events are the fishing gear encounter is a type that can result in entanglement, which is a combination of the proportions of gear types that are used in the region and the types of gear that have been observed to cause entanglements; whales are present in the region; the proportion of regional fishing gear that is lost annually or over some specified time scale; and the removal rate of fishing gear from the regional body of water. The discrete model analysis demonstrated its ability to generate average, multi-year, and multi-regional estimates. Several visualization techniques were utilized to demonstrate the influence of each sub-event on the overall risk calculation. Probability distributions were incorporated into the model by treating each sub-event as a random variable. Visualization demonstrated how to capture uncertainty in the data and model parameters. The probability of exceedance was used to calculate the likelihood of underestimating the true number of whale entanglements using the current definitions of the sub-events and generated data.

Section 6 addresses debris-structure interactions in the form of collisions and accumulations of shipping containers at a fixed structure. The identified collision sub-events are that debris enters the body of water and becomes waterborne, the path of the waterborne debris intersects with the placement of the structure causing a spatial overlap, and the waterborne debris collides at a certain force. Accumulation included an additional sub-event related to the stability of the accumulation at the structure. Two illustrative examples were conducted to demonstrate the flexibility of the model utilizing sampling and simulation methods to generate predictions. The first example estimated the

probability of collision with a single container of length 6.1 m or 12.2 m using the unmodified flexible impact model. The second example estimated the probability of collision for accumulated shipping containers of length 6.1 m using a drag force model. These examples demonstrate how detailed design specifications can be incorporated into the risk model.

The ability to create risk models that can be tailored to specific applications is invaluable. Many natural systems and processes contain inherent randomness that deterministic models cannot capture. Using a risk model requires understanding of the fundamental events that dictate the function of a system. Implementing risk models can generate solutions to reduce losses by specifically targeting risk reductions in the fundamental events. It can be concluded from this research that the generalized event specific risk-based model developed is suitable for generating valid predictions for the applications studied. The probability density functions selected were tailored to fit each sub-event. As the knowledge of each application grows, the model allows for the alteration of both function and parameter selection.

For future work it is recommended that additional data be collected for each application as it becomes available and additional sub-events identified and added to further improve the depth and accuracy of the models. For the application of whale entanglement, the current model considers the temporal overlap between fishing seasons and whale migration routes. Knowledge of the physical migration routes of whales using whale siting data to overlap with fishing vessel locations to model spatial variability will enhance the strength of the model predictions. For the application of debris-structure

interactions, a deeper understanding of how debris accumulations form, including predictions of vertical accumulation geometry, and the stability of non-instantaneous accumulations can be explored. The relative motion between the containers and structure can also be examined by focusing on redefining the probability of overlap between objects. Other hydrodynamic or hydrostatic forces can be investigated in a similar manner to address other phenomena such as erosion and the depth of scour at bridge piers or wave action at breakwater structures. Validation of the model results can be completed through laboratory and field testing. Future studies may consider other applications for which to adopt a quantitative risk model. Applications must be carefully chosen based on the appropriateness of a risk model because although the risk model remains valid, it may not be feasible to pursue.

REFERENCES

Aghl, P.P., Naito, C.J., and Riggs, H.R. (2014). "Full-scale experimental study of impact demands resulting from high mass, low velocity debris." *Journal of Structural Engineering*. 140(5): 04014006.

American Association of State Highway and Transportation Officials (AASHTO) (2012). *AASHTO LFRD Bridge Design Specifications*. AASHTO. Washington, D.C.

Andreescu, T. and Feng, Z. (2004). *A Path to Combinatorics for Undergraduates: Counting Strategies*. Boston, US: Birkhäuser.

Ang, A.H-S. and Tang, W.H. (1984). *Probability Concepts in Engineering Planning and Design: Vol II Decision, Risk, and Reliability*. New York, US: John Wiley & Sons, Inc.

Ang, A.H-S. and Tang, W.H. (2007). *Probability Concepts in Engineering: Emphasis on Applications in Civil & Environmental Engineering*. New York, US: John Wiley & Sons, Inc.

ASCE (2017). *Minimum design loads and associated criteria for buildings and other structures*. Reston (VA).

Aven, T. (2008). *Risk Analysis: Assessing Uncertainties Beyond Expected Values and Probabilities*. Chichester, UK: John Wiley & Sons, Ltd.

Barnes, D.K.A., Galgani, F., Thompson, R.C., and Barlaz, M. (2009). "Accumulation and fragmentation of plastic debris in global environments." *Phil. Tran. R. Soc B*. 364:1985-1998.

Benjamin, J.R. and Cornell, C.A. (2014). *Probability, Statistics, and Decision for Civil Engineers*. Mineola, US: Dover Publications, Inc.

Bearman, P.W. and Trueman, D.M. (1972). "An investigation of the flow around rectangular cylinders." *The Aeronautical Quarterly*. 23(3): 229-237.

Brown, A.H. and Niedzwecki, J.M. (2020). “Assessing the risk of whale entanglement with fishing gear debris.” *Marine Pollution Bulletin*. 161(2020): 111720.

Brown, J. and Macfadyen, G. (2007). “Ghost fishing in European waters: Impacts and management responses.” *Marine Policy*. 31(2007): 488-504.

Burkardt, J. (2014, 17 Oct). *The Truncated Normal Distribution*. Tallahassee, FL: Department of Scientific Computing, Florida St University. Retrieved from <https://people.sc.fsu.edu/~%20jburkardt/presentations/truncated_normal.pdf>

Castro, F.S.d., Katsuno, E.T, Assi, G.R.d.S., and Dantas, J.L.L. (2018). “Structural investigation of the log accumulation effect in a debris containment grid through towing tank experiments.” Proceedings of the ASME 2018 37th International Conference on Ocean, Offshore and Arctic Engineering. Madrid, Spain. OMAE2018-78097.

Chang, F.F.M and Shen, H.W (1979). “Debris Problems in River Environment” Fairfax (VA): U.S. Department of Transportation Federal Highway Association (US); 1979 Mar. Report No. FHWA-RD-79-62

Chuenpagdee, R., Morgan, L.E., Maxwell, S.M., Norse, E.A., and Pauly, D. (2003). “Shifting gears: assessing collateral impacts of fishing methods in U.S. waters.” *Frontiers in Ecology and the Environment*. 1(10): 517-524.

Crum, N., Gowan, T., Krzystan, A., and Martin, J. (2019) “Quantifying risk of whale-vessel collisions across space, time, and management policies.” *Ecosphere*. 10(4):e02713.

Daniel, P., Jan, G., Cabioc’h, F., Landau, Y., and Loiseau, E. (2002). “Drift Modeling of Cargo Containers.” Spill Science & Technology Bulletin. 7(5- 6): 279-288.

Design Manual for Roads and Bridges (DMRB). (2012) “The Assessment of Scour and Other Hydraulic Actions at Highway Structures.” *Design Manual for Roads and Bridges BD 97/12*. London. Retrieved from <https://www.standardsforhighways.co.uk/dmrb/ >

Diehl, T.H. (1997). “Potential Drift Accumulation at Bridges.” Nashville (TN): U.S. Department of Transportation Federal Highway Administration (US); 1997 Apr. Report No. FHWA-RD-97-028.

Discover New England. (n.d.). *Whale Watch Tours*. Retrieved from <https://www.discovernewengland.org/things-do/whale-watch-tours>

Dolman, S.J., Asmutis-Silvia, R., and Ryan, C. (2018). "Whale Entanglement – a 21st-Century Challenge in the Ocean." *Animal Welfare in a Changing World*. Wallingford, UK: CAB International. p. 14-23.

Eriksen, M., Lebreton, L.C.M., Carson, H.S., Thiel, M., Moore, C.J., Borerro, J.C., Galgani, F., Ryan, P.G., and Reisser, J. (2014). "Plastic Pollution in the World's Oceans: More than 5 Trillion Plastic Pieces Weighing over 250,000 Tons Afloat at Sea." *PLOS ONE*. 9(12): e111913.

Gilman, E., Chopin, F., Suuronen, P, and Kuemlangan B. (2016). "Abandoned, lost and discarded gillnets and trammel nets: Methods to estimate ghost fishing mortality, and the status of regional monitoring and management." FAO Fisheries and Aquaculture Tech. Paper No. 600. Retrieved from <http://www.fao.org/3/i5051e/i5051e.pdf>.

Haehnel, R.B. and Daly, S.F. (2002). "Maximum impact force of woody debris on floodplain structures." Vicksburg (MS): US Army Corp of Engineers, Engineer Research and Development Center; 2002 Feb. Technical Report No. ERDC/CRREL. TR-02-2.

Haehnel, R. B. and Daly, S.F. (2004). "Maximum impact force of woody debris on floodplain structures." *Journal of Hydraulic Engineering*. 130(2): 112-120.

Haldar, A. and Mahadevan, S. (2000) *Probability, Reliability, and Statistical Methods in Engineering Design*. New York, US: John Wiley & Sons, Inc.

Hoff, P.D. (2009). *A First Course in Bayesian Statistical Methods*. New York, US: Springer.

Ikeno, M., Takabatake, D., Kihara, N., Kaida, H., Miyagawa, Y., and Shibayama, A. (2016). "Improvement of Collision Force Formula for Woody Debris by Airborne and Hydraulic Experiments." *Coastal Engineering Journal*. 58(4): 1640022.

Johnson, A., Salvador, G., Kenney, J., Robbins, J., Kraus, S., Landry, S., and Clapham, P. (2005). "Fishing gear involved in entanglements of right and humpback whales." *Marine Mammal Science*. 21(4): 635-645.

Katsuno, E.T., Gomes, G.d.G, Castro, F.S.d., and Dantas, J.L.D. (2018). "Numerical analysis of debris containment grid fluid-body interaction." Proceedings of the ASME 2018 37th International Conference on Ocean, Offshore and Arctic Engineering. Madrid, Spain. OMAE2018-78106.

Ko, H. T.-S., Cox, D.T., Riggs, H.R., and Naito, C.J. (2014). "Hydraulic Experiments on Impact Forces from Tsunami-Driven Debris." *J. Waterway, Port, Coastal, Ocean Eng.* 141(3): 04014043.

Lagasse, P.F., Clopper, P.E., Zevenbergen, L.W., Spitz, W.J, and Girard, L.G. (2010). "Effects of Debris on Bridge Pier Scour." Washington, D.C.: Transportation Research Board – National Research Council (US); NCHRP Report 653.

Lebreton, L.C.-M, Zwet, J.v.d, Damsteeg, J.-W, Slat, B., Andrady, A., Reisser, J. (2016). "River Plastic Emissions to the World's Oceans." *Nature Communications*. 8:15611.

Lee, W.S., Grosh, D.L., Tillman, F.A., and Lie, C.H. (1985). "Fault tree analysis, methods, and applications – a review." *IEEE Transactions on Reliability*. R-34(3): 194-203.

Lee, K.T., Ho, Y.-H., and Chyan, Y.-J. (2006). "Bridge Blockage and Overbank Flow Simulations Using HEC-RAS in the Keelung River during the 2001 Nari Typhoon." *Journal of Hydraulic Engineering*. 132(3):319-323.

Lyman, E. (2014) Hawaiian Islands Humpback Whale National Marine Sanctuary/NOAA Fisheries Marine Mammal Health and Stranding Response Program (Permit #932-1905).

Lyn, D.A., Cooper, T.J., Condon, C.A., and Gan, L. (2007). "Factors in debris accumulation at bridge piers." West Lafayette (IN): Indiana Department of Transportation and US DOT Federal Highway Association (US); 2007 Aug. Report No. FHWA/IN/JTRP-2006/36.

Macfadyen, G., Huntington, T., and Cappell, R. (2009). "Abandoned, lost or otherwise discarded fishing gear." FAO Fisheries and Aquaculture Tech. Paper No. 523 and UNEP Regional Seas Reports and Studies No. 185. Retrieved from <http://www.fao.org/3/i0620e/i0620e00.htm>

Manaadiar, H. (2018, March 26). “Containers lost at sea..!!!! Why it happens and what to do when it happens.” *Shipping and Freight Resource*. Retrieved from <https://shippingandfreightresource.com/containers-lost-at-sea/>.

Manners, R.B. and Doyle, M.W. (2008). “A mechanistic model of woody debris jam evolution and its application to wood-based restoration and management.” *River Research and Applications*. 24: 1104-1123.

Manuel, L., Kallivokas, L.F., Williamson, E.B., Bomba, M., Berlin, K.B., Cryer. A., and Henderson, W.R. (2006) “A Probabilistic Analysis of the Frequency of Bridge Collapses due to Vessel Impact.” Austin (TX): Texas Department of Transportation and US DOT Federal Highway Association (US); 2006 Nov. Report No. FHWA/TX-07/0-4650-1

Maria, C.S. (2020, December 8). “ONE Apus ship returns to Japan after losing over 1,800 containers in ocean.” *The Weather Network*. Retrieved from <https://www.theweathernetwork.com/ca/news/article/one-apus-ship-returning-to-japan-after-losing-number-of-containers-in-north-pacific-ocean>.

Martin, J., Sabatier, Q., Gowan, T.A., Giraud, C., Gurarie, E., Calleson. C.S., Ortega-Ortiz, J.G., Deutsch, C.J., Rycyk, A., and Koslovsky, S.M. (2015). “A quantitative framework for investigating risk of deadly collisions between marine wildlife and boats.” *Methods in Ecology and Evolution*. 7(1):42-50.

Matsutomi, H. (2009). “Method for estimating collision force of driftwood accompanying tsunami inundation flow.” *Journal of Disaster Research*. 4(6): 435-440.

Mattila, D.K. and Lyman, E. (2014). “A note on the entanglement of large whales in marine debris.” 58th Annual Meeting of the Scientific Committee of the International Whaling Commission, Anchorage, Alaska. Report SC/58/BC2. Retrieved from <https://hawaiihumpbackwhale.noaa.gov/protect/publications.html>

Melchers, R.E. and Beck A.T. (2018). *Structural Reliability Analysis and Prediction*. Hoboken, NJ: John Wiley & Sons, Ltd.

Melville, B.W. and Dongol, D.M. (1992). “Bridge Pier Scour with Debris Accumulation” *Journal of Hydraulic Engineering*. 118(9): 1306-1310.

Morgan, L.E. and Chuenpagdee, R. (2003). "Shifting gears: addressing the collateral impacts of fishing methods in U.S. waters." *PEW Science Series*. Washington, D.C.: Island Press.

Naito, C.J., Cercone, C., Riggs, H.R., and Cox, D. (2014). "Procedure for site assessment of the potential for tsunami debris impact." *J. Waterway, Port, Coastal, Ocean Engineering*. 140(2): 223-232.

Nistor, I., Goseberg, N., and Stolle, J. (2017). "Tsunami-driven debris motion and loads: a critical review." *Frontiers in Built Environment*. 3:2.

NOAA Fisheries (2019, 13 Dec). *West Coast Large Whale Entanglement Response Program*. NOAA Fisheries. Retrieved from <https://www.fisheries.noaa.gov/west-coast/marine-mammal-protection/west-coast-large-whale-entanglement-response-program#reports>

NOAA Marine Debris Program (2015). *2015 Report on the impacts of 'ghost fishing' via derelict fishing gear*. Silver Spring, MD. Retrieved from <https://marinedebris.noaa.gov/sites/default/files/publications-files/Ghostfishing_DFG.pdf >

NOAA Office of Response and Restoration (2017, 9 Aug). *How Marine Debris is Impacting Marine Animals*. NOAA. Retrieved from <https://response.restoration.noaa.gov/about/media/how-marine-debris-impacting-marine-animals.html>.

Paczkowski, K., Riggs, H.R., Naito, C.J., and Lehmann, A. (2012). "A one-dimensional model for impact forces resulting from high mass, low velocity debris." *Structural Engineering and Mechanics*. 42(6): 831-847.

Padgett, J., DesRoches, R., Nielson, B., and Yashinsky, M. (2008). "Bridge damage and repair costs from Hurricane Katrina." *Journal of Bridge Engineering*. 13(1): 6-14.

Panici, D., Kripakaran, P., Djordjević, S, and Dentith, K. (2020). "A practical method to assess risks from large wood debris accumulations at bridge piers." *Science of the Total Environment*. 728(2020):138575.

Parola, A.C., Apelt, C.J., and Jempson, M.A. (2000). "Debris Forces on Highway Bridges." Washington, D.C.: Transportation Research Board – National Research Council (US); NCHRP Report 445.

Pettis, H.M., Pace, R.M. III, and Hamilton, P.K. (2020). "North Atlantic Right Whale Consortium 2019 Annual Report Card". *Report to the North Atlantic Right Whale Consortium*. Retrieved from < https://www.narwc.org/uploads/1/1/6/6/116623219/2019reportfinal.pdf>.

Richardson, K., Hardesty, B.D., and Wilcox, C. (2019). "Estimates of fishing gear loss rates at a global scale: A literature review and meta-analysis." *Fish and Fisheries*. 20(6): 1218-1231.

Riggs, H.R., Cox, D.T., Naito, C.J., Kobayashi, M.H., Aghl, P.P., Ko, H.T.-S, and Khowitar, E. (2013). "Water-driven debris impact forces on structures: experimental and theoretical program." Proceedings of the ASME 2013 32nd International Conference on Ocean, Offshore and Arctic Engineering. Nantes, France. OMAE2013-11128.

Riggs, H.R., Cox, D.T., Naito, C.J., Kobayashi, M.H., Aghl, P.P, Ko, H.T.-S., and Khowitar, E. (2014). "Experimental study of water-driven debris impact forces on structures." *Journal of Offshore Mechanics and Artic Engineering*. 136: 041603.

Roberts, F.S. and Tesman, B. (2009). *Applied Combinatorics: Second Edition*. Boca Raton, US: CRC Press.

Roberts, N.J., Nadim, F., and Kalsnes, B. (2009). "Quantification of vulnerability to natural hazards." *Georisk*. 3(3): 164-173.

Robinson, K. (2020, September 18). "Hurricane Sally: Skanska says removing barges before storm was neither 'safe nor feasible.'" *Pensacola News Journal*. Retrieved from <https://www.pnj.com/story/news/2020/09/18/hurricane-sally-damage-3-mile-bridge-pensacola-skanska-says-barge-removal-neither-safe-nor-feasible/3492153001/>

Ruiz-Villanueva, V., Piégay, H., Gurnell, A.M., Martson. R.A., and Stoffel, M. (2016). "Recent advances quantifying the large wood dynamics in river basins: New methods and remaining challenges." *Review of Geophysics*. 54: 611-652.

Saez, L., Lawson, D., and DeAngelis, M. (2020). "Large whale entanglements off the U.S. West Coast, from 1982-2017." NOAA Tech. Memo. NMFS-OPR-63, 48 p.

Skanska USA (2020, October 21). "Pensacola Bay Bridge Update." *Skanska*. Retrieved from <https://www.usa.skanska.com/who-we-are/media/featured-news/hurricane-sally/>

Slowey, K. (2020, September 24). "22 barges broke loose from Florida bridge project during Hurricane Sally, Skanska confirms." *Contruction Dive*. Retrieved from <https://www.constructiondive.com/news/skanskas-florida-bridge-project-shut-down-after-construction-barges-slam-i/585642/>

Smolowitz, R.J. (1978). "Trap design and ghost fishing: discussion." *Marine Fisheries Review*. MFR Paper 1310: 59-67.

Stelfox, M., Hudgins, J., and Sweet, M. (2016). "A review of ghost gear entanglement amongst marine mammals, reptiles and elasmobranchs." *Marine Pollution Bulletin*. 111(2016): 6-17.

Stolle, J., Goseberg, N., Nistor, I., and Petriu, E. (2018). "Probabilistic investigation and risk assessment of debris transport in extreme hydrodynamic conditions." *J. Waterway, Port, Coastal, Ocean Engineering*. 144(1): 04017039.

U.S. Department of Transportation Federal Highway Association (U.S. DOT FHWA) (2020). *National Bridge Inventory*. Washington, D.C. Retrieved from <https://www.fhwa.dot.gov/bridge/nbi.cfm>

U.S. Regional Fishery Management Councils. (n.d.). *U.S. Regional Fishery Management Councils*. Retrieved from < http://www.fisherycouncils.org/>

Van Sickle, J. and Gregory, S.V. (1990). "Modeling inputs of large woody debris to streams from falling trees." *Canadian Journal of Forest Research*. 20(1990):1593-1601.

Visit California. (2019, August 21). *Top Places for Whale Watching in California*. Retrieved from <https://www.visitcalifornia.com/feature/top-places-whale-watching-california>

Wallerstein, N., Thorne, C.R., and Abt, S.R. (1997) “Debris Control at Hydraulic Structures in Selected Areas of the United States and Europe.” London (UK): U.S. Army Research Development & Standardization Group (UK); 1997 Dec. Contract Report CHL-97-4.

Waters, H. (2016, Nov). *Slow Down for Right Whales*. Smithsonian Ocean. Retrieved from <https://ocean.si.edu/ocean-life/marine-mammals/slow-down-right-whales>

World Animal Protection (2018). *Ghost beneath the waves*. London, UK: World Animal Protection International.

Yeom, G.-S., Nakamura, T., and Mizutani, N. (2009). “Collision analysis of container drifted by runup tsunami using drift collision coupled model.” *Journal of Disaster Research*. 4(6): 441-449.

APPENDIX A

MATLAB CODE: WHALE ENTANGLEMENT

Objects are linked to documents that contain the code.

 EntanglementPlots.pdf	This script conducts the discrete valued analysis and generates scatter plots
 EntanglementSimulation.pdf	This script simulates analysis using continuous probability distribution functions and generates visualization
 TrunDi.pdf	This function is used to conduct the sensitivity analysis calculations
 RunTrunDi.pdf	This script runs the above function to perform generate visualization
 Entanglement3D.pdf	This script generates the 3D histogram and contour graphics

APPENDIX B

MATLAB CODE: DEBRIS COLLISION

Objects are linked to documents that contain the code.

Collision.pdf

This script calculates the probability of collision for individual container sizes and the convolution of sizes

AccumulationLoop.pdf

This script simulates the accumulation of a specified number of containers for a single size.